

***Hydrogeology, Geochemistry and Microbiology  
of a Reactive Barrier for  
Acid Mine Drainage***

by

Shawn Gavin Benner

A thesis

Presented to the University of Waterloo

in fulfillment of the

thesis requirement for the degree of

Doctor of Philosophy

in

Earth Sciences

Waterloo, Ontario, Canada, 1999

© Shawn G. Benner 1999



**National Library  
of Canada**

**Acquisitions and  
Bibliographic Services**

**395 Wellington Street  
Ottawa ON K1A 0N4  
Canada**

**Bibliothèque nationale  
du Canada**

**Acquisitions et  
services bibliographiques**

**395, rue Wellington  
Ottawa ON K1A 0N4  
Canada**

*Your file* *Votre référence*

*Our file* *Notre référence*

**The author has granted a non-exclusive licence allowing the National Library of Canada to reproduce, loan, distribute or sell copies of this thesis in microform, paper or electronic formats.**

**The author retains ownership of the copyright in this thesis. Neither the thesis nor substantial extracts from it may be printed or otherwise reproduced without the author's permission.**

**L'auteur a accordé une licence non exclusive permettant à la Bibliothèque nationale du Canada de reproduire, prêter, distribuer ou vendre des copies de cette thèse sous la forme de microfiche/film, de reproduction sur papier ou sur format électronique.**

**L'auteur conserve la propriété du droit d'auteur qui protège cette thèse. Ni la thèse ni des extraits substantiels de celle-ci ne doivent être imprimés ou autrement reproduits sans son autorisation.**

0-612-51179-0

**Canada**

The University of Waterloo requires the signatures of all persons using or photocopying this thesis. Please sign below and give address and date.

## *Abstract*

A full-scale permeable reactive barrier was installed in August 1995 into an aquifer impacted by mine drainage waters at the Nickel Rim mine site, near Sudbury, Ontario. The reactive barrier (3.6 m x 15 m x 4 m) contains organic compost to promote bacterially mediated sulfate reduction and subsequent metal sulfide precipitation. Dramatic changes in concentrations of  $\text{SO}_4$  (decrease of 2000-3000 mg/L), Fe (decrease of 270-1300 mg/L), trace metals (e.g., Ni decreases 30 mg/L) and alkalinity (increase of 800-2700 mg/L) are observed. Populations of sulfate reducing bacteria, dissolved sulfide concentrations, and isotope  $^{34}\text{S}$  are elevated compared to the up-gradient aquifer. Solid phase analysis of the reactive mixture indicates the accumulation of Fe mono-sulfide precipitates.

The overall rate of  $\text{SO}_4$  and Fe removal declines with time from initial rates of 58 and 38  $\text{mmol L}^{-1} \text{a}^{-1}$  respectively, to 40 and 18  $\text{mmol L}^{-1} \text{a}^{-1}$  respectively, 38 months after installation, likely due to declining organic carbon reactivity. Heterogeneous flow, and resulting variation in residence times, produces spatially variable treatment and decreases barrier performance. The  $\text{SO}_4$  reduction rate varies seasonally by a factor of 2 which is attributed to seasonal shifts in groundwater temperature (3-16 °C); an effective activation energy of  $E_a=10 \text{ kcal mol}^{-1}$  can account for this change.

Enumeration of bacterial populations in the Nickel Rim groundwater flow system indicate elevated populations of iron and sulfur oxidizing bacteria are restricted to zones of groundwater recharge and discharge. Sulfur oxidizers are highest in the tailings ( $1.27 \times 10^3$  MPN/g) where sulfide minerals are exposed to oxygen and iron oxidizers are highest ( $9.56 \times 10^5$  MPN/g) where effluent discharges to the surface. Comparatively low populations of oxidizing bacteria in the tailings reflect low rates of sulfide oxidation due to the high water content in the zone of active oxidation. An observed positive correlation between populations of sulfate reducing bacteria and sulfur oxidizing bacteria suggests interdependency.

Numerical flow modeling shows that heterogeneities in hydraulic conductivity within the aquifer will strongly affect thin barrier performance, while thicker barrier performance will be more strongly affected by variation in barrier hydraulic conductivity. More uniform flow can be attained utilizing thicker, homogeneous barriers.

## *Acknowledgements*

This thesis would have not been possible without the support of a large and varied cast of characters.

I have been blessed with exceptional mentors who have guided my educational journey through this thesis. David Blowes provided me with guidance and support and taught me the power of a quantitative and interdisciplinary approach to groundwater geochemistry. Carol Ptacek's always available and sage advice has left a large mark on both me and this thesis. Doug Gould's dedication to this project has been exceptional and without him the breadth of this thesis would have been greatly narrowed. Dave, Carol, and Doug shaped my education at Waterloo and working with them has been both enjoyable and rewarding.

To my committee members Jim Barker and Barbara Butler and Janet Herman: thank you for your criticisms, comments, and insights; they have helped to focus my thesis and have enhanced the quality of the final product.

To those who came before: David Blowes and Carol Ptacek conceived the idea of reactive barriers for acid mine drainage. Kathy Waybrant conducted "proof-of-concept" laboratory column studies. Ray Johnson, John Jambor and Jeff Bain characterized the hydrogeochemistry of the Nickel Rim tailings impoundment. Without these pioneers, this thesis would not have been possible.

A special thanks to my colleagues Tom Al, Mike Baker, Ty Ferré, and Uli Mayer: our conversations often sparked the creative juices and their influences are found throughout this thesis. Numerous discussions on physical flow and barrier performance with Rick Devlin also provided valuable insight. Roger Herbert conducted solid phase analysis of the barrier material and I benefited greatly, in many ways, from the year he spent at Waterloo.

This project would not have been possible without the support and vision of folks at Falconbridge Ltd. In particular, Mike Sudbury, Glen Hall, and the people in the analytical laboratory provided their support, assistance, and expertise.

This was a labor-intensive and technically diverse endeavor and would have taken eons without the assistance of many talented people. In particular, Jeff Bain, Mike Moncur, Lynn Lortie, Scott Sale, and Cheryl Sue contributed many hours of hard work in the laboratory and field to make this thesis a reality. Kathy Chalykoff, David Dillon, Louise Durham, Patty Forester, Linda Gogal, Andrea Hulshof, Che McRae, Shane Matheson, Jennifer Nadeau, Erin Parker, Cheryl Ross, and Sierra Shea, all contributed their time to this project. John Molson gave his time and assistance with the FLOTRANS computer code. Karen Critchley went well beyond the call of duty preparing many batches of last minute slides over the years. Chris Hanton-Fong assisted in method development, field sampling, logistical and managerial support and generally kept the grime ship afloat.

Thank you, one and all!

This project was made possible by generous funding from Falconbridge Ltd., Canada, Centre for Mineral and Energy Technology Biotechnology Fund, Canadian National Science and Engineering Research Council (NSERC), and the Waterloo Centre for Groundwater Research Ontario Centre for Research in Earth and Space Technology (CRESTech).

*This thesis is dedicated to*

*my wife Juliana,*

*she has always believed in me*

*and has made it possible for me to pursue my dream.*

# Table of Contents

CHAPTER 1 INTRODUCTION.....	1
1.1 THESIS OBJECTIVES .....	3
1.2 THESIS STRUCTURE .....	3
1.3 REFERENCES .....	5
CHAPTER 2 INSTALLATION AND INITIAL RESULTS.....	6
2.1 CHAPTER SUMMARY .....	6
2.2 INTRODUCTION .....	7
2.2.1 <i>Sulfate reduction</i> .....	9
2.2.2 <i>Reactive barrier technology</i> .....	10
2.2.3 <i>Site description</i> .....	12
2.3 METHODS .....	13
2.3.1 <i>Selection of reactive material</i> .....	13
2.3.2 <i>Barrier installation</i> .....	17
2.3.3 <i>Installation and sampling of monitoring wells</i> .....	17
2.4 RESULTS AND DISCUSSION .....	19
2.4.1 <i>Surface water recharge</i> .....	19
2.4.2 <i>Groundwater velocity</i> .....	21
2.4.3 <i>Water chemistry</i> .....	21
2.4.4 <i>Estimating reactive barrier longevity</i> .....	23
2.4.5 <i>Cost of installation</i> .....	25
2.5 CONCLUSIONS .....	25
2.6 REFERENCES .....	27

<b>CHAPTER 3 GEOCHEMISTRY AND MICROBIOLOGY .....</b>	<b>33</b>
3.1 CHAPTER SUMMARY .....	33
3.2 INTRODUCTION .....	34
3.2.1 <i>Acid mine drainage</i> .....	34
3.2.2 <i>Sulfate reduction</i> .....	34
3.2.3 <i>Nickel Rim Reactive Barrier</i> .....	35
3.2.4 <i>Nickel Rim Aquifer</i> .....	36
3.2.5 <i>Water Sampling and Analysis</i> .....	38
3.2.6 <i>Solid Phase Methods</i> .....	38
3.2.7 <i>Geochemical Modeling</i> .....	39
3.3 RESULTS AND DISCUSSION .....	40
3.3.1 <i>Four Distinct Zones</i> .....	42
3.3.2 <i>Up-Gradient Zone</i> .....	42
3.3.3 <i>Organic Mixture Zone</i> .....	45
3.3.4 <i>Down-Gradient Zone</i> .....	48
3.3.5 <i>Vertical trends within barrier</i> .....	49
3.4 REFERENCES .....	51
<b>CHAPTER 4 RATES OF REACTION AND TREATMENT .....</b>	<b>55</b>
4.1 CHAPTER SUMMARY .....	55
4.2 INTRODUCTION .....	56
4.3 METHODS .....	56
4.3.1 <i>Water Sampling and Analysis</i> .....	56
4.3.2 <i>Bacterial Enumeration</i> .....	57
4.3.3 <i>Groundwater Flow Modeling</i> .....	58
4.4 RESULTS AND DISCUSSION .....	58

4.4.1	<i>Physical Flow through the Barrier</i> .....	58
4.4.2	<i>Spatial Heterogeneities</i> .....	65
4.4.3	<i>Comparing Transects Parallel to Flow</i> .....	66
4.4.4	<i>Profiles Perpendicular to Flow</i> .....	68
4.4.5	<i>Lower Barrier in Values</i> .....	70
4.4.6	<i>Reactivity vs. Residence Time</i> .....	70
4.4.7	<i>Horizontal Trends</i> .....	73
4.4.8	<i>Comparing Fe and SO<sub>4</sub> removal rates</i> .....	77
4.4.9	<i>Aqueous Phase Removal Rates</i> .....	78
4.4.10	<i>Solid Phase Accumulation Rates</i> .....	81
4.4.11	<i>Comparing Solid and Aqueous Phase Rates</i> .....	82
4.4.12	<i>Changing Groundwater Temperature</i> .....	84
4.4.13	<i>Effect of Temperature on Reactions in the Barrier</i> .....	87
4.4.14	<i>Coupling Temperature to the Rate of Sulfate Reduction</i> .....	87
4.4.15	<i>Calculating an effective E<sub>a</sub></i> .....	89
4.4.16	<i>Effect of Temperature on Sulfide Solubility</i> .....	91
4.4.17	<i>Implications for Barrier Performance and Design</i> .....	93
4.5	REFERENCES .....	96
<b>CHAPTER 5 AQUIFER MICROBIAL POPULATIONS</b> .....		99
5.1	CHAPTER SUMMARY .....	99
5.2	INTRODUCTION .....	100
5.2.1	<i>The Nickel Rim Research Site</i> .....	101
5.3	METHODS .....	103
5.4	RESULTS AND DISCUSSION .....	105

5.4.1	<i>Recharge Zone (Tailings)</i> .....	105
5.4.2	<i>Profiles along Flow Lines</i> .....	109
5.4.3	<i>Vertical Profiles within the Aquifer</i> .....	115
5.5	CONCLUSIONS.....	118
5.6	REFERENCES.....	120
<b>CHAPTER 6 MODELING BARRIER FLOW</b> .....		124
6.1	CHAPTER SUMMARY.....	124
6.2	INTRODUCTION.....	125
6.3	METHODS.....	127
6.4	RESULTS AND DISCUSSION.....	129
6.4.1	<i>Homogeneous Conditions</i> .....	129
6.4.2	<i>Heterogeneous Aquifer</i> .....	133
6.4.3	<i>Heterogeneous Barrier</i> .....	140
6.5	CONCLUSIONS.....	142
6.6	REFERENCES.....	144
<b>CHAPTER 7 CONCLUSIONS</b> .....		147

## *List of Tables*

<b>TABLE 1.1</b> .....	15
Hydraulic conductivity of mixtures of gravel and reactive material determined by constant head permeameter.	
<b>TABLE 4.1</b> .....	80
Rates of S and Fe removal based on changes in aqueous concentrations (influent - effluent) and estimated residence times.	
<b>TABLE 4.2</b> .....	82
Rates of S and Fe removal based on solid phase digestions (from <i>Herbert et al., 2000</i> ).	

# List of Figures

<b>FIGURE 1.1</b> .....	2
Schematic of de-coupled sulfur and iron oxidation associated with acid mine drainage and treatment using sulfate reduction in a permeable reactive barrier.	
<b>FIGURE 2.1</b> .....	12
Map view of the Nickel Rim mine site, location of permeable reactive barrier installation, location of monitoring cross section A-A'.	
<b>FIGURE 2.2</b> .....	13
Cross sectional profile along transect A-A' in Figure 2.1 shows groundwater discharging both at the foot of the dam and to Moose Lake.	
<b>FIGURE 2.3</b> .....	16
Results of FLONET modeling showing idealized aquifer in cross-section. $K_x$ and $K_z$ = hydraulic conductivity in the X and Z directions, respectively. (a) Aquifer with no reactive barrier, lower layer is more permeable than upper layer. (b) Same as (a) but with reactive barrier with permeability equivalent to lower layer of aquifer. (c) Same as (b) but with reactive barrier 10X more permeable than aquifer. (d) Same as (b) but with small layer of higher permeability within reactive barrier.	
<b>FIGURE 2.4</b> .....	18
Schematic diagram of permeable reactive barrier installation.	
<b>FIGURE 2.5</b> .....	20
Cross-sectional profiles of reactive barrier and adjoining aquifer. Small squares indicate sample locations. (a) Schematic diagram showing zone of aquifer receiving surface water recharge based on head profiles and water chemistry prior to reactive barrier installation (From Bain, 1996). (b) Profile of chloride concentrations one month after installation. (c) Profile of chloride concentrations nine	

months after installation.

**FIGURE 2.6** ..... 22

Cross-sectional view of reactive barrier and adjoining aquifer. Small squares indicate sample locations. Concentrations of sulfate and iron in groundwater and calculated "Potential Acidity" nine months after installation are shown.

**FIGURE 3.1** ..... 37

Cross-sectional profiles of aquifer and reactive barrier: (a) shows flow lines for the Nickel Rim aquifer prior to the installation of the reactive barrier determined by field-collected data and flow modeling from Bain (2000). (b) sample well and core locations in aquifer and reactive barrier. (c) location of geochemically distinct zones along groundwater flow path.

**FIGURE 3.2** ..... 40

Cross-sectional profiles of dissolved constituents for September 1996:  $\text{SO}_4$ , Fe, alkalinity (as  $\text{CaCO}_3$ ), and Ni.

**FIGURE 3.3** ..... 41

Vertically averaged constituent concentrations for each well nest. (a)  $\text{SO}_4$ , alkalinity (as  $\text{CaCO}_3$ ), and  $\text{S}^{2-}$  (b) Fe, Ca, and Mg (c) Ni and Zn (d) Si, Al, and Mn (e) pH and Eh and (f) vertically averaged most probable numbers (MPN) for sulfate reducing bacteria (SRB), and Dehydrogenase enzyme activity (DH).

**FIGURE 3.4** ..... 43

Vertically averaged saturation indices for selected mineral phases for each well nest: (a) gypsum ( $\text{CaSO}_4$ ), calcite ( $\text{CaCO}_3$ ), and dolomite ( $\text{CaMg}(\text{CO}_3)_2$ ) (b) siderite ( $\text{FeCO}_3$ ) and rhodochrosite ( $\text{MnCO}_3$ ) (c) gibbsite ( $\text{Al}(\text{OH})_3$ ), amorphous  $\text{Al}(\text{OH})_3$ , and amorphous  $\text{SiO}_2$  (d) amorphous FeS, and pyrite ( $\text{FeS}_2$ ). Note: sulfide saturation indices outside Organic Material Zone were calculated from measured Eh.

**FIGURE 3.5** ..... 46

Vertical profiles of "acid volatile sulfide-AVS" and "total reduced (inorganic) sulfides-TRS" concentrations for organic material from Core #2, September 1996. Dashed line indicates TRS concentration in organic material prior to installation of the barrier. Data taken from Herbert et al. (1998).

**FIGURE 4.1** ..... 57

Map view of Nickel Rim reactive barrier installation showing mine tailings impoundment, groundwater flow path, and locations of reactive barrier and monitoring well transects.

**FIGURE 4.2.** ..... 59

Flow and transport modeling boundary and initial conditions.

**FIGURE 4.3** ..... 60

Field-measured cross-sectional profile of chloride concentrations with time

**FIGURE 4.4** ..... 60

Modeled cross-sectional profiles of chloride concentrations with time

**FIGURE 4.5** ..... 62

Chloride concentrations with time for sampling points in well nests RW29, RW30 and RW31 located 0.5 m, 2 m and 3.5 m into the barrier (Figure 3). Dashed line indicates maximum observed Cl concentration of influent water. Arrow marks time at which background would be reached under plug flow conditions and a groundwater velocity of 16 m a<sup>-1</sup>. Each plot is labeled with the approximate depth below surface.

**FIGURE 4.6** ..... 63

Cross-sectional profiles along Transect A (Figure 1) of SO<sub>4</sub> concentrations through the reactive barrier for each sampling period.

**FIGURE 4.7** ..... 64

Cross-sectional profiles along Transect A (Figure 1) of Fe concentrations through the reactive barrier for each sampling period.

<b>FIGURE 4.8</b> .....	65
Cross-sectional profiles along Transect A (Figure 1) of alkalinity values through the reactive barrier for each sampling period.	
<b>FIGURE 4.9</b> .....	67
Cross-sectional profiles along transects F, A, and E, parallel to groundwater flow, of SO <sub>4</sub> concentrations for the May and October 1998 sampling periods.	
<b>FIGURE 4.10</b> .....	67
Cross-sectional profiles along transects F, A, and E parallel to groundwater flow, of Fe concentrations for the May and October 1998 sampling periods.	
<b>FIGURE 4.11</b> .....	68
Cross-sectional profiles along transects B, C, and D, perpendicular to groundwater flow, of SO <sub>4</sub> concentrations for the May and October 1998 sampling periods. Flow direction is out of the page.	
<b>FIGURE 4.12</b> .....	69
Cross-sectional profiles along transects B, C, and D perpendicular to groundwater flow, of Fe concentrations for the May and October 1998 sampling periods. Flow direction is out of the page.	
<b>FIGURE 4.13</b> .....	71
Vertical profiles of populations of sulfate reducing bacteria (SRB) and overall bacterial activity as measured by dehydrogenase activity (DH) for cores taken adjacent to well nests RW29, RW30, and RW31.	
<b>FIGURE 4.14</b> .....	72
Vertically averaged trends in concentrations of SO <sub>4</sub> , Fe, S <sup>2-</sup> , and the saturation index for mineral phase mackinawite for all sampling periods.	
<b>FIGURE 4.15</b> .....	74

Trends in concentrations of SO<sub>4</sub> along slow flow path at bottom of the barrier and fast flow path in the middle of the barrier.

**FIGURE 4.16** ..... 75

Trends along fast and slow, and all flow paths averaged for all sampling periods and modeled rates of SO<sub>4</sub> removal based on Monod formulation.

**FIGURE 4.17** ..... 77

Trends in concentrations of Fe along slow flow path at bottom of the barrier and fast flow path in the middle of the barrier.

**FIGURE 4.18** ..... 79

(a) Vertically averaged concentrations of SO<sub>4</sub> in the well nests RW23 (up gradient) and RW26 (down gradient) versus time. (b) Vertically averaged concentrations of Fe in the well nests RW23 (up gradient) and RW26 (down gradient) versus time. (c) Removal of SO<sub>4</sub> and Fe based on the difference between RW23 and RW26 (up gradient - down gradient) concentrations versus time. Error bars reflect ± one standard error.

**FIGURE 4.19** ..... 85

Recorded temperature data within the barrier over a one year period. Curves are shown for surface ground temperature, 1.1 meter, 2.0 m and 3.6 m depths.

**FIGURE 4.20** ..... 86

Average concentrations of SO<sub>4</sub> and Fe removed and alkalinity added with time. Based on the RW23 concentrations - concentrations of all points (n=12) within the barrier.

**FIGURE 4.21** ..... 88

Temperature at 2 m depth (solid line) and plot of four parameter sine function (dotted line) for that data.

**FIGURE 4.22** ..... 89

Predicted rate of sulfate removal versus time based on average removal rate (Figure 16), the Arrhenius equation and an apparent activation energy of E<sub>a</sub> = 25 kcal mol<sup>-1</sup>.

**FIGURE 4.23** ..... 90

The curve based on Arrhenius equation (solid line) for observed temperature induced fluctuations in  $\text{SO}_4$  removal (square boxes) yielding an apparent activation energy  $E_a = 10 \text{ kcal mol}^{-1}$ . Dashed curve shows sensitivity of fit to changing  $E_a$  by  $\pm 5 \text{ kcal mol}^{-1}$ . Stepped solid line indicates maximum rate based on observed removal in well nest RW23 (down gradient).

**FIGURE 4.24** ..... 92

Observed (square boxes) and predicted Fe concentrations with time based on: 1) changing solubility of mackinawite (based on Van't Hoff equation,  $\Delta H$ ) and 2) changing rates of  $\text{H}_2\text{S}$  generation expressed as  $\text{SO}_4$  removal (based on Arrhenius equation,  $E_a$ ).

**FIGURE 5.1** ..... 102

a) Shows the flow system for the Nickel Rim Aquifer based on hydrologic flow modeling of Bain et al. (1999). Diagram also shows water sampling points and sediment core locations. (b) Shows idealized flow paths: Both flow paths originate in the tailings, but Flow Path A discharges to the surface at the base of the tailings dam, while Flow Path B remains in the aquifer and passes through the reactive barrier.

**FIGURE 5.2** ..... 106

The mineralogy of the tailings from the surface to the 1.6 m depth (Adapted from *Jambor and Owens (1993)*). The narrow (2-5 cm) zone of active sulfide oxidation is located at bottom of the previously oxidized, orange-stained, tailings.

**FIGURE 5.3** ..... 107

Vertical profiles for location NR6 in the tailings impoundment of pH, Eh, alkalinity, Fe,  $\text{SO}_4$ , IOB (iron oxidizing bacteria), SOB (sulfur oxidizing bacteria), SRB (sulfate reducing bacteria and FOC (solid phase fraction organic carbon). Hashed marks denotes oxidized tailings, horizontal dotted line indicates the location of the water table. See Figure 1 for location of profile.

**FIGURE 5.4** ..... 112

Flow Path A profiles of pH, Eh, Alkalinity, Fe, SO<sub>4</sub>, IOB (iron oxidizing bacteria), SOB (sulfur oxidizing bacteria), SRB (sulfate reducing bacteria and DOC (dissolved phase organic carbon). See Figure 1 for location of Flow Path A.

**FIGURE 5.5** ..... 114

Flow Path B profiles of pH, Eh, Alkalinity, Fe, SO<sub>4</sub>, IOB (iron oxidizing bacteria), SOB (sulfur oxidizing bacteria), SRB (sulfate reducing bacteria. See Figure 1 for location of Flow Path B.

**FIGURE 5.6** ..... 116

Vertical profiles for location NR63 at the base of the tailings dam of pH, Eh, Alkalinity, Fe, SO<sub>4</sub>, IOB (iron oxidizing bacteria), SOB (sulfur oxidizing bacteria), SRB (sulfate reducing bacteria and FOC (solid phase fraction organic carbon). Horizontal line indicates the ground surface (G.S.). See Figure 1 for location of profile.

**FIGURE 5.7** ..... 117

Vertical profiles for location RW21 up-gradient of the reactive barrier of pH, Eh, Alkalinity, Fe, SO<sub>4</sub>, IOB (iron oxidizing bacteria), SOB (sulfur oxidizing bacteria), SRB (sulfate reducing bacteria. Horizontal line indicates the ground surface (G.S.). See Figure 1 for location of profile.

**FIGURE 5.8** ..... 117

Vertical profiles for location RW29 within the reactive barrier of pH, Eh, Alkalinity, Fe, SO<sub>4</sub>, IOB (iron oxidizing bacteria), SOB (sulfur oxidizing bacteria), SRB (sulfate reducing bacteria. Horizontal line indicates the ground surface (G.S.). See Figure 1 for location of profile.

**FIGURE 5.9** ..... 118

Vertical profiles for location RW24 down-gradient of the reactive barrier of pH, Eh, Alkalinity, Fe, SO<sub>4</sub>, IOB (iron oxidizing bacteria), SOB (sulfur oxidizing bacteria), SRB (sulfate reducing bacteria. Horizontal line indicates the ground surface (G.S.). See Figure 1 for location of profile.

**FIGURE 6.1** ..... 128

Shows a three dimensional view of idealized reactive barrier. Simulations can represent horizontal or vertical cross sectional views of flow through the barrier.

**FIGURE 6.2** ..... 130

Scenario I shows flow with a homogenous K distribution in the aquifer and barrier. The barrier K is ten times greater than the aquifer. a) 3.0 m thick barrier, b) 1.0 m thick barrier, c) 0.2 m thick barrier, d) same as (b), but with low K material bounding top and bottom of domain.

**FIGURE 6.3** ..... 132

Scenario II shows the affect of varying the barrier K on the "edge effect". Homogenous K distribution in the aquifer and barrier. All simulations the same as Scenario I (b), but the barrier K is varied. Barrier is a) 100 times greater than the aquifer, b) 10 times greater than the aquifer, c) 2 times greater than the aquifer.

**FIGURE 6.4** ..... 134

Scenario III shows the affect of an aquifer with heterogeneous K distribution. Same as Scenario I, but a 1.0 m thick high K layer (10 times rest of aquifer) has been placed up and down gradient of the barrier.

**FIGURE 6.5** ..... 135

Scenario IV shows the affect of varying barrier K on flow in heterogeneous aquifer. The barrier K is varied. Barrier K is a) 100 times greater, b) 10 greater, c) equal to, the K of the aquifer, d) same as (b), but with low K material bounding top and bottom of domain.

**FIGURE 6.6** ..... 137

Scenario V shows the affect of varying the K distribution in aquifer. The total flux across the domain remains constant, but the distribution of high K layers is varied. a) The high K layer in the aquifer is 0.5 m wide with a K 20 times that of the rest of the aquifer. b) The high K layer is 1.0 m wide with a K 10 times that of the rest of the aquifer. c) The high K layer is split into 2 layers each 0.5 m wide with a K 10 times that of the rest of the aquifer. d) same as (c), but with low K material bounding top and bottom of domain.

**FIGURE 6.7** ..... 139

Scenario VI shows the affect of adding homogeneous mixing zones. Mixing zones are added up and down gradient of the barrier. a) Same as Scenario III (c). b) High K, 2 m thick block added up gradient of the barrier. c) High K, 1 m blocks added up and down gradient of the barrier. d) Same as (c) but high K blocks are separated from the barrier by 0.5 m of aquifer.

**FIGURE 6.8** ..... 141

Scenario VII shows the affect of heterogeneous K in the barrier. Same as Scenario I but 1.0 m wide high K layer added to barrier. a) 3.0 m thick barrier. b) 1.0 m thick barrier. c) 0.2 m thick barrier. d) same as (b), but with low K material bounding top and bottom of the domain.

# Chapter 1

## *Introduction*

Discharge of acidic effluent, often containing high concentrations of toxic trace metals, from mines and mine waste is an intractable, worldwide environmental problem with estimated costs of treatment in the 10's of billions of dollars. The oxidation of residual sulfide minerals in mines and mine waste can produce acidic waters containing high concentrations of sulfate, Fe(II) and trace metals (Figure 1). This effluent often enters underlying and adjacent aquifers where buffering by mineral dissolution raises the pH to 4-7 (*Morin and Cherry, 1988*). However, on discharge to the surface, the oxidation of Fe(II) to Fe(III) and the precipitation of ferric oxyhydroxides re-generates acidic conditions (pH < 3), mobilizing toxic trace metals and adversely impacting the surface water ecosystem. Discharge from mines and mine waste can continue for decades, even centuries (*Dubrovsky et al., 1985*). Treatment of this effluent is extremely difficult due to the high dissolved metal concentrations and low pH conditions.

Current methods for the prevention and treatment of acid mine drainage include preventing the infiltration of meteoric water, preventing the oxidation of sulfides and treating the acidic water discharge (*Blowes et al., 1994*). Recognition of the significance and causes of acidic drainage has resulted in changes in the approaches used in the design and operation of tailings disposal systems. The objectives of these changes are to prevent the oxidation of sulfides and the mobilization and subsequent release and transport of reaction products. There is often a time delay of tens of years between the oxidation of the sulfides within the tailings and the eventual discharge to surface water

bodies. Therefore, even at many tailings impoundments with remedial measures imposed, discharge of poor quality water will continue for many years (*Blowes et al., 1994*). Conventional treatment of discharge waters involves precipitation of Fe-oxhydroxides by addition of lime. This approach can be effective but often involves high operating costs and produces large volumes of metal-rich sludge from which metals may subsequently leach. The remediation and prevention of acid mine drainage through the use of permeable reactive barriers to promote bacterially mediated sulfate reduction and metal sulfide precipitation may provide an effective, inexpensive alternative to conventional collection and treatment programs (Figure 1).

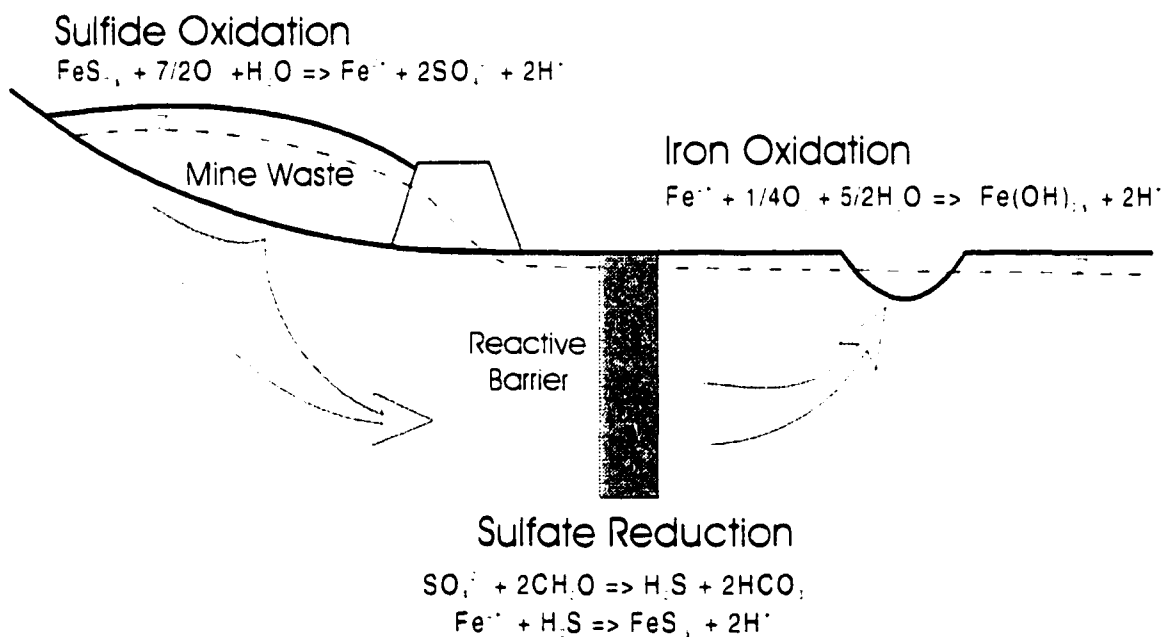


**Figure 1.1** Schematic of de-coupled sulfur and iron oxidation associated with acid mine drainage and treatment using sulfate reduction in a permeable reactive barrier.

## 1.1 THESIS OBJECTIVES

In this thesis I have assessed the use of a full-scale, permeable reactive barrier to treat acid mine drainage utilizing bacterially mediated sulfate reduction. The objectives of this thesis can be summarized in five broad questions:

*Can a full-scale reactive barrier promote sulfate reduction and metal sulfide precipitation, and will the installation result in improved groundwater quality?*

*What are the physical and chemical processes occurring in the reactive barrier that impact groundwater chemistry?*

*What are the rates of these processes, and what are the implications for reactive barrier performance?*

*What is the distribution of bacterial populations associated with the generation and treatment of acid mine drainage within the aquifer and reactive barrier?*

*What is the impact of reactive barrier geometry on groundwater flow in a heterogeneous flow field?*

## 1.2 THESIS STRUCTURE

This thesis is presented in a series of chapters. Chapters 2 through 6 have each been written in manuscript form for submittal to a peer-reviewed journal. Each chapter is written to stand alone, resulting in some repetition of introductory material. Chapters 2, 3 and 4 form the core of the thesis while Chapters 5 and 6 pursue related topics. Chapter 2 describes the installation of the barrier and shows the initial impact on groundwater chemistry. Chapter 3 describes the biogeochemical processes occurring within the barrier. Chapter 4 addresses the kinetics of the reactions within the barrier that lead to improved groundwater quality and also discusses the controlling factors on barrier performance. Chapter 5 examines the distribution throughout the Nickel Rim aquifer of bacterial populations which catalyze the generation and treatment of acid mine drainage.

Chapter 6 presents the results of computer flow modeling that illustrate the importance of reactive barrier geometry on reactive barrier performance and provides assistance for reactive barrier design and assessment.

### 1.3 REFERENCES

- Blowes DW, Ptacek CJ, Jambor JL. 1994. Remediation and prevention of low-quality drainage from tailings impoundments. In: Blowes DW, Jambor JL, eds. Short Course Handbook on Environmental Geochemistry of Sulfide Mine-Wastes. 22 ed. Nepean, ON: Mineralogical Association of Canada.: 365-379.
- Morin KA, Cherry JA. 1988. Migration of acidic groundwater seepage from uranium-tailings impoundments. 3. Simulation of the conceptual model with application to seepage area A. *J. Contam. Hydro.* 2 p. 323-342.
- Dubrovsky NM, Cherry JA, Reardon EJ, Vivyurka AJ. 1985. Geochemical evolution of inactive pyritic tailings in Elliot Lake uranium district. *Can. Geotech. J.* 22 p. 110-128.

## Chapter 2

### *Installation and Initial Results*

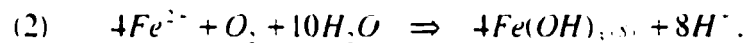
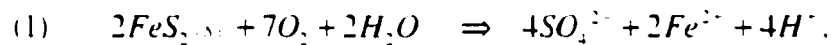
#### **2.1 CHAPTER SUMMARY**

The generation and release of acidic drainage, containing high concentrations of dissolved metals, from decommissioned mine wastes is an environmental problem of international scale. A potential solution to many acid drainage problems is the installation of permeable reactive barriers into aquifers affected by drainage water derived from mine waste materials. A permeable reactive barrier was installed in August 1995 into an aquifer impacted by low quality mine drainage waters at the Nickel Rim mine site, near Sudbury, Ontario. The reactive mixture, containing organic matter, was designed to promote bacterially mediated sulfate reduction and subsequent metal sulfide precipitation. The reactive barrier is installed to an average depth of 12 feet (3.6 m) and is 49 feet (15 m) long perpendicular to groundwater flow. The barrier thickness (flow path length) is 13 feet (4 m). Initial results, collected nine months after installation, indicate that sulfate reduction and metal sulfide precipitation is occurring. Comparing water entering the barrier to treated water exiting the barrier: sulfate concentrations decrease from 2400-4600 mg/L to 200-3,600 mg/L, Fe concentrations decrease from 250-1,300 mg/L to 1.0-40 mg/L, pH increases from 5.8 to 7.0 and alkalinity (as CaCO<sub>3</sub>) increases from 0-50 mg/L to 600-2,000 mg/L. The reactive barrier has effectively removed the capacity of the groundwater to generate acidity on discharge to the surface. Calculations based on comparison to previously run laboratory column experiments indicate that the reactive barrier should remain effective for at least 15 years.

## 2.2 INTRODUCTION

Acidic metal-rich drainage from mines and mine wastes is the largest environmental problem facing the North American mining industry (*Feasby, 1991; USDA, 1993*). On United States Forest Service lands there are between 20,000 and 50,000 mines generating acidic drainage (*USDA, 1993*). In Canada, potential acid generating sites from base metal mining total over 37,000 acres (*Feasby, 1991*). In the Eastern United States over 4,000 miles of rivers and streams are adversely impacted by acid mine drainage from coal mining (*Kleinmann, 1991*). In the Western United States between 5,000 and 10,000 miles of streams are impacted by metal mining (*USDA, 1993*). Estimated costs for the stabilization of these sites are in the billions of dollars (*Feasby, 1991*).

Production of acidic drainage results from the oxidation of residual sulfide minerals and the subsequent oxidation of dissolved Fe(II) (*Boorman and Watson, 1976; Nordstrom, 1979; Dubrovsky et al., 1984*). These reactions can be described as:



Similar reactions, involving other sulfide minerals, can release dissolved As, Cd, Cu, Ni, Pb and Zn. The oxidation of sulfide minerals and the oxidation of Fe<sup>2+</sup> are often decoupled in mine tailings impoundments. Sulfide oxidation (Reaction #1) occurs in the unsaturated zone of the tailings releasing Fe<sup>2+</sup>, SO<sub>4</sub><sup>2-</sup>, and H<sup>+</sup> to the tailings pore water. At many mine sites infiltrating precipitation water carries these reaction products downwards through the tailings and into underlying aquifers. Mineral phases within the mine waste material and aquifer sediment can buffer acidity, resulting in the formation of

a groundwater plume containing high concentrations of  $\text{SO}_4^{2-}$ ,  $\text{Fe}^{2+}$  and other metals but at near-neutral pH (*Morin et al., 1988; Blowes, 1990; Blowes and Ptacek 1994*). As this contaminated groundwater discharges to oxygenated surface-water bodies,  $\text{Fe}^{2+}$  oxidizes, releasing a second pulse of acidity to the environment (Reaction #2). Not only are the resulting low pH conditions harmful to biota, but these conditions also increase the mobility of toxic trace metals such as Cd, Cu, Ni, and Pb, greatly enhancing their bioavailability. In many cases the flux of poor quality water from tailings impoundments will continue for many decades, even centuries (*Morin et al., 1988; Blowes, 1990*). It was the objective of this project to significantly decrease the toxicity of mine drainage effluent by preventing the generation of acidity at discharge to the surface by utilizing sulfate reduction in a porous reactive barrier.

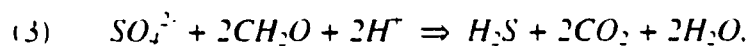
Current methods for the prevention and treatment of acid mine drainage include preventing the infiltration of meteoric water, preventing the oxidation of sulfides and treating the acidic water discharge (*Blowes et al., 1994*). Recognition of the significance and causes of acidic drainage has resulted in changes in the approaches used in the design and operation of tailings disposal systems. The objectives of these changes are to prevent the oxidation of sulfides and the mobilization and subsequent release and transport of reaction products. There is often a time delay of tens of years between the oxidation of the sulfides within the tailings and the eventual discharge to surface water bodies. Therefore, even at many tailings impoundments with remedial measures imposed, discharge of poor quality water will continue for many years (*Blowes et al., 1994*). Conventional treatment of discharge waters involves precipitation of Fe-oxyhydroxides by addition of lime. This approach can be effective but often involves high operating costs and produces large volumes of metal-rich sludge from which metals may subsequently leach.

The remediation and prevention of acid mine drainage through the use of permeable, geochemically reactive barriers may provide an effective, inexpensive

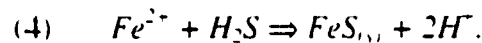
alternative to conventional collection and treatment programs (*Blowes, 1990; Blowes et al., 1995*). This paper describes the design and installation of a full-scale reactive barrier for the treatment of acid mine drainage at the inactive Nickel Rim mine tailings impoundment near, Sudbury, Ontario.

### 2.2.1 Sulfate reduction

Bacterially mediated reduction of sulfate can be expressed as:



where  $\text{CH}_2\text{O}$  represents a generic organic carbon compound. In the presence of soluble metals, hydrogen sulfide can react to form metal sulfides:



Elements such as As, Cd, Cu, Ni, Pb and Zn can also react with  $\text{H}_2\text{S}$  to form other sulfide minerals.

This reaction sequence results in decreased concentrations of dissolved  $\text{SO}_4^{2-}$ , Fe, and other metals, and an increase in alkalinity and pH. All of these changes are desirable in waters affected by mine drainage. Tuttle (*1968*) documented naturally occurring sulfate reduction in a stream contaminated by acid mine waters. Wakao (*1979*) suggested that mine waters could be treated using sulfate-reducing bacteria.

Recently, interest in sulfate reduction has focused on its utility during wetland remediation of acid mine drainage. Wetlands are often designed to treat acid mine drainage using processes of adsorption to solids within the wetland and Fe oxidation and precipitation (Reaction #2). Wetlands are also designed to incorporate anaerobic sulfate reduction (Reactions #3-4) (*McIntire et al., 1990; Hedin, 1989*). The primary method of

exploiting sulfate reduction has been to force acidic, metal and sulfate-rich surface water into the subsurface of the wetland by an induced hydraulic gradient (*McIntire et al., 1990; Machermer and Wildeman, 1992*). Others have attempted to utilize sulfate reduction within bioreactors containing a variety of organic materials (*Dvorak et al., 1992; Hammack and Edenborn, 1992; Bechard, 1993 and 1995; Eger and Wagner, 1995*).

The success of utilizing sulfate reduction for treatment of acidic mine waters has been mixed. In many cases sulfate reduction and metal sulfide precipitation have resulted in improved water quality. However, two factors have hampered this approach. First, high acidity can quickly consume any buffering capacity within the reactive organic material, resulting in a drop in pH. Acidic conditions limit bacterially mediated sulfate reduction (*Brock and Madigan, 1991*), decreasing treatment capacity. Second, where neutral pH conditions have been maintained, the residence times within the reactive mixture are often not sufficient to remove the mass of sulfate and metals entering the system (*Eger and Wagner, 1995*).

### *2.2.2 Reactive barrier technology*

Blowes (*1990*) proposed in situ sulfate reduction to treat water contaminated with mine-related wastes within the saturated zone of tailings or within permeable reaction zones installed into the aquifer down-gradient of tailings impoundments. By treating the water prior to the oxidation of  $\text{Fe}^{2+}$  (Reaction #2), the generation of additional acidity, and accompanying enhanced metal mobility, is prevented. Because contaminated groundwater is treated without pumping, the volume of water that is necessary to treat is smaller. It is also easier to maintain the reduced geochemical conditions necessary for sulfate reduction below the water table within the aquifer. Finally, sulfate reduction is optimized at the near-neutral pH conditions found in many aquifers.

We have attempted to exploit advantages of treatment within the aquifer using

the emerging remediation technology of a permeable reactive barrier. This method consists of installing an appropriate reactive material into the aquifer, so that contaminated water flows through the material. The reactive material induces chemical reactions that remove the contaminants from the water or otherwise cause a change that decreases the toxicity of the contaminated water. Methods have been developed for the treatment of chromate (*Blowes and Ptacek, 1992*), halogenated organic compounds (*Gillham and O'Hannesin, 1992 and 1994*), nitrate, (*Robertson and Cherry, 1995*), phosphate (*Baker, 1993, Ptacek et al., 1994, Baker, 1996*), and water contaminated by mine wastes (*Blowes and Ptacek, 1994, Blowes et al., 1994*). For the treatment of groundwater affected by leachate derived from mine wastes, the porous reactive barrier contains organic carbon to enhance sulfate reduction.

Laboratory and field pilot studies have established the potential utility of this remedial method. Waybrant et al., (1995) and Waybrant (1995) tested a variety of carbon substrates in both batch and column experiments. Batch experiments identified optimal organic carbon substrate materials. Column experiments evaluated the extent and duration of water treatment under dynamic flow conditions. Influent water contained elevated concentrations of  $\text{SO}_4^{2-}$  and dissolved Fe and was similar in composition to aquifer water at the Nickel Rim mine site. The results of these experiments indicate that sulfate reduction and metal sulfide precipitation are the dominant mechanisms responsible for removing  $\text{SO}_4^{2-}$ , Fe and other metals from the water. An ongoing column experiment continued to remove 1000 mg/L sulfate after more than 24 months. Small-scale field test cells were installed at the Nickel Rim site in the fall of 1993 and 1994. These test cells continue to induce sulfate reduction and metals removal within the aquifer 12 and 24 months after installation, indicating that this technology is transferable to a field setting (*Blowes, 1995*).

### 2.2.3 Site description

The physical and chemical hydrogeology of the site has been well characterized. Johnson (1993), Bain et al., (1995) and Bain (1996) describe the physical hydrogeology and aqueous geochemistry of the tailings impoundment and associated groundwater plume. The tailings impoundment is located at the head of a small alluvial-filled valley which drains into Moose Lake, approximately 130 m from the tailings dam (Figures 1 and 2). The tailings are located in a zone of groundwater recharge. Groundwater from the tailings follows two flow paths. Approximately half the water originating from the tailings discharges to the surface at the foot of the dam and then flows towards Moose Lake as surface water. The remaining groundwater flows to Moose Lake within the alluvial aquifer. The water table throughout the alluvial valley is at or very near ground surface. The aquifer is composed of fine-grained, glacio-fluvial quartz-feldspar sand and is 3 to 8 meters thick. Bounded on the sides and at the base by bedrock, the aquifer can be thought of as a long, sediment-filled trough in which groundwater is flowing. Bain et al., (1995) estimated a groundwater velocity in the aquifer of 15 m/a.

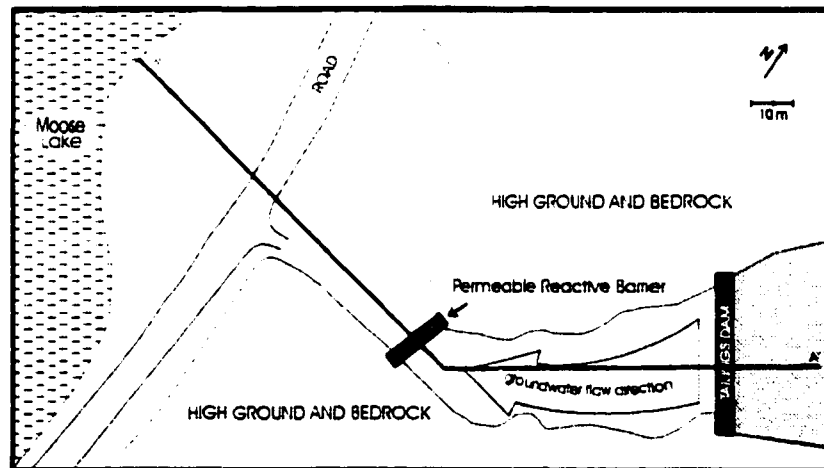


**Figure 2.1** Map view of the Nickel Rim mine site, location of permeable reactive barrier installation, location of cross section A-A'.

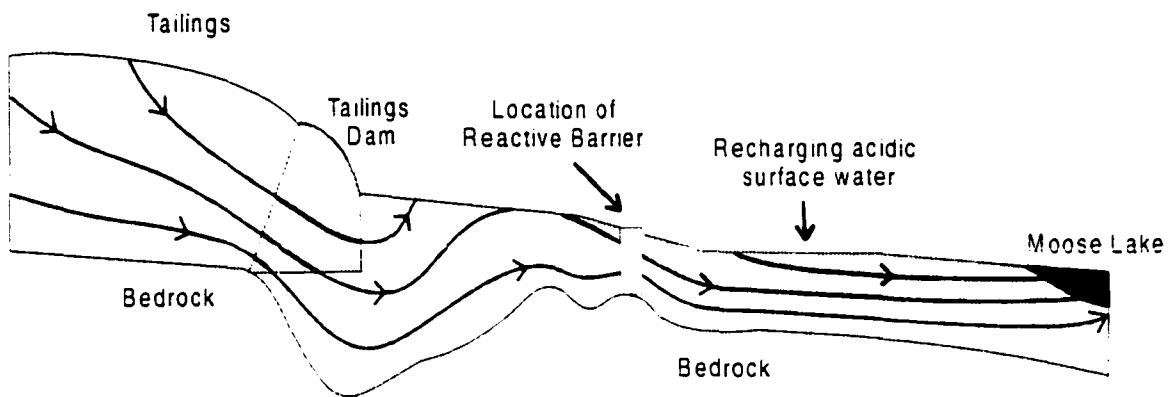


**Figure 2.2** Cross sectional profile along transect A-A' in Figure 2.1 shows groundwater discharging both at the foot of the dam and to Moose Lake.

Residual sulfide minerals contained in the tailings impoundment are being oxidized and water, migrating downward into the underlying aquifer, is acidic and contains high sulfate and metal concentrations. The chemical composition of the contaminated water is evolving as a result of a sequence of acid neutralization reactions as minerals in the tailings and aquifer sediment are gradually depleted. These reactions result in a progressive increase in pH along the groundwater flow path. This increase in pH enhances the attenuation of most metals other than Fe. The resulting plume contains high Fe and sulfate concentrations (500 to 2000 mg/L Fe and 1000 to 7000 mg/L sulfate) and is slightly acidic (pH 4-6) (Bain, 1996). Both Bain (1995) and Johnson (1993) predict that poor quality water will continue to discharge from the tailings for at least 50 years.

## 2.3 METHODS

### 2.3.1 Selection of reactive material

The material for the porous reactive barrier must satisfy five criteria: it must be reactive, permeable, have sufficient longevity, and be readily available and inexpensive.

The material must be sufficiently reactive to reduce sulfate concentrations found in the aquifer at Nickel Rim. The material must be permeable enough to accommodate the groundwater flux rates at the site. The material must sustain its permeability and reactivity over a time period of years. Finally, the material must be readily available and affordable with respect to site conditions.

The selection of organic carbon source material for this study was based on laboratory experiments conducted by Waybrant (1995). The results of these experiments indicate that leaf compost is an effective material for promoting sulfate reduction, and that mixtures containing a variety of different carbon sources are most effective. Fresh organic carbon sources are superior to older sources because they likely contain a higher concentration of short-chain, single-carbon-bond aliphatics, the primary substrate of sulfate reducing bacteria (Brock and Madigan, 1991). In addition to an available carbon source, sulfate reducing bacteria also require nitrogen, phosphate and other trace elements for growth (Brock and Madigan, 1991). Based on these considerations, a substrate composed of 40% municipal compost, 40% leaf compost, and 20% wood chips was selected. Municipal compost was selected because it is readily available, is composed of a variety of materials, is rich in nitrogen and phosphate, as well as other trace nutrients, and can be acquired at a point during the composting sequence when only partial decomposition has occurred. Leaf compost was selected because it is readily available and was shown to be effective in long-term column experiments. Wood chips were selected because they are readily available, are a source of fresh carbon and their larger size may provide additional longevity.

The reactive mixture must maintain a hydraulic conductivity that is sufficient to accommodate the groundwater flow in the aquifer. To increase the hydraulic conductivity of the reactive mixture, pea gravel was mixed with the substrate material. Constant head permeameter tests were conducted to determine an appropriate ratio of pea gravel to organic material. These tests indicate that hydraulic conductivity of the

mixture is very sensitive to the ratio of gravel to substrate (Table I) and that small variations in mixing and packing can have a dramatic impact on hydraulic conductivities. The hydraulic conductivities of all mixture ratios were high enough for use as a reactive barrier material in the Nickel Rim aquifer. It was anticipated that dissolution of organics would result in some mass loss of the organic material fraction. To maintain hydraulic conductivity after installation, a ratio of gravel to organics was selected that would be essentially gravel supported (50% gravel and 50% organic material).

**Table I**

*Hydraulic conductivity of mixtures of gravel and reactive material determined by constant head permeameter.*

Percentage Gravel	Hydraulic Conductivity (cm/sec)
70%	1.0
60%	0.5
55%	0.5
50%	0.4
45%	0.05
40%	0.02
30%	0.0005
Aquifer	0.002

To evaluate the effect of variations in the hydraulic conductivity of the reactive material on the flow regime within the aquifer, groundwater flow modeling using the two dimensional finite element model FLONET was conducted. Aquifer parameters for the Nickel Rim aquifer were taken from Bain (1996). This modeling suggests that if the hydraulic conductivity of the reactive barrier is an order of magnitude greater than the adjacent aquifer, good flow distribution within the barrier is achieved (Figure 2). There is little change in the flow regime with additional increases in barrier hydraulic

conductivity (Figure 2). These results are consistent with the observations of Start and Cherry (1994).

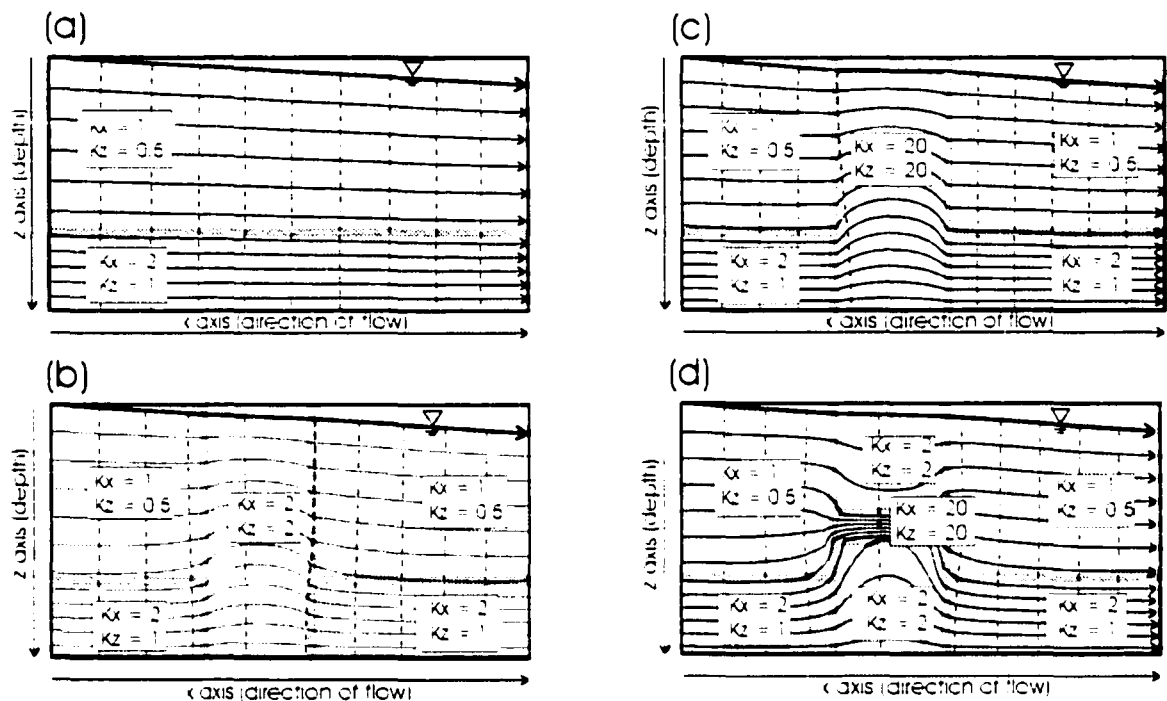


**Figure 2.3** Results of FLONET modeling showing idealized aquifer in cross-section.  $K_x$  and  $K_z$  = hydraulic conductivity in the X and Z directions, respectively. (a) Aquifer with no reactive barrier, lower layer is more permeable than upper layer. (b) Same as (a) but with reactive barrier with permeability equivalent to lower layer of aquifer. (c) Same as (b) but with reactive barrier 10X more permeable than aquifer. (d) Same as (b) but with small layer of higher permeability within reactive barrier.

Channeling of flow decreases the contact time between the dissolved contaminants and the reactive material and decreases the total mass of carbon available, potentially leading to reductions in the effectiveness of the reactive barrier. Simulations suggest that even small layers of higher hydraulic conductivity material within the barrier will result in significant channeling of flow (Figure 2). To avoid preferential flow the mixture must be homogeneous. To achieve a homogeneous mixture, a 130 ft. (40 m)

conveyer was used to mix the organic material and pea gravel. Gravel and compost were loaded onto the conveyor simultaneously, and dumped into a single pile. This process was repeated with the mixed pile until a uniform mixture was obtained.

### **2.3.2 Barrier installation**

The reactive barrier at Nickel Rim was installed where the bedrock valley narrows to minimize the costs in materials and installation while ensuring that all groundwater flowing within the aquifer would pass through the treatment barrier (Figure 1). The reactive barrier was installed by cut and fill excavation: as the aquifer material was removed to bedrock, the hole was back-filled with the organic carbon and gravel mixture. The resulting structure stretches across the alluvial valley and is in direct contact with the bedrock on both sides and at the base. Sand fill was added at the up and down-gradient sides of the barrier to square off the organic mixture with the sloping sides of the trench. These sand zones help to distribute flow evenly through the barrier and facilitate sampling of the inflow and the outflow. A 12 inch (30 cm) clay cap was applied on top the barrier to minimize oxygen diffusion into, and water flow out of, the reactive mixture. The installed reactive mixture is approximately 49 feet (15 m) long, 12 feet (3.6 m) deep and 13 feet (4 m) wide (Figure 3).

### **2.3.3 Installation and sampling of monitoring wells**

Monitoring wells (2" (5 cm) wells and bundle piezometers) were installed in nests along a transect roughly parallel to groundwater flow (Figure 4), establishing monitoring points up and down-gradient of, as well as within, the newly installed porous reactive barrier. These wells were installed using a gasoline powered vibrating hammer (*Blair, 1981; and Dubrovsky, 1986*).

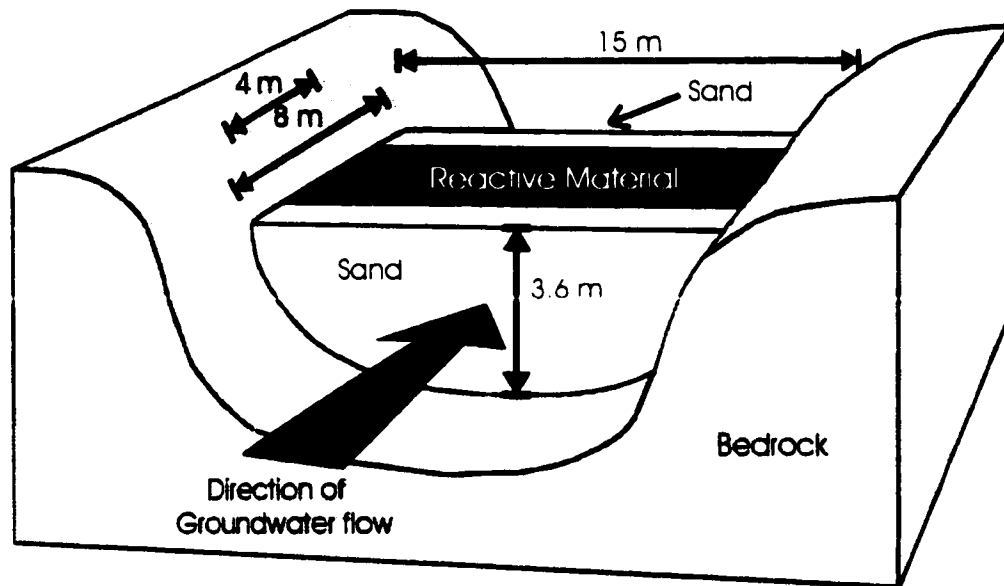


**Figure 2.4** Schematic diagram of permeable reactive barrier installation.

Samples of groundwater were collected approximately one month and nine months after installation. Water samples were collected from installed wells using a peristaltic pump and passed through 0.45  $\mu\text{m}$  filters. Samples for cation analyses were acidified to  $\text{pH} < 1$  using 12 N HCl. All samples were refrigerated at the field site and stored refrigerated until analyzed at the University of Waterloo or Falconbridge Ltd. Analytical Laboratory. Chemical analyses were conducted to determine the concentrations of Al, As, Ca, Cd, Co, Cr, Cu, Fe, K, Mg, Mn, Ni, Pb, S, Sr, Zn, by Inductively Coupled Plasma Emission Spectrometry (ICP) or Atomic Adsorption Spectrometry (AA), and  $\text{SO}_4$ ,  $\text{NO}_3$ , F and Cl, by ion chromatography. All dissolved Fe is assumed to be in the Fe (II) oxidation state. Dissolved organic carbon was analyzed by a Total Organic Carbon method using a platinum catalyst and an infrared detector (*Standard Methods, 1996*). Replicate samples were collected from several locations. Determinations of pH (ORION™ Ross 815600 Combination Electrode or Accumet™ Standard 13-620-108 Gel Filled Combination Electrode) and Eh (ORION™ 9678BN Combination Electrode) were made at each

piezometer using sealed cells maintained at ground-water temperature. The pH electrode was calibrated using pH 4.0 and 7.0 buffer solutions (traceable to NIST). The performance of the Eh electrode was confirmed using prepared Zobell's solution (Zobell, 1946; Nordstrom, 1977) and Light's solution (Light, 1972). Determinations of alkalinity were made in the field by titration with standardized H<sub>2</sub>SO<sub>4</sub> using a digital titrator (Hach Instruments Ltd.).

## **2.4 RESULTS AND DISCUSSION**

### *2.4.1 Surface water recharge*

A cross-sectional view of the flow field at the installation site (Figure 4) provides a physical framework for assessing the impact of the reactive barrier on the aquifer. The organic material used in the reactive barrier contained high Cl<sup>-</sup> concentrations compared with the aquifer. The leaching of Cl<sup>-</sup> from the reactive material resulted in the development of a distinguishable zone of water one month after installation. This zone contained concentrations of dissolved Cl<sup>-</sup> of up to 6000 mg/L, much greater than the background concentration in the aquifer, approximately 7 mg/L. In addition to groundwater flowing through the barrier, untreated surface water recharged the aquifer down-gradient of the reactive barrier (Figure 2). This recharging surface water was acidic, with high concentrations of SO<sub>4</sub><sup>2-</sup> and Fe. Before entering the aquifer, the untreated surface water flowed through a pile of compost material left over from the reactive barrier installation and, therefore, also contained high Cl<sup>-</sup> concentrations. As a result of this recharge, the aquifer down-gradient of the reactive barrier contained two merging plumes of Cl<sup>-</sup>. One plume of treated water flowing from the barrier, occupied the lower portion of the aquifer and a second plume of untreated water, emanating from the Cl<sup>-</sup>-rich surface water recharge, occupied the upper portion of the aquifer (Figure 4). This Cl<sup>-</sup> profile correlates well with the physical flow field profile. It indicates that

treated water flowing from the reactive barrier will occupy only the lower portion of the down-gradient aquifer.

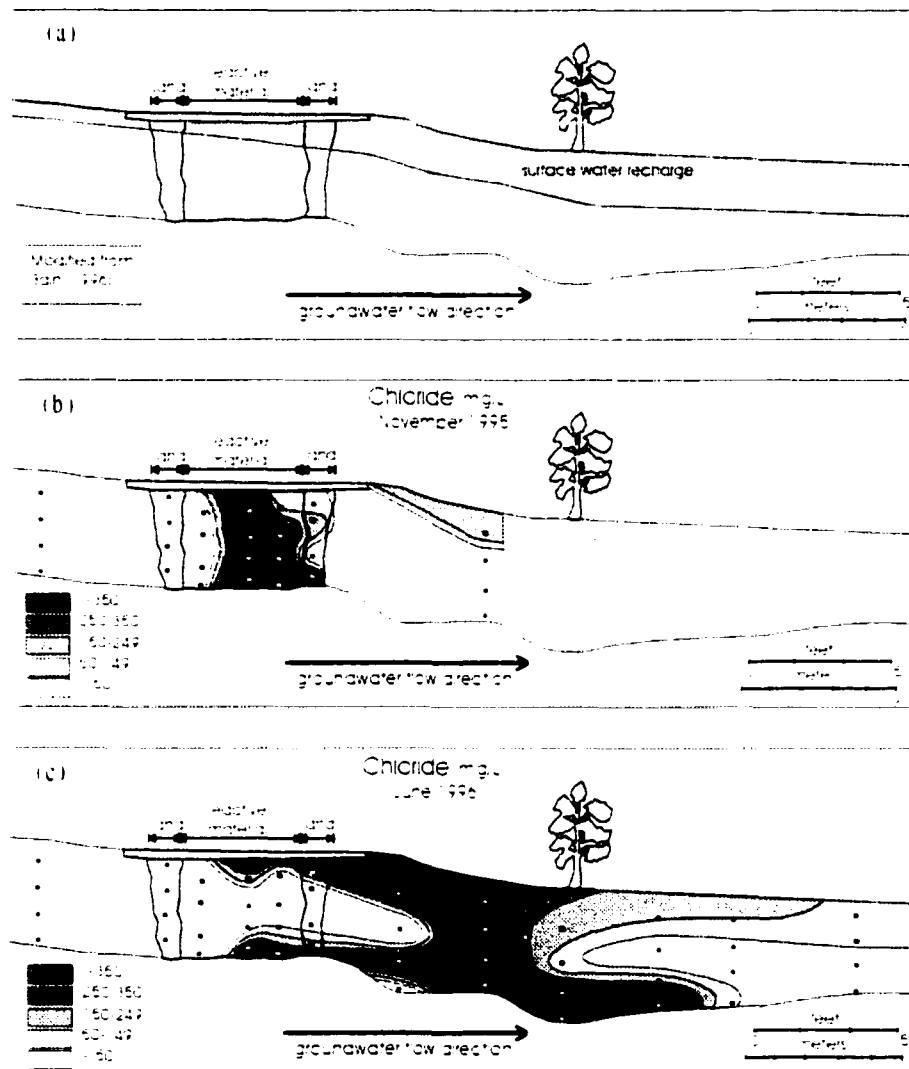


**Figure 2.5** Cross-sectional profiles of reactive barrier and adjoining aquifer. Small squares indicate sample locations. (a) Schematic diagram showing zone of aquifer receiving surface water recharge based on head profiles and water chemistry prior to reactive barrier installation (From Bain, 1996). (b) Profile of chloride concentrations one month after installation. (c) Profile of chloride concentrations nine months after installation.

### 2.4.2 Groundwater velocity

The Cl<sup>-</sup> profile after nine months shows the high-Cl plug was located about 12 meters down-gradient indicating an average groundwater velocity of 16 meters a year. This value is in good agreement with estimates of groundwater velocities in the aquifer prior to installation of the permeable reactive barrier (Bain, 1995). The Cl<sup>-</sup> profile within the barrier shows high concentrations along the top and base, suggesting there is some preferential flow through the center of the barrier.

### 2.4.3 Water chemistry

Comparing water entering the barrier to treated water exiting the barrier along transect A-A' (Figure 1) nine months after installation, sulfate concentrations decrease from 2400-4800 mg/L to 200-3600 mg/L, dissolved Fe concentrations decrease from 250-1300 mg/L to 1.0-40 mg/L, pH increases from 4-6 to 6.6-7.0 and alkalinity (as CaCO<sub>3</sub>) increases from 0-66 mg/L to 690-2300 mg/L (Figure 5). To assess the objective of preventing the mine effluent from generating acidity on discharge, the capacity of the groundwater to generate acidity must be calculated. The acid producing capacity of the water is a function of the concentration of ions that will generate acidity on discharge. In most mine effluents, Fe, which forms sparingly soluble oxyhydroxides (Reaction # 2), is the dominant, acid-generating ion. In addition to acid producing capacity, the ability of the water to buffer acidity, the alkalinity, must be known. The tendency of the water to produce acidic drainage on discharge can be calculated by subtracting the acid buffering capacity (the molar equivalents of dissolved carbonate alkalinity) from the acid producing potential (molar equivalents of acid produced by oxidation of dissolved Fe):

$$\text{Potential Acidity} = 2(\text{moles/L Fe}^{2+}) - \text{moles/L Alkalinity (as CaCO}_3\text{)}.$$

This is called the potential acidity and is a predictive form of mineral acidity as

defined by Snoeyink and Jenkins (1980). A positive value indicates a net acid producing potential and a negative value indicates a net acid consuming potential. The water entering the barrier had net potential acidity of 7.8 to 46 meq/L, while the water exiting the barrier had net potential acidity of -16 to -45 meq/L (Figure 5).

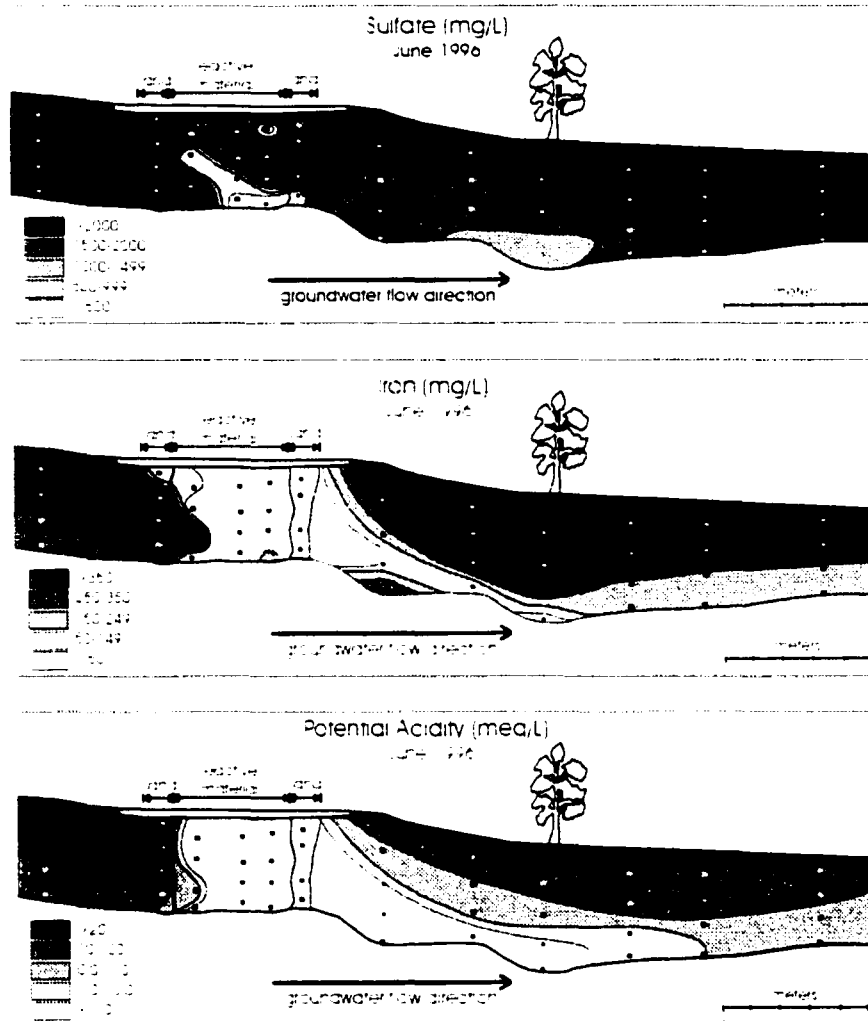


**Figure 2.6** Cross-sectional view of reactive barrier and adjoining aquifer. Small squares indicate sample locations. Concentrations of sulfate and iron in groundwater and calculated "Potential Acidity" nine months after installation are shown.

Iron and  $\text{SO}_4$  removal occurred at a 1:1 molar ratio, consistent with the precipitation of a Fe mono-sulfide ( $\text{FeS}$ ). This stoichiometric constraint on the removal of Fe and  $\text{SO}_4$  by sulfide mineral precipitation appeared to limit the removal of  $\text{SO}_4$ . Once all of the Fe was removed, approximately half of the  $\text{SO}_4$  remained. Because Fe was the primary acid generating constituent in the contaminated groundwater, a removal ratio that results in excess  $\text{SO}_4$  is preferable to a ratio that results in excess Fe.

#### 2.4.4 Estimating reactive barrier longevity

The ultimate success of the porous reactive barrier will be determined by the longevity over which sulfate reduction and metal sulfide precipitation is maintained. The ability of the barrier to transform the groundwater from acid producing to acid consuming is dependent on the removal of Fe. Therefore, change in Fe concentration as water passes through the barrier is a useful measure of the reactive barrier effectiveness. It may be assumed that the limiting factor will be the ability of the organic carbon to induce sulfate reduction. Previous work suggests that not all of the carbon is "available" for sulfate reduction (*Eger and Wagner, 1995*). If the total usable carbon for sulfate reduction is limited, the thickness of the permeable reactive barrier will be proportional to its longevity. In addition, the amount of available organic carbon may also be a function of the amount of time that the sulfate and organic carbon are in contact. Longer residence times may overcome potential kinetic limitations on organic carbon reactivity and may increase the fraction of reactive carbon.

Reactive barrier longevity can be estimated by comparison with results of laboratory column experiments conducted by Waybrant et al (*1995*). In the laboratory 300-1000 mg/L Fe was removed in a column with a residence time of 15 days and a travel path length of 0.3 m. Assuming a groundwater velocity in the Nickel Rim aquifer of 16 meters/year and a barrier thickness of 4 meters, the residence time is 90 days.

Therefore the barrier residence times are six times longer, and path length is 12 times longer than the laboratory columns. Concentrations of Fe entering the reactive barrier are 200-1000 mg/L, which is similar to concentrations used in the laboratory columns. Comparison of Fe concentration, path length, and residence time suggests that an estimate of reactive barrier longevity based on laboratory column longevity is appropriate.

In the laboratory column (Waybrant *et al.*, 1995), a minimum of 10% of the carbon has been consumed by sulfate reduction and metal sulfide precipitation. Assuming that 10% of the carbon in the reactive barrier at Nickel Rim is available, an estimate of longevity can be made. The barrier contains approximately 1,500,000 moles of carbon. Assuming that a minimum of 10% of that carbon (~150,000 moles) is available, the minimum amount of Fe that can be precipitated as sulfides by that carbon is 75,000 moles (based on stoichiometry of Reactions #3 and #4). Given a porosity of 0.4, groundwater velocity of 16 m/a, and a cross-sectional area of 45 m<sup>2</sup>, the flux of water through the barrier is 288 m<sup>3</sup>/a. With an Fe concentration of 1000 mg/L, the annual flux will be about 5,100 moles/yr. This suggests that the reactive barrier will be effective for a minimum of 15 years. This estimate neglects potential losses in efficiency due to preferential flow within the barrier, variations in the reactive mixtures used or other differences due to scaling-up from bench-scale column experiments to field application. It is likely that there will be some preferential flow within the barrier, this will result in decreased efficiency and a shorter operating lifetime. Plugging of the barrier by accumulation of sulfide precipitates is not anticipated. With the reduction of sulfate and precipitation of a sulfide mineral phase, there is a corresponding conversion of organic material to HCO<sub>3</sub><sup>-</sup> (Reactions #3 and #4). Therefore, the process results in the exchange of organic material, with a specific gravity of 1 to 2, for solid phase sulfides which have a specific gravity of 3 to 5. Laboratory column studies indicate no change in hydraulic conductivity after more than 30 pore volumes (Waybrant, 1996).

The accumulation of sulfides within the saturated reactive barrier provides long term mineral stability. The re-oxidation of the sulfides will be limited by the availability of an electron donor to oxidize the sulfide. Possible oxidizers include  $O_2$ ,  $NO_3^-$ , and  $Fe^{3+}$ . Assuming that the hydraulic regime does not undergo significant change and the reactive barrier remains below the water table, oxygen concentrations are limited to aqueous solubility. Even at saturation, the product of sulfide oxidation by oxygen would be on the order of tens of milligrams per liter. Nitrate is also rarely found in groundwater at concentrations greater than 10 mg/L. Ferric iron concentrations are limited by the low solubility of iron oxyhydroxides. Significant concentrations of ferric iron occur at pH of less than 3, pH values less than 3 in groundwater are rare, even in mine drainage settings (*Blowes and Ptacek, 1994*). In addition, all other readily oxidizable material (e.g. sulfides and organic matter) along the flow path within the tailings material and aquifer must be oxidized before an electron acceptor would become available to oxidize sulfides within the reactive barrier.

#### *2.4.5 Cost of installation*

Materials and installation costs for the permeable reactive barrier were approximately \$30,000.00 (U.S. funds). Approximately half of that cost was materials and half was installation. This value does not include costs of monitoring and assessment. Costs will vary from site to site depending on the physical and chemical characteristics of the contaminated groundwater plume.

## **2.5 CONCLUSIONS**

Installation of a permeable reactive barrier for prevention of acid mine drainage has resulted in dramatic improvement in down-gradient groundwater quality. Removal of >90% of soluble Fe and a greater than ten-fold increase in alkalinity has converted the groundwater system from acid producing to acid consuming. Calculations based on

comparison with previous column studies suggest an operational life time of >15 years. These results indicate that *in situ* sulfate reduction is a potentially effective treatment strategy for remediation of groundwater plumes impacted by drainage from mining activities. Monitoring of the water quality exiting the barrier will continue for a minimum of three years. Studies of the biogeochemical transformations within the barrier and the aquifer are underway.

## 2.6 REFERENCES

- Bain, J.G. 1995. *The Physical and Chemical Hydrogeology of Sand Aquifer Affected By Drainage From the Nickel Rim Tailings Impoundment*. M.Sc.Thesis, University of Waterloo, Waterloo, Ontario.
- Bain, J.G., Blowes, D.W., and Robertson, W.D. 1995. The hydrogeochemistry of a sand aquifer affected by discharge from the Nickel Rim tailings, Sudbury, Ontario. *Proceedings of Sudbury '95 - Mining and the Environment, May 28- June 1, 1995, Sudbury, Ontario, Canada*, Sudbury, Ontario, May 28 - June 1, 1995. Hynes, T.P. and Blanchette, M.C. Eds. Vol. 2., pp. 715-723.
- Baker, M.J. 1993. *Laboratory investigations into the potential for solid mixtures containing industrial products to remove phosphate from solution*. M. Sc.Thesis, University of Waterloo, Waterloo, Ontario.
- Baker, M.J., Blowes, D.W., and Ptacek, C.J. 1996. Development of a reactive mixture to remove phosphorous from on-site wastewater disposal systems. *Waterloo Centre for Groundwater Research Conference Proceedings for Disposal Trenches, Pre-Treatment, and Re-Use of Wastewater*, University of Waterloo, Waterloo, Ontario, May 13, 1996. pp. 51-56.
- Bechard, G., McCready, R.G.L., Koren, D.W., and Rajan, S. 1995. Microbial treatment of acid mine drainage at Halifax International Airport. *Proceedings of Sudbury '95- Mining and the Environment*, Sudbury, Ontario, May 28 - June 1, 1995. Hynes, T.P. and Blanchette, M.C. Eds. Vol. 2., pp. 545-554.
- Bechard, G., Rajan, S., and Gould, W.D. Torma, A.E., Apel, M.L., and Brierley, C.L. editors. Characterization of microbiological processes for the treatment of acidic mine drainage. Warrendale, PA: TMS. 1993. 2. p.277
- Blair, R.D. 1981. *Hydrogeochemistry of an Inactive Pyritic, Uranium Tailings Basin, Nordic Mine, Elliot Lake, Ontario*. M. Sc.Thesis, University of Waterloo, Waterloo, Ontario, Canada.

- Blowes, D.W. 1990. *The geochemistry, hydrogeology and mineralogy of decommissioned sulphide tailings: A comparison study*. Ph.D.Thesis. University of Waterloo. Waterloo, Ontario.
- Blowes, D.W. and Jambor, J.L. 1990. The pore-water geochemistry and the mineralogy of the vadose zone of sulfide tailings. Waite Amulet, Quebec, Canada. *Appl. Geochem.* 5, 327-346.
- Blowes, D.W. and Ptacek, C.J. 1992. Geochemical remediation of groundwater by permeable reactive walls. Removal of chromate by reduction with iron bearing solids. *Proceedings of the Subsurface Restoration Conference, Third International Conference on Groundwater Quality Research.*, Dallas, Texas. June 21-24, 1992. pp. 214-216.
- Blowes, D.W. and Ptacek, C.J. 1994. System for Treating Contaminated Groundwater. U.S. 5514279.
- Blowes, D.W. and Ptacek, C.J. 1994. Acid neutralization mechanisms in inactive tailings impoundments. *Short Course Handbook on Environmental Geochemistry of Sulfide Mine-Wastes, Mineralogical Association of Canada, May, 1994 Waterloo, Ontario, Canada*. Jambor, J.L., Blowes, D.W., Eds. p. 271-292.
- Blowes, D.W., Ptacek, C.J., Bain, J.G., Waybrant, K.R., and Robertson, W.D. 1995. Treatment of mine drainage water using in situ permeable reactive walls. *Proceedings of Sudbury '95 - Mining and the Environment*, Sudbury, Ontario. May 28-June 1, 1995. Hynes, T.P. and Blanchette, M.C. Eds. Vol. 3., pp. 979-987.
- Blowes, D.W., Ptacek, C.J., and Jambor, J.L. 1994. Remediation and prevention of low-quality drainage from tailings impoundments. Blowes, D.W., Jambor, J.L. Eds. 22th ed. Nepean, ON: Mineralogical Association of Canada. p. 365-379.
- Brock, T.D. and Madigan, M.T. 1995. *Biology of Microorganisms*. 6th ed. Englewood Cliffs, New Jersey: Prentice Hall.

- Christensen, T.H. et al., 1994. Attenuation of landfill leachate pollutants in aquifers. *Crit. Rev. Environ. Sci. Tech.*, 24, 119-202.
- Dubrovsky, N.M. 1986. *Geochemical Evolution of Inactive Pyritic Tailings in the Elliot Lake Uranium District*. Ph.D.Thesis, University of Waterloo, Waterloo, Ontario.
- Dubrovsky, N.M., Morin, K.A., Cherry, J.A., and Smyth, D.J.A. 1984. Uranium tailings acidification and subsurface contaminant migration in a sand aquifer. *Water Poll. Res. J. Canada*, 19, 55-89.
- Dvorak, D.H., Hedin, R.S., Edenborn, H.M., and McIntire, P.E. 1992. Treatment of metal-contaminated water using bacterial sulphate reduction: Results from pilot-scale reactors. *Biotech. Bioeng.* 40, 609-616.
- Eger, P. and Wagner, J. 1995. Sulfate reduction for the treatment of acid mine drainage: Long term solution or short term fix? *Proceedings of Sudbury '95- Mining and the Environment.*, Sudbury, Ontario, May 28-June 1, 1995. Hynes, T.P. and Blanchette, M.C. Eds. Vol. 2., pp. 515-524.
- Feasby, D.G., Blanchette, M., and Tremblay, G. 1991. The mine environment neutral program. *Second International Conference on the Abatement of Acidic Drainage.*, Montreal, Quebec, Sept. 16-18, 1991. Vol. 1., pp. 1-26.
- Gillham, R.W. and O'Hannesin, S.F. 1992. Metal-catalysed abiotic degradation of halogenated organic compounds. *IAH Conference "Modern Trends in Hydrogeology"*, Hamilton, Ontario, May 10-13, 1992. pp. 94-103.
- Gillham, R.W. and O'Hannesin, S.F. 1994. Enhanced degradation of halogenated aliphatics by zero-valent iron. *Ground Water*, 32, 958-967.
- Hammack, R.W. and Edenborn, H.M. 1992. The removal of nickel from mine waters using bacterial sulphate reduction. *Appl. Microbiol. Biotechnol.* 37, 674-678.
- Hedin, R.S. 1989. Treatment of coal mine drainage with constructed wetlands. *Wetlands Ecology and Conservation: Emphasis in Pennsylvania*. Majumdar, S.K., Brooks,

- R.P., Brenner, F.J., Tiner, R.W. Eds. The Pennsylvania Academy of Science, p. 349-362.
- Johnson, R.H. 1993. *The Physical and Chemical Hydrogeology of the Nickel Rim Mine Tailings, Sudbury, Ontario*. M.Sc.Thesis. University of Waterloo, Waterloo, Ontario.
- Kleinmann, R.L.P. 1991. Acid Mine Drainage: An Overview. *Proceedings of Conference Energy in the 90's*, Pittsburgh, Pennsylvania, March 10-13, 1991. Hobbs, B.F. Eds. pp. 281-282.
- Light, T.S. 1972. Standard solution for redox measurements. *Anal. Chem.* 44, 1038-1039.
- Machemer, S.D. and Wildeman, T.R. 1992. Adsorption compared with sulphide precipitation as metal removal processes from acid mine drainage in a constructed wetland. *J. Contam. Hydro.* 9, 115-131.
- McIntire, P.E., Edenborn, H.M., and Hammack, R.W. 1990. Incorporation of bacterial sulphate reduction into constructed wetlands for the treatment of acid and metal mine drainage. *National Symposium on Mining*, University of Kentucky, Lexington, Kentucky, May 14-18, 1990. pp. 207-213.
- Morin, K.A., Cherry, J.A., Dave, N.K., Lim, T.P., and Vivyurka, A.J. 1988. Migration of acidic groundwater seepage from uranium-tailings impoundments. 1. Field study and conceptual hydrogeochemical model. *J. Contam. Hydro.* 2, 271-303.
- Nordstrom, D.K., Jenne, E.A., and Ball, J.W. 1977. Thermochemical redox equilibria of Zobell's solution. *Chemical Modeling of Natural Systems*. Everett, A.J., Ball, J.W. Eds. p. 51-79.
- Nordstrom, D.K., Jenne, E.A., and Ball, J.W. 1979. Redox equilibria of iron in acid mine waters. *Chemical modeling of natural systems*. Everett, A.J., Ball, J.W. Eds.
- Ptacek, C.J., Blowes, D.W., Robertson, W.D., and Baker, M.J. 1994. Adsorption and mineralization of phosphate from septic system effluent on aquifer materials.

*Proceedings of the Waterloo Centre for Groundwater Research Annual Septic System Conference: Wastewater Nutrient Removal Technologies and Onsite Management Districts*, Waterloo, Ontario, June 6. pp. 26-44.

Robertson, W.D. and Cherry, J.A. 1995. In situ denitrification of septic system nitrate using reactive porous media barriers: Field trials. *Ground Water*, Vol. 33 (1) p 99-111.

Snoeyink, V.L. and Jenkins, D. 1980. *Water Chemistry*. New York: John Wiley and Sons 183p.

Standard Methods, 1996. Eaton AD, Clesceri LS, and Greenberg AE, editors. *Standard Methods for the Examination of Water and Wastewater*. 19th ed. Washington DC: APHA. 5-16p.

Starr, R.C. and Cherry, J.A. 1994. In situ remediation of contaminated groundwater: The funnel-and-gate system. *Ground Water*, 97, 465-476.

Tuttle, J.H., Randles, C.I., and Dugan, P.R. 1968. Activity of microorganisms in acid mine water. I. Influence of acid water on aerobic heterotrophs of a normal stream. *J. Bacteriol.* 95, 1495-1503.

USDA 1993. Acid drainage from mines on the National Forest: A management challenge. *U. S. Forest Service Publication*, 1505, 1-12.

Wakao, N., Takahashi, T., Sakurai, Y., and Shita, H. 1979. The treatment of acid mine water using sulphate-reducing bacteria. *J. Ferment. Technol.* 57, 445-452.

Waybrant, K.R. 1995. *The Prevention of Acid Mine Drainage Using In Situ Porous Reactive walls: A Laboratory Study*. M. Sc. Thesis, University of Waterloo, Waterloo, Ontario, Canada.

Waybrant, K.R., Blowes, D.W., and Ptacek, C.J. 1995. Selection of reactive mixtures for the prevention of acid mine drainage using porous reactive walls. *Proceedings of Sudbury '95 - Mining and the Environment*, Sudbury, Ontario, May 28 - June 1, 1995. Hynes, T.P. and Blanchette, M.C. Eds. Vol. 3., pp. 945-953.

Zobell, C.E. 1946. Studies of redox potential of marine sediments. *Bul. Amer. Ass. Petrol. Geol.* 30. 477-513.

## Chapter 3

### *Barrier Geochemistry and Microbiology*

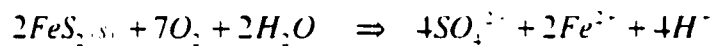
#### 3.1 CHAPTER SUMMARY

A permeable reactive barrier, designed to remove metals and generate alkalinity by promoting sulfate reduction and metal sulfide precipitation, was installed in August 1995 into an aquifer containing effluent from mine tailings. Passage of groundwater through the barrier results in striking improvement in water quality. Dramatic changes in concentrations of  $\text{SO}_4$  (decrease of 2000-3000 mg/L), Fe (decrease of 270-1300 mg/L), trace metals (e.g., Ni decreases 30 mg/L) and alkalinity (increase of 800-2700 mg/L) are observed. Populations of sulfate reducing bacteria are 10,000 times greater and bacterial activity, as measured by dehydrogenase activity, is 10 times higher within the barrier compared to the up-gradient aquifer. Dissolved sulfide concentrations increase by 0.2-120 mg/L and the isotope  $^{34}\text{S}$  is enriched relative to  $^{32}\text{S}$  in the dissolved phase  $\text{SO}_4^{2-}$  within the barrier. Water chemistry, coupled with geochemical speciation modeling, indicates the pore water in the barrier becomes supersaturated with respect to amorphous Fe sulfide. Solid phase analysis of the reactive mixture indicates the accumulation of Fe mono-sulfide precipitates. Shifts in the saturation states of carbonate, sulfate, and sulfide minerals and most of the observed changes in water chemistry in the barrier and down-gradient aquifer can be attributed, either directly or indirectly, to bacterially-mediated sulfate reduction.

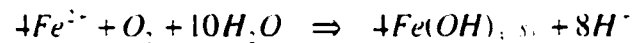
## 3.2 INTRODUCTION

### 3.2.1 Acid mine drainage

Discharge of acidic effluent, often containing high concentrations of toxic trace metals, from mines and mine waste is an intractable, worldwide environmental problem with estimated costs of treatment in the 10's of billions of dollars. The oxidation of residual sulfide minerals in mines and mine waste can produce acidic waters containing high concentrations of sulfate, Fe(II) and trace metals. The oxidation of iron sulfide can be expressed as:



This effluent often enters underlying and adjacent aquifers where buffering by mineral dissolution raises the pH to 4-7 (*Morin and Cherry, 1988*). However, on discharge to the surface, the oxidation of Fe(II) to Fe(III) and the precipitation of ferric oxyhydroxides can re-generate acidic conditions (pH < 3):

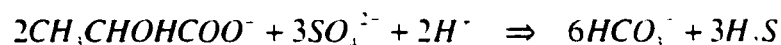


This generated acidity can mobilize toxic trace metals and adversely impact surface water ecosystems. Discharge from mines and mine waste can continue for decades, even centuries (*Dubrovsky et al., 1985*). Conventional treatment by lime neutralization produces large volumes of metal-rich sludge and often involves long-term operating costs.

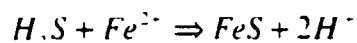
### 3.2.2 Sulfate reduction

Sulfate reduction and metal sulfide precipitation have the potential to remediate acid mine drainage (*Wakeo et al., 1979*). In natural settings, sulfate reduction is mediated by sulfate reducing bacteria (SRB). Sulfate reducing bacteria are phylogenetically diverse and utilize a variety of biochemical pathways to reduce sulfate by oxidation of organic carbon. Sulfate reducing bacteria utilize short chain organic

carbon compounds or  $H_2$  to reduce  $SO_4$  and are often dependent on a consortium of microorganisms to provide these substrates (Chapelle, 1993). A simplified expression of the reduction of sulfate by lactate can be expressed as:



The reduction of  $SO_4$  and the production of dissolved sulfide species in the presence of dissolved metals can result in precipitation of metal sulfide mineral phases:



Other potential contaminants, including As, Cd, Cu, Fe, Ni, Pb, and Zn, can also react with sulfide to form sparingly-soluble sulfide minerals. However, acidic waters can consume generated alkalinity and limit the ability of sulfate reducing bacteria to promote this reaction sequence (Hao *et al.*, 1996). This limitation has hampered attempts to utilize sulfate reduction to treat acidic surface water associated with mine drainage (Machemer and Wildeman, 1992; Dvorak *et al.*, 1992; Bechard *et al.*, 1995). We have overcome this obstacle by promoting sulfate reduction within the aquifer, prior to increased acidification of the effluent upon discharge to the surface. Treatment within the aquifer is accomplished using a passive *in situ* permeable reactive barrier composed of organic material (Blowes and Ptacek, 1994). The organic carbon promotes sulfate reduction and metal sulfide precipitation as the contaminated groundwater flows through the structure.

### 3.2.3 Nickel Rim Reactive Barrier

The reactive barrier, containing a mixture of municipal compost (20 vol. %), leaf mulch (20%), wood chips (9%), gravel (50%), and limestone (1%), was keyed to underlying bedrock at the base and outcropping bedrock at the sides. The installed barrier extends 20 m across the aquifer, is 3.5 m deep and the barrier is 4 m thick in the direction of flow. Zones of sand, approximately 1 m thick, were also installed at the up and down-gradient sides of the organic carbon mixture. These sand zones square off the

barrier with the sloping sides of the trench, help to redistribute flow, and facilitate uniform sampling. A protective clay cap (30 cm) was placed over the barrier to minimize oxygen diffusion and flow of infiltrating water into the barrier. The barrier installation is described in detail in Benner et al. (1997). This barrier is the first full-scale reactive barrier in the world designed to treat metals and acid mine drainage using reductive processes. The installation provides a unique opportunity to evaluate, under controlled conditions, changes in groundwater geochemistry. Though the barrier is an engineered system, geochemical changes closely match processes associated with sulfate reduction in natural settings such as sediments and aquifers. This paper describes geochemical, microbiological and mineralogical processes occurring within the permeable reactive barrier and adjoining aquifer.

#### 3.2.4 Nickel Rim Aquifer

A groundwater plume, containing high concentrations of  $\text{SO}_4$  (1000-5000 mg/L), Fe (200-2000 mg/L), and a pH of 4 to 6, flows from the inactive Nickel Rim tailings impoundment into an adjoining alluvial aquifer (Bain et al., 2000; Johnson et al., 1999). At the site of the installation, acidic surface water is recharging the aquifer. Figure 1(a) shows the flow field for the Nickel Rim aquifer prior to the reactive barrier installation (Benner et al., 1997; Bain et al., 2000). The aquifer receives water that has entered the aquifer through the tailings impoundment as well as acidic water infiltrating directly from the surface above the aquifer. This flow regime results in water entering the barrier from two distinct sources. The protective clay cap prevents infiltration directly into the barrier, but acidic surface water continues to enter the aquifer on both the up-gradient and down-gradient sides. Treated water exiting the down-gradient side of the barrier occupies only the lower half of the aquifer whereas the upper half of the aquifer contains acidic water which has not undergone treatment. Groundwater velocity is approximately 15 m/a (Benner et al., 1997).

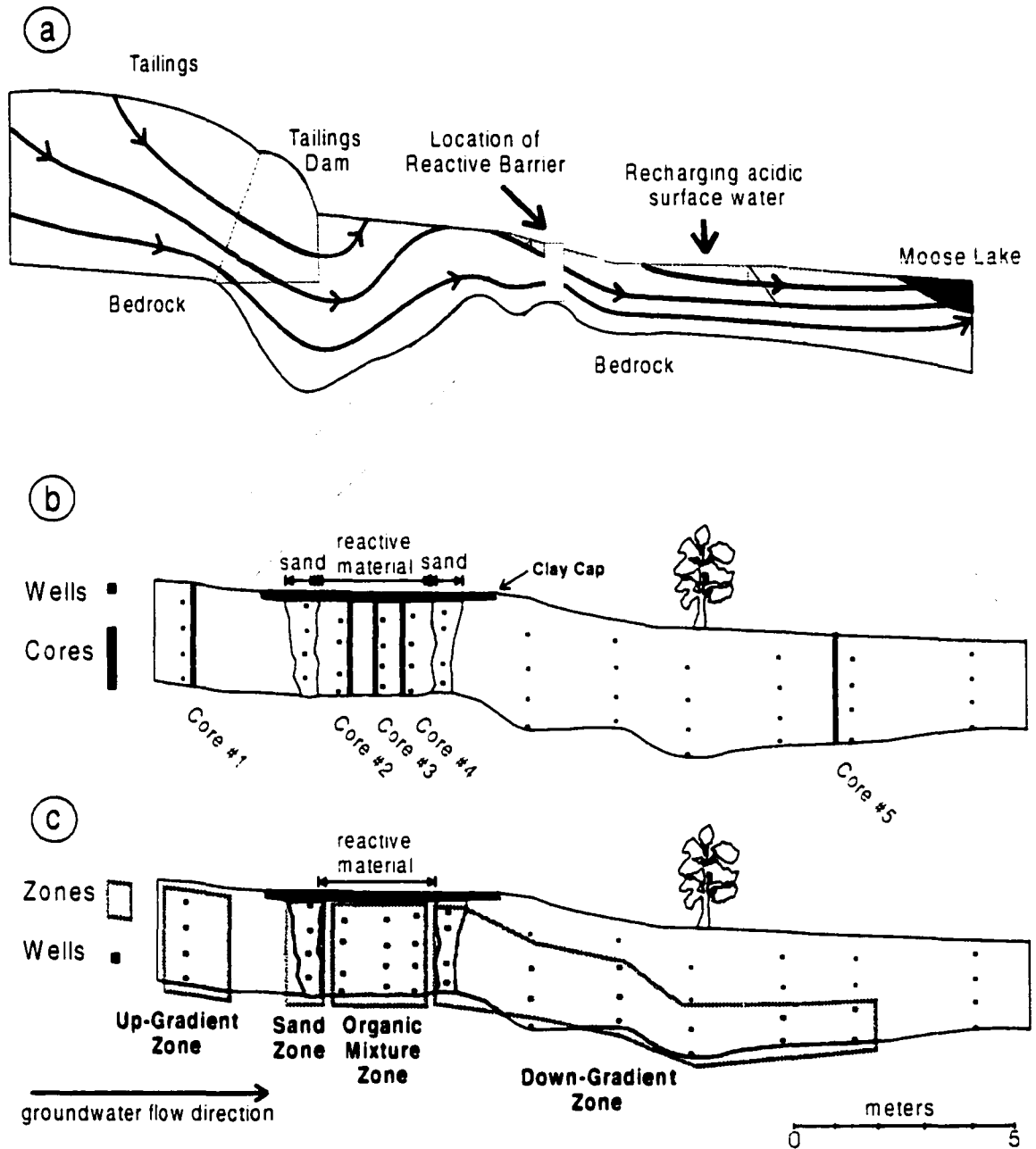


**Figure 3.1** Cross-sectional profiles of aquifer and reactive barrier: (a) shows flow lines for the Nickel Rim aquifer prior to the installation of the reactive barrier determined by field-collected data and flow modeling from Bain (2000). (b) sample well and core locations in aquifer and reactive barrier. (c) location of geochemically distinct zones along groundwater flow path.

## METHODS

### 3.2.5 Water Sampling and Analysis

Monitoring wells were installed in nests along a transect roughly parallel to groundwater flow (Figure 1). Samples of groundwater were collected in September 1995, June and September 1996, and July 1997 (1, 9, 12, and 22 months after installation). A detailed description of well installation, water sampling and field and laboratory analysis can be found in Benner et al. (1997). Additional analyses include dissolved organic carbon by combustion and infrared detection (*Standard Methods, 1996*), total dissolved sulfide by methylene blue method (*Standard Methods, 1996*) and sulfur isotope determination by thermal decomposition of barium sulfate and analysis on a mass spectrometer (*Yanagisawa and Sakai, 1983*).

### 3.2.6 Solid Phase Methods

Samples were collected using a 5 cm diameter driven coring device. Cores were collected in September 1996 for solid phase and mineralogical analysis and in September 1997 for bacterial analysis (Figure 1b). Cores, collected in aluminum casing, were sealed with plastic caps and refrigerated until analyzed.

The sulfate reducing bacteria were grown in a modified Postgate medium C in 20 mL serum bottles (*Postgate, 1984*). The medium had the following composition in g/L:  $\text{KH}_2\text{PO}_4$ , 0.5;  $\text{NH}_4\text{Cl}$ , 1.0;  $\text{Na}_2\text{SO}_4$ , 4.5;  $\text{CaCl}_2 \cdot 2\text{H}_2\text{O}$ , 0.04;  $\text{MgSO}_4 \cdot 7\text{H}_2\text{O}$ , 0.06; Na lactate (60%), 2.92; Na acetate, 1.28; yeast extract, 1.0;  $\text{FeSO}_4 \cdot 7\text{H}_2\text{O}$ , 0.004; Na citrate  $\cdot 2\text{H}_2\text{O}$ , 0.3; resazurin, 0.005 (pH adjusted to 7.5 using NaOH). Serum bottles containing medium were autoclaved and 1 g sediment was added to each of five replicates. Inoculated samples were sequentially diluted and incubated in an anaerobic glove box for 30 days. Positive growth of SRB was indicated by precipitation of Fe-sulfides. Values are reported as Most Probable Number (MPN) determinations (*Alexander and Black, 1965*). Triphenyl tetrazolium chloride is a substrate for a number

of non-specific dehydrogenases present in microflora and can be generally correlated with respiratory activity and used as an index of microbial activity (Ladd, 1978). To determine dehydrogenase activity (DH), five grams of sediment was buffered with  $\text{CaCO}_3$  (to a pH >6) and 1.75 mL of 0.5% 2,3,5-Triphenyl tetrazolium chloride and distilled water were added. The samples were incubated for 24 hours and extracted sequentially with two 10 mL aliquots of methanol and filtered through Whatman #42 paper. The aliquots were combined in a volumetric flask and made up to 50 mL with methanol. Optical density of the extract was measured at 485  $\mu\text{m}$ . The enzyme activity assay was performed in triplicate and averaged.

Accumulations of mono-sulfides (operationally defined as acid volatile sulfides, AVS) and the AVS fraction plus disulfides and elemental sulfur (total reduced inorganic sulfur, TRS) were determined from core location #2 (Figure 1) within the organic mixture. The AVS and TRS extraction methods are described in detail in Herbert et al. (Herbert et al., 1998), and involve the reaction of samples with cold 6M HCl and hot chromous chloride solutions (Canfield et al., 1986), respectively. Following reaction the evolved  $\text{H}_2\text{S}$  is trapped in a zinc acetate solution as ZnS and determined by idiometric titration. A field emission scanning electron microscope employing energy-dispersive X-ray analysis was used to obtain high-magnification images and elemental compositions of black accumulations on a sampling tube from within the permeable reactive barrier.

### 3.2.7 Geochemical Modeling

The geochemical speciation/mass transfer computer code MINTQA2 (Allison et al., 1990), adjusted to be consistent with the WATEQ4F database (Ball and Nordstrom, 1991), was used to aid in the interpretation of aqueous geochemical data. Input parameters were Al, Ca, Cl, Fe, K, Mg, Mn, Na, Ni, Si,  $\text{SO}_4$ , Zn, alkalinity and pH. For water collected outside the reactive barrier installation, Eh was input from field platinum electrode measurements. The calculated saturation state for sulfide mineral phases was

based on measured concentrations of dissolved sulfide. Most points outside the barrier were below level of detection. For these samples the level of detection (0.005 mg/L) was used.

### 3.3 RESULTS AND DISCUSSION

A striking improvement in water quality is observed after groundwater enters the reactive barrier. Concentrations of almost all measured dissolved species change (e.g. alkalinity increases 800-2700 mg/L,  $\text{SO}_4$  decreases 2000-3000 mg/L, Fe decreases 270-1300 mg/L, Ni decreases 30 mg/L; Figures 2.3). These changes indicate that significant geochemical transformations are occurring within the barrier.

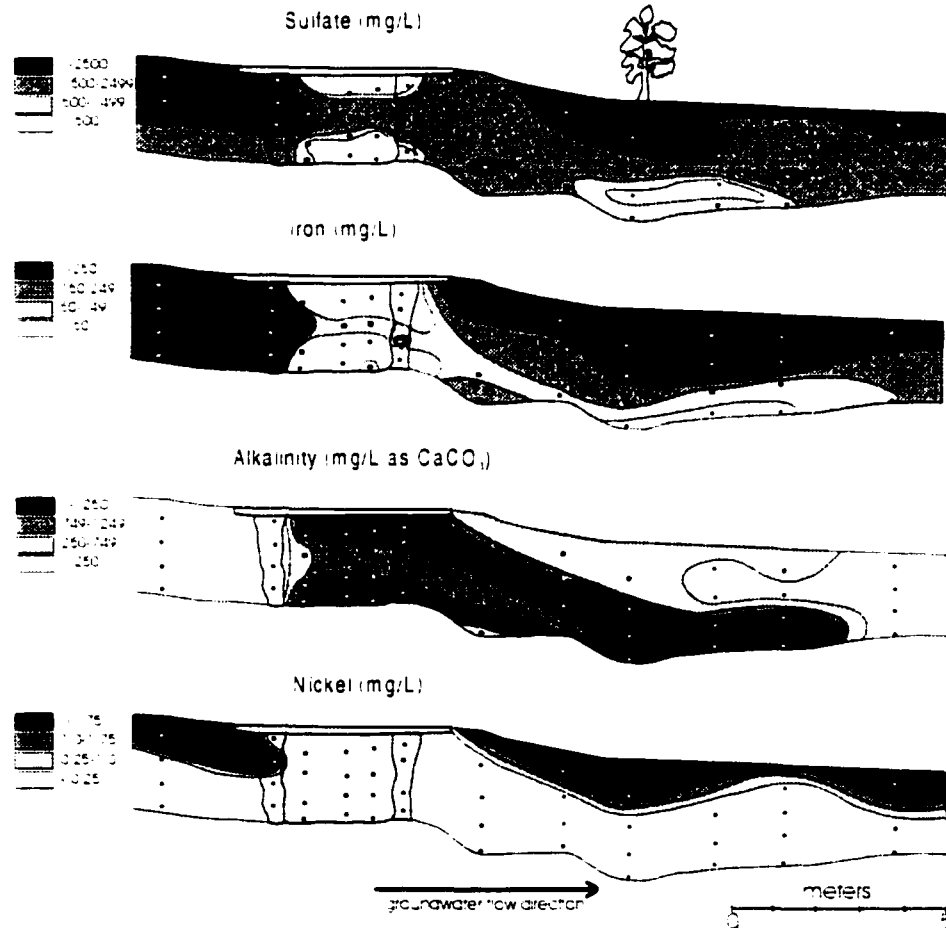


**Figure 3.2** Cross-sectional profiles of dissolved constituents for September 1996:  $\text{SO}_4$ , Fe, alkalinity (as  $\text{CaCO}_3$ ), and Ni.

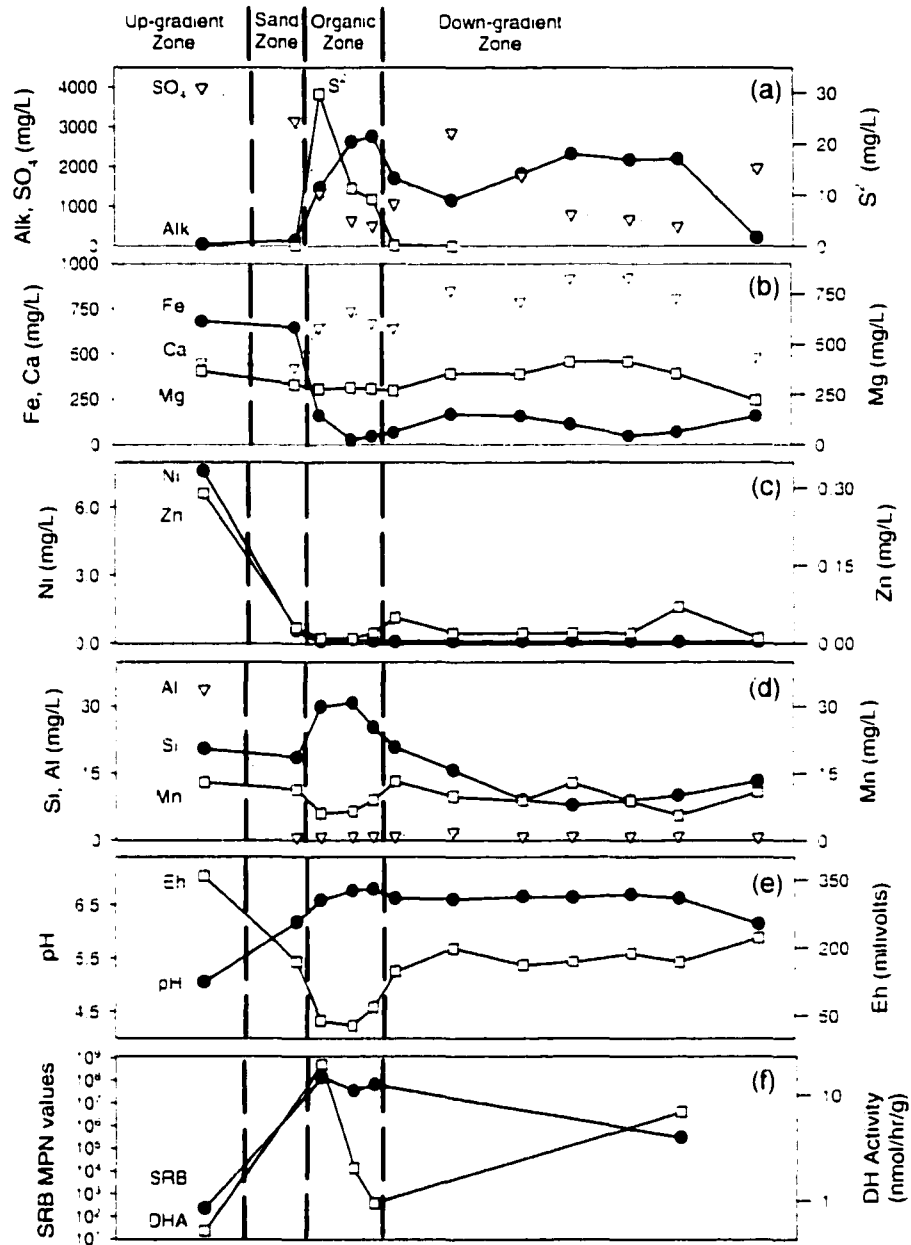


**Figure 3.3** Vertically averaged constituent concentrations for each well nest. (a)  $SO_4$ , alkalinity (as  $CaCO_3$ ), and  $S^{2-}$  (b) Fe, Ca, and Mg (c) Ni and Zn (d) Si, Al, and Mn (e) pH and Eh and (f) vertically averaged most probable numbers (MPN) for sulfate reducing bacteria (SRB), and Dehydrogenase enzyme activity (DH).

### *3.3.1 Four Distinct Zones*

For the purpose of evaluating geochemical, mineralogical and microbiological changes attributed to the barrier, the aquifer can be viewed as being comprised of four zones. (Figure 1c). The up-gradient aquifer (Up-gradient Zone) contains mine-waste effluent water. This water first passes through the up-gradient sand fill (Sand Zone) and then the organic carbon mixture (Organic Mixture Zone). Treated water flows into the lower portion of the down-gradient aquifer (Down-Gradient Zone). Water chemistry analyses obtained during September 1996 from each vertical well nest along the flow path were averaged (Figure 3). Although these zones are chemically distinct, there is some variability from well point to well point within each zone (Figure 2).

### *3.3.2 Up-Gradient Zone*

Bain et al. (2000) described the aquifer geochemistry prior to the reactive barrier installation. Geochemical analysis and modeling in this study are consistent with those results. The groundwater in the Up-Gradient Zone is characterized by high concentrations of  $\text{SO}_4$  (2500 to 5200 mg/L), Fe (250 to 1350 mg/L), and Ni (0.12 to 30 mg/L), pH between 2.8 and 5.9 and < 1 to 60 mg/L alkalinity (as  $\text{CaCO}_3$ ). The recharging acidic surface water (occupying the top meter of the up-gradient aquifer) contains higher concentrations of Al (130 mg/L), Ni (30 mg/L), Zn (1.0 mg/L), Cr (0.3 mg/L) and Cu (3.0 mg/L) and lower pH (<4).

Sulfate and Ca concentrations appear to be controlled by gypsum precipitation in the Up-Gradient Zone (Figure 4). The groundwater is near saturated with respect to siderite ( $\text{FeCO}_3$ ) in the lower portion of the aquifer, and near saturated or supersaturated with respect to jarosite ( $\text{KFe}(\text{SO}_4)_2(\text{OH})_6$ ) or  $\text{Fe}(\text{OH})_3$  in the upper portion of the aquifer (Bain et al., 2000).

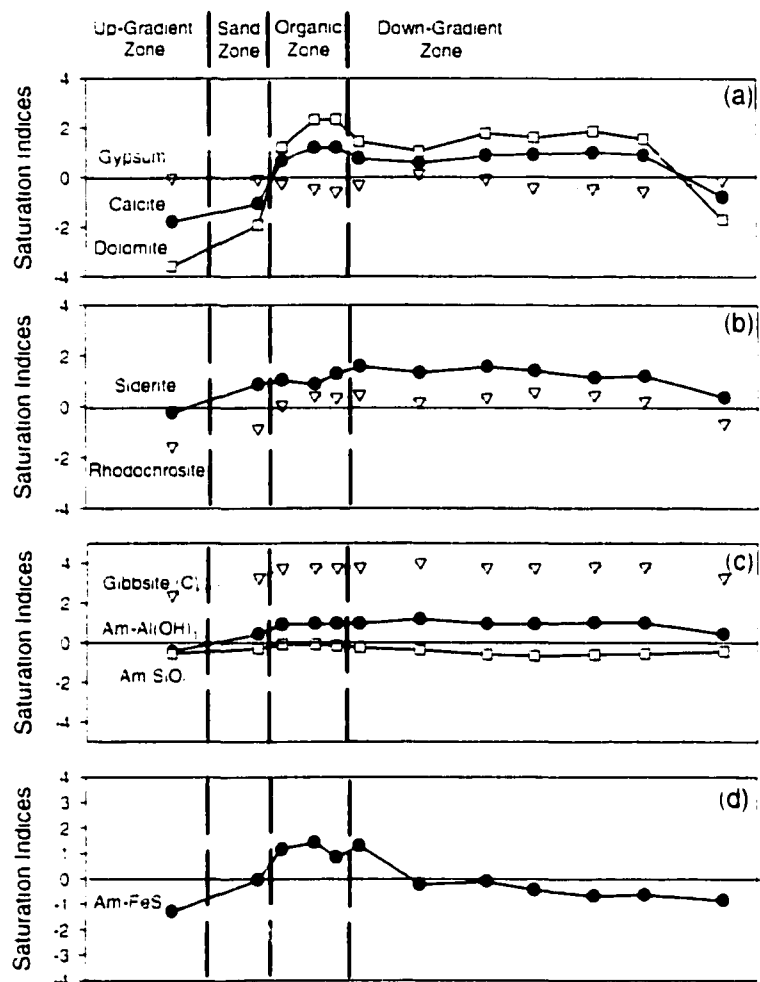


**Figure 3.4** Vertically averaged saturation indices for selected mineral phases for each well nest: (a) gypsum ( $\text{CaSO}_4$ ), calcite ( $\text{CaCO}_3$ ), and dolomite ( $\text{CaMg}(\text{CO}_3)_2$ ) (b) siderite ( $\text{FeCO}_3$ ) and rhodochrosite ( $\text{MnCO}_3$ ) (c) gibbsite ( $\text{Al}(\text{OH})_3$ ), amorphous  $\text{Al}(\text{OH})_3$ , and amorphous  $\text{SiO}_2$  (d) amorphous  $\text{FeS}$ . Note: sulfide saturation indices outside Organic Material Zone were calculated using level of detection sulfide concentrations.

Siderite dissolution has been proposed as a buffer to decreasing pH in this aquifer (*Bain et al., 2000*). Amorphous  $\text{Al}(\text{OH})_3$  probably controls aluminum concentrations. Silica concentrations range from 51 to 9 mg/L and appear to be limited at the higher concentrations by the solubility of amorphous  $\text{SiO}_2$ . No secondary mineral phase controls for Cl, Mg, Mn, Na, and Ni were identified. Other mechanisms such as coprecipitation or adsorption/desorption reactions with aquifer solids may limit concentrations of these species (*Bain et al., 2000*). Within the Up-Gradient Zone, MPN for sulfate reducing bacteria average  $2.3 \times 10^3$ . Dehydrogenase activity (DH) values average  $0.5 \text{ nmol hr}^{-1} \text{ g}^{-1}$  (Figure 3).

### 3.3.3 Sand Zone

As water enters the Sand Zone, vertically averaged alkalinity increases to 150 mg/L, likely the result of calcite dissolution. MINTEQA2 calculations indicate slightly undersaturated conditions for calcite (Figure 4). Water entering the barrier is at equilibrium with gypsum. Calcium, released to the water by calcite dissolution, promotes gypsum precipitation. A corresponding decrease in  $\text{SO}_4$  concentrations (to 3200 mg/L) is observed. Calcium concentrations, meanwhile, remain largely unchanged. Calcite dissolution coupled with gypsum precipitation commonly occurs in carbonate aquifers receiving acid mine drainage effluent (*Bain et al., 2000; Morin and Cherry, 1988*). Calcite dissolution may also produce the observed increase in pH. Though dissolved sulfide concentrations are low, it is also possible that sulfate reduction is occurring in the Sand Zone. Sulfate reduction can also explain the increase in alkalinity and pH and the decrease in  $\text{SO}_4$  and Fe.

Geochemical calculations indicate near saturation with respect to amorphous  $\text{Al}(\text{OH})_3$ . The precipitation of amorphous  $\text{Al}(\text{OH})_3$ , driven by the increase in pH, likely explains the observed decreased Al concentrations (to <1.0 mg/L) (*Stumm and Morgan, 1981*). Within the Sand Zone, trace metal concentrations decrease to below analytical

detection limits for Cu (<0.01 mg/L) and near detection levels for Zn (0.015 mg/L). Nickel concentrations decrease to 0.6 mg/L. Geochemical speciation calculations did not suggest precipitating mineral phases for these metals. High concentrations of trace metals originate from recharging acidic surface water. Declines in concentrations of these species may also be the result of reactions with aquifer sediment prior to entering the Sand Zone.

#### 3.3.4 Organic Mixture Zone

As groundwater enters the Organic Mixture Zone, average concentrations of  $\text{SO}_4^{2-}$  decrease 74% to 840 mg/L, while average alkalinity increases 1400% to 2300 mg/L, and  $\text{S}^{2-}$  increases 12,000% to 17 mg/L. Average populations of sulfate reducing bacteria ( $9.1 \times 10^7$ ) are  $10^5$  times greater and DH ( $9 \text{ nmol hr}^{-1} \text{ g}^{-1}$ ) is 20 times greater than Up-Gradient Zone values (Figure 4), indicating an elevated population of sulfate reducing bacteria is present and active within the barrier. Enrichment in  $^{34}\text{S}$  in the remaining aqueous phase  $\text{SO}_4$  ( $30 \text{ ‰} \delta^{34}\text{S}$  compared to the up-gradient aquifer value of  $5 \text{ ‰} \delta^{34}\text{S}$ ) confirms that the observed decreases in  $\text{SO}_4$  concentrations are due to bacterially-mediated sulfate reduction (Chamber and Trudinger, 1979). The large increase in alkalinity can be attributed to production of bicarbonate by sulfate reducing and fermentative bacteria.

Elevated sulfide concentrations produce saturated to slightly supersaturated conditions for mackinawite ( $\text{Fe}_{1+x}\text{S}$ ) and amorphous FeS (Figure 4). These phases commonly precipitate under sulfate reducing conditions in shallow ground and surface water systems (Morse et al., 1987). The results of solid-phase analysis conducted by Herbert et al., 1998 indicate an accumulation of total reduced inorganic sulfur in the Carbon Mixture Zone of up to 0.5 wt. % S, compared with 0.025 wt. % S in "unreacted" organic mixture (Figure 5). SEM-EDX analysis of black precipitates that accumulated on sampling tubes within the barrier indicate a Fe-S composition with a 1:1 stoichiometry.

while X-ray diffraction (XRD) analysis confirmed that the precipitates were poorly-crystalline mackinawite ( $\text{Fe}_{1+x}\text{S}$ ) (Herbert *et al.*, 1998). The precipitation of these sulfide phases provides a sink for dissolved Fe which decreases >85% to an average of 80 mg/L. MINTEQA2 modeling indicates that the groundwater is near saturation with respect to siderite ( $\text{FeCO}_3$ ) within the Organic Mixture Zone. The precipitation of siderite may also contribute to the observed decrease in Fe concentrations.

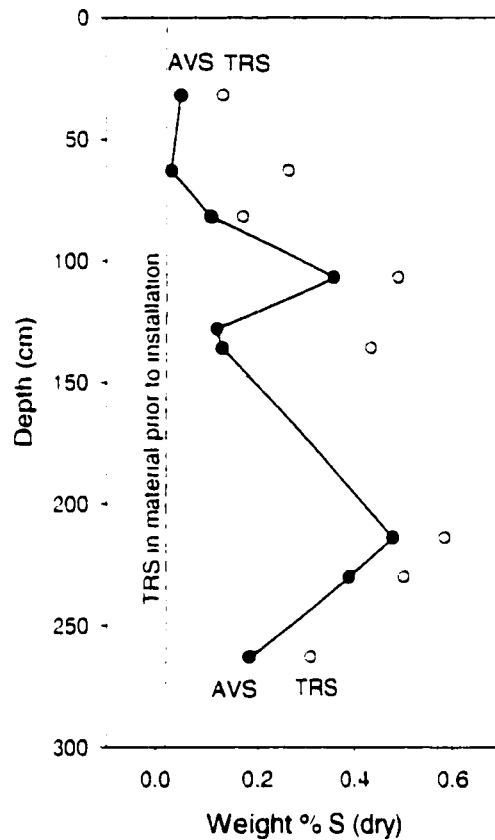


**Figure 3.5** Vertical profiles of "acid volatile sulfide-AVS" and "total reduced (inorganic) sulfides-TRS" concentrations for organic material from Core #2, September 1996. Dashed line indicates TRS concentration in organic material prior to installation of the barrier. Data taken from Herbert *et al.*, 1998.

Decreased  $\text{SO}_4$  concentrations result in a shift from near equilibrium conditions for gypsum in the Sand Zone to undersaturated conditions in the Organic Mixture Zone

(Figure 5). Dissolution of gypsum may be the source of observed increases in Ca concentrations. Conversely, high alkalinity results in a shift in calcite stability from undersaturated in the Sand Zone to supersaturated conditions in the Organic Mixture Zone. Increased alkalinity also results in supersaturation with respect to rhodochrosite ( $\text{MnCO}_3$ ). Precipitation of rhodochrosite, or a less crystalline precursor, can explain the observed decrease in Mn concentrations. Mn may also be removed by coprecipitation with FeS or as a discrete manganese sulfide phase (*Morse et al., 1987*). The increase in pH to an average 6.7 versus 6.2 in the Sand Zone, can be attributed to buffering between the carbonate and sulfide systems (*Boudreau and Canfield, 1993*), and reflects the ability of this system to regulate pH conditions. Silica concentrations increase to an average value of 27 mg/L (Figure 3). This increase may be the result of enhanced silicate dissolution resulting from bacterial activity on silicate mineral surfaces (*Hiebert and Bennett, 1992*) or may reflect increased Si solubility due to organic acid complexation (not accounted for by MINTEQA2 modeling) (*Bennett, 1991*). Both of these mechanisms have been observed in organic-rich groundwater environments.

Concentrations of Ni decline to  $<0.1$  mg/L within the Organic Mixture Zone. MINTEQA2 calculations indicate slightly supersaturated conditions for millerite ( $\text{NiS}$ ). Though Cu and Zn are present below detection within the Organic Mixture Zone, geochemical calculations were made using analytical detection values. These calculations indicate that the pore water would be supersaturated with respect to the sulfide minerals chalcopyrite ( $\text{FeCuS}_2$ ) and sphalerite ( $\text{ZnS}$ ) suggesting a potential for these minerals, or less crystalline precursors, to precipitate. Laboratory studies have also shown effective removal of Ni, Cd, and Zn under sulfate reducing conditions (*Waybrant et al., 1998*). However, mechanisms removing trace metals from the water in natural anoxic sedimentary analogs are not well understood. Depending on geochemical conditions, trace metals can adsorb, coprecipitate or form discrete sulfide mineral phases under sulfate-reducing conditions (*Machemer and Wildeman, 1992*).

Barium concentrations increase from below analytical detection ( $< 0.1$  mg/L) in the Up-Gradient Zone to 0.4 mg/L within the barrier. Geochemical calculations indicate that the water is locally undersaturated with respect to barite. If present, barite may be dissolving within the barrier (Baldi *et al.*, 1996). Boron concentrations also increase from below analytical detection ( $< 0.1$  mg/L) to 0.6 mg/L. A solid phase source for boron within the barrier was not identified. Phosphorous concentrations increase from below analytical detection 0.1 mg/L in the Up-gradient Zone to 5 to 20 mg/L in the Organic Material Zone. The increase in P can be attributed to release from degradation of organic matter under anaerobic conditions (Stumm and Morgan, 1981).

### 3.3.5 Down-Gradient Zone

As the plume of treated water exits the permeable reactive barrier into the down-gradient aquifer, water chemistry again changes. Silica concentrations decrease to 13 mg/L. Depletion of dissolved organic carbon may eliminate enhanced silicate dissolution observed in the barrier. The sulfide concentrations decrease to an average 0.14 mg/L in the Down-Gradient Zone. These sulfide concentrations are much lower (often less than the analytical level of detection) than within the Organic Mixture Zone.

The absence of measurable sulfide concentrations precludes the direct determination of saturation indices for sulfide-bearing phases. Sulfide speciation using level of detection values indicates that sulfide mineral phases may be near saturation but are less saturated compared to within the barrier. Evidence exists that sulfate reduction is occurring in the down-gradient aquifer. Black precipitates, similar in appearance to those identified as sulfides within the reactive barrier, were observed on well sampling tubes in the Down-Gradient Zone. Dissolved organic carbon (DOC), a potential electron donor for sulfate reduction, is elevated in the down-gradient aquifer (50 to 200 mg/L). MPN values indicate populations of SRB (averaging  $3 \times 10^5$ ) are  $10^3$  greater than in the Up-Gradient Zone (Figure 3). Bacterial activity is also elevated with DH at  $7 \text{ nmol hr}^{-1} \text{ g}^{-1}$ .

Geochemical modeling indicates that this water is supersaturated with respect to calcite, which is consistent with generation of alkalinity by SRB metabolic activity. Precipitation of sulfides may be occurring in reduced micro-environments associated with suspended or dissolved organic carbon. The most down-gradient sampling point in Figures 2 and 3 represents water that passed through the aquifer prior to the reactive barrier installation.

### 3.3.6 Vertical trends within barrier

Within the Organic Carbon Zone, aqueous phase concentrations exhibit trends suggesting a greater degree of sulfate reduction at the top and bottom, compared to the middle, of the barrier. Concentrations of  $\text{SO}_4$  are generally higher ( $>1500$  mg/L) within the middle half than at the top and bottom ( $< 500$  mg/L) (Figure 2). Iron shows a similar trend with values in the center  $>50$  mg/L and generally  $<50$  mg/L at the top and bottom. Conversely, alkalinity is generally  $<1250$  mg/L in the central part of the barrier and  $>1250$  mg/L at the top and bottom (Figure 2). Input water within the up-gradient Sand Zone does not exhibit these trends, suggesting they are the products of processes within the barrier.

Vertical stratification is likely caused by higher rates of flow through the middle portion of the organic mixture zone. Slower flow rates along the top and bottom of the barrier will result in longer residence times and may produce more complete reduction of sulfate, metal sulfide precipitation and alkalinity generation. Shorter residence times through the middle of the barrier result in less  $\text{SO}_4$  removed from a given pore volume. However, the higher flow rates through this zone may still produce higher rates of sulfide accumulation compared with slower zones above and below. Vertical profiles exhibiting higher accumulations of solid phase sulfides within the middle portion of the barrier are consistent with this conclusion (Figure 5). Most Probable Numbers for SRB and bacterial activity values do not exhibit obvious, clearly definable, trends within the reactive barrier. However, bacterial activity, as measured by dehydrogenase activity, and

MPN values for SRB do suggest slightly higher bacterial populations are present in the middle of the barrier. These trends are consistent with trends in aqueous phase concentrations.

The permeable reactive barrier appears to be quite effective at maintaining Eh and pH conditions that support bacterially-mediated sulfate reduction (*Hao et al., 1996; Connell and Patrick, 1968*). The major changes in water chemistry and bacterial populations as groundwater passes through the barrier and the accumulation of solid phase sulfides within the barrier indicate that sulfate reduction and metal sulfide precipitation are the dominant mechanisms producing improved water quality. Nearly all observed changes in groundwater chemistry can be attributed, directly or indirectly, to these processes. Groundwater toxicity has been lowered in three significant ways: the addition of alkalinity, the elimination of acid generating potential, and the removal of trace metals. In addition, the precipitation of carbonate minerals within and down-gradient of the barrier results in the accumulation of solid-phase buffering capacity against the future influx of acidic groundwater. Lack of oxidizing agents within the groundwater, coupled with low mineral solubility, renders the accumulating sulfide phases within the barrier quite stable.

There is enough carbon within the barrier to treat the groundwater for 100's of years, however, it is likely that only a fraction of the organic carbon is sufficiently reactive to promote rapid reduction of sulfate. Calculations, based on the long-term performance of column studies, indicate that the reactive barrier has a theoretical treatment lifetime of >15 years (*Benner et al., 1997*). However, direct transfer of these results from the laboratory neglects the potential complexities that exist in a field setting. Factors that may limit barrier performance in the field include preferential flow or preferential mass flux, and low temperatures inhibiting bacterial activity. The long-term treatment capacity for the Nickel Rim reactive barrier will be determined by continued monitoring.

## REFERENCES

- Alexander, M.; Black, C. A. Ed. 1965. Most-probable-number method for microbial populations. *Agronomy* 9, 1467-1472.
- Allison, J.D.; Brown, D.S.; Nova-Gradac, K.J. *MINTEQA2/PRODEFA2, A geochemical assessment model for environmental systems: Version 3.0 user's manual.*; U.S.E.P.A.: Athens, GA, 1990.
- Bain, J.G.; Blowes, D.W.; Robertson, W.D. The hydrogeochemistry of a sand aquifer affected by drainage from the Nickel Rim tailings impoundment. Proceedings of Sudbury '95- Mining and the Environment, Sudbury Ontario, May 28- June 1, 1995, 715-723.
- Bain, J.G.; Blowes, D.W.; Robertson, W.D. 2000. The physical and chemical hydrogeology of a sand aquifer affected by drainage from the Nickel Rim tailings impoundment. *J. Contam. Hydrol.*, (In Press).
- Baldi, F.; Pepi, M.; Burrini, D.; Kniewald, G.; Scali, D.; Lanciotti, 1996. E. Dissolution of barium from barite in sewage sludges and cultures of *Desulfotomaculum desulfuricans* *Appl. Environ. Microbiol.* 62 (7) 2398-2404.
- Ball, J.W.; Nordstrom, D.K. *User's manual for WATEQ4F, with revised thermodynamic data base*; U.S.G.S., Open File Report 91-183:1991.
- Bechard, G.; McCready, R.G.L.; Koren, D.W.; Rajan, S. Microbial treatment of acid mine drainage at Halifax international airport. Proceedings of Sudbury '95- Mining and the Environment, Sudbury Ontario, May 28- June 1, 1995, 545-554.
- Bennett, P.C. 1991. Quartz dissolution in organic-rich aqueous systems. *Geochim. Cosmochim. Acta* 55, 1781-1897.
- Benner, S.G.; Blowes, D.W.; Ptacek, C.J. 1997. Full-scale porous reactive wall for the prevention of acid mine drainage. *Ground Water Monit. Remed.* 1997, 17, 99-107.

- Blowes, D.W.; Ptacek, C.J. (1994) U.S. Patent # 5514279.
- Boudreau, B.P.; Canfield, D.E. 1993. A comparison of closed- and open-system models for porewater pH and calcite-saturation state. *Geochim. Cosmochim. Acta* 57, 317-334.
- Canfield, D.E.; Raiswell, R.; Westrich, J.T.; Reaves, C.M.; Berner, R.A. 1986. The use of chromium reduction in the analysis of reduced inorganic sulfur in sediments and shales. *Chem. Geol.* 54, 149-155.
- Chambers, L.A.; Trudinger, P.A. 1979. Microbiological fractionation of stable isotopes: a review and critique. *Geomicrobiol. J.* 1, 249-293.
- Chapelle, F.H. 1993. *Ground-Water Microbiology and Geochemistry*; John Wiley & Sons Inc.: New York, p 87.
- Connell, W.E.; Patrick, W.H. 1968. Sulfate reduction in soil: Effects of redox potential and pH *Sci.* 159, 86-87.
- Dubrovsky, N.M.; Cherry, J.A.; Reardon, E.J.; 1985. Geochemical evolution of inactive pyritic tailings on the Elliot Lake uranium district. *Can. Geotech. J.* 22, 110.
- Dvorak, D.H.; Hedin, R.S.; Edenborn, H.M.; McIntire, P.E. 1992. Treatment of metal-contaminated water using bacterial sulfate reduction: results from pilot-scale reactors. *Biotech. Bioeng.* 40, 609-616.
- Hao, O.J., Chen, J.M., Huang, L., Buglass, R.L. 1996. Sulfate Reducing Bacteria *Crit. Rev. Environ. Sci. Tech.* 26 (1), 155-187.
- Herbert Jr., R.B.; Benner, S.G.; Blowes, D.W. Reactive barrier treatment of groundwater contaminated by acid mine drainage: Sulfur accumulation and sulfide formation. *Groundwater Quality: Remediation and Protection*. Tübingen, Germany. IAHS Publication no. 250, September 21-25, 1998, 451-458.
- Hiebert, F.K.; Bennett, P.C. 1992. Microbial control of silicate weathering in organic-rich ground water. *Sci.* 258, 278-281.

- Johnson, R.H.; Blowes, D.W.; Robertson, W.D.; Jambor, J.L. 1999. The hydrogeochemistry of the Nickel Rim mine tailings impoundment, Sudbury, Ontario. *J. Contam. Hydrol.* (In Press).
- Ladd, J.N. 1978. Origin and range of enzymes in soil. *Soil Enzymes*; Burns, R.G. Ed. Academic Press, New York. 51-96.
- Machemer, S.D.; Wildeman, T.R. 1992. Adsorption compared with sulfide precipitation as metal removal processes from acid mine drainage in a constructed wetland. *J. Contam. Hydrol.* 9, 115-131.
- Morin, K.A.; Cherry, J.A. 1988. Migration of acidic groundwater seepage from uranium-tailings impoundments. 1. Field study and conceptual hydrogeological model. *J. Contam. Hydrol.*, 2, 323.
- Morse, J.W.; Miller, F.J.; Cornwell, J.C.; Rickard, D. 1987. The chemistry of the hydrogen sulfide and iron sulfide system in natural waters. *Earth Sci. Rev.* 24, 1-42.
- Postgate, J.R. 1984. *The Sulphate-Reducing Bacteria*. Cambridge University Press: Cambridge, England.
- Standard Methods for the Examination of Water and Wastewater*; APHA: Washington DC, 1996; 5-11.
- Stumm, W.; Morgan, J.J. *Aquatic Chemistry*; John Wiley & Sons: New York, 1981; p 543.
- Wakao, N; Takahashi, T; Sakurai, Y.; Shiota, H. 1979. A treatment of acid mine water using sulfate-reducing bacteria. *J. Ferment. Technol.*, 57, 445.
- Waybrant, K.R.; Blowes, D.W.; Ptacek, C.J.. Selection of reactive mixtures for use in permeable reactive walls for the treatment of acid mine drainage. *Environ. Sci. Technol.*, 1998, 32, 1972-1979.

Yanagisawa, F.; Sakai, H. 1983. Thermal decomposition of barium sulfate-vanadium pentoxide-silica glass mixtures for preparation of sulfur dioxide in sulfur ratio measurements. *Anal. Chem.* 55, 985.

## Chapter 4

### *Rates of Reactions and Treatment*

#### 4.1 CHAPTER SUMMARY

A full-scale reactive barrier, utilizing bacterially mediated sulfate reduction to promote metal sulfide precipitation and alkalinity generation, was installed in August 1995. Monitoring of groundwater chemistry up-gradient and down-gradient of and within the reactive barrier over a three-year period allows assessment of long term reactive barrier performance. The overall rate of sulfate removal within the barrier declines with time from an initial rate of 58 to 40 mmol L<sup>-1</sup> a<sup>-1</sup> 38 months after installation. Over the same time period, the rate of Fe removal declines from 38 to 18 mmol L<sup>-1</sup> a<sup>-1</sup>. The degree of sulfate reduction and Fe sulfide precipitation within the barrier is both spatially and temporally variable. Spatial differences are primarily the result of different residence times. Variations in hydraulic conductivity of a factor of three within the treatment material produce large differences in the degree of SO<sub>4</sub> and Fe removal. Temporal variations are likely the result of a decline in organic carbon reactivity over time. Temperatures in the aquifer fluctuate from a low of 2 °C in the winter to a high of 16 °C in the summer and the rate of SO<sub>4</sub> reduction in the summer is nearly two times greater than the winter rate. An effective activation energy of  $E_a=10$  kcal mol<sup>-1</sup> can account for the temperature induced changes.

## 4.2 INTRODUCTION

A full-scale permeable reactive barrier was installed August 1995 in a sand aquifer at the Nickel Rim mine site in Ontario, Canada (Benner et al., 1997). The reactive barrier intercepts a groundwater plume, emanating from a tailings impoundment, that is characterized by elevated concentrations of Fe(II),  $\text{SO}_4$  and Ni (Bain et al., 1999). The barrier is installed into an alluvium filled valley and abuts underlying bedrock at the sides and base. The reactive barrier contains organic carbon which promotes sulfate reduction and metal sulfide precipitation and increases the alkalinity of the effluent (Benner et al., 1999). Sulfate reduction is bacterially mediated and populations of sulfate reducing bacteria are five orders of magnitude higher within the barrier compared to the up gradient aquifer (Benner et al., 1999, Benner et al., 2000). Iron and  $\text{SO}_4$  are primarily removed by precipitation of Fe sulfides and the mineral phase mackinawite ( $\text{FeS}$ ) is precipitating in the barrier (Herbert Jr. et al., 2000). Removal of Fe(II) prevents the generation of acidity when the groundwater discharges to the surface and the addition of alkalinity increases groundwater buffering capacity. This paper presents results of three years of monitoring, defines rates of sulfate and iron removal, and describes the performance of the barrier.

## 4.3 METHODS

### 4.3.1 Water Sampling and Analysis.

Monitoring wells were installed in a network of nests forming six transects, three parallel and three perpendicular to groundwater flow (Figure 1). Samples of groundwater were collected bi-annually from November 1995 to October 1998. A detailed description of well installation, water sampling and field and laboratory analysis can be found in Benner et al. (1997). Well nests installed into the aquifer up gradient, within and down gradient of the barrier were sampled for anion and cation analysis. The parameters pH, Eh, alkalinity and total dissolved sulfide concentration were measured in the field. The

geochemical speciation/mass transfer computer code MINTEQA2 (Allison et al., 1990), adjusted to be consistent with the WATEQ4F database (Ball et al., 1991), was used to aid in the interpretation of aqueous geochemical data. Input parameters were Al, Ca, Cl, Fe, K, Mg, Mn, Na, Ni, Si,  $\text{SO}_4$ , Zn, alkalinity and pH. For water collected outside the reactive barrier installation, Eh was input from field platinum electrode measurements. Within the barrier, Eh was not specified and measured concentrations of dissolved sulfide were input to calculate sulfide mineral saturation indices. All dissolved iron was assumed to be in the Fe (II) oxidation state.

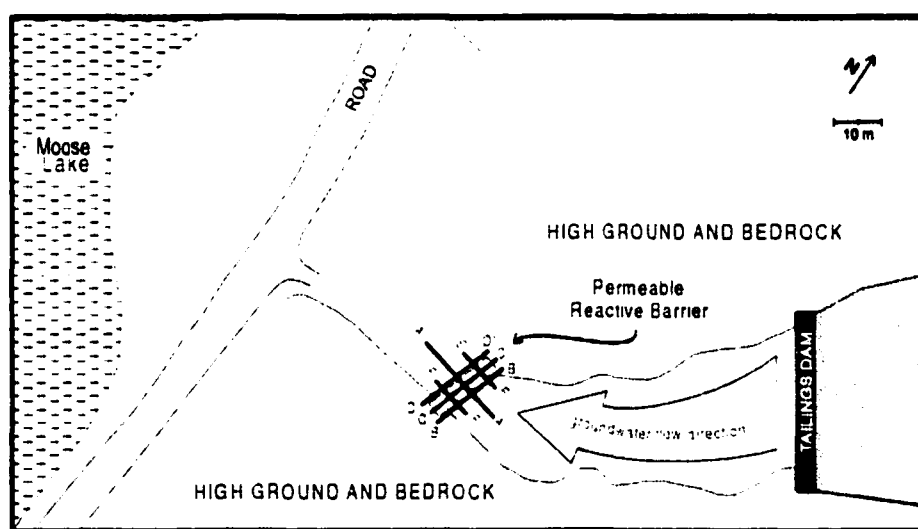


**Figure 4.1** Map view of Nickel Rim reactive barrier installation showing mine tailings impoundment, groundwater flow path, and locations of reactive barrier and monitoring well transects.

#### 4.3.2 Bacterial Enumeration

Sediment cores were collected adjacent to well nests RW29, 30, and 31 (Figure 6). Sediment was analyzed for most probable numbers (MPN) of sulfate reducing bacteria and dehydrogenase activity which can be generally correlated with bacterial respiratory activity and used as an index of microbial activity (Ladd, 1978). A detailed description of these methods can be found in Benner et al. (1999).

### 4.3.3 Groundwater Flow Modeling

The two-dimensional finite element model FLOTRANS (Guiguer et al., 1994) was used to conduct simulations of flow and conservative chloride transport along a 30 m transect parallel to flow passing through the reactive barrier. A uniform grid of 100 by 100 nodes was used to represent a 30 by 3.5 m domain. The left and right boundaries were assigned specified head so that a gradient of 0.016 was established with flow from left to right (Figure 2). The top and bottom of the domain were assigned no flow boundaries with the exception of the top boundary, down gradient from the barrier, which was assigned as specified flux to reflect surface water recharge to the aquifer in this region. Transport boundary and initial conditions were assigned to reflect low background Cl concentrations in the aquifer, high initial Cl concentrations in the barrier and elevated Cl concentrations in the surface recharge water down gradient of the barrier. The initial hydraulic conductivity field was consistent with previous flow modeling of Bain et al. (1999).

## 4.4 RESULTS AND DISCUSSION

### 4.4.1 Physical Flow through the Barrier

Field measured water levels indicate that flow is perpendicular to the barrier installation and generally parallel to Transect A-A' (Figure 1). The hydraulic gradient across the barrier (0.016) is slightly lower than the average gradient for the adjacent aquifer (0.02) indicating that the average hydraulic conductivity of the barrier is greater than that of the aquifer. Direct measurement of hydraulic parameters within the barrier has proven difficult. Clogging of well screens by the reactive organic material has prevented development of a good hydraulic connection between monitoring wells and the barrier groundwater. However, high concentrations of soluble Cl contained in the installed compost material provide an *in situ* tracer and yield information about the nature of groundwater flow through the barrier. The Cl data indicate that flow through the barrier

is heterogeneous, with higher flow velocities through the central portion of the barrier (Figure 3).

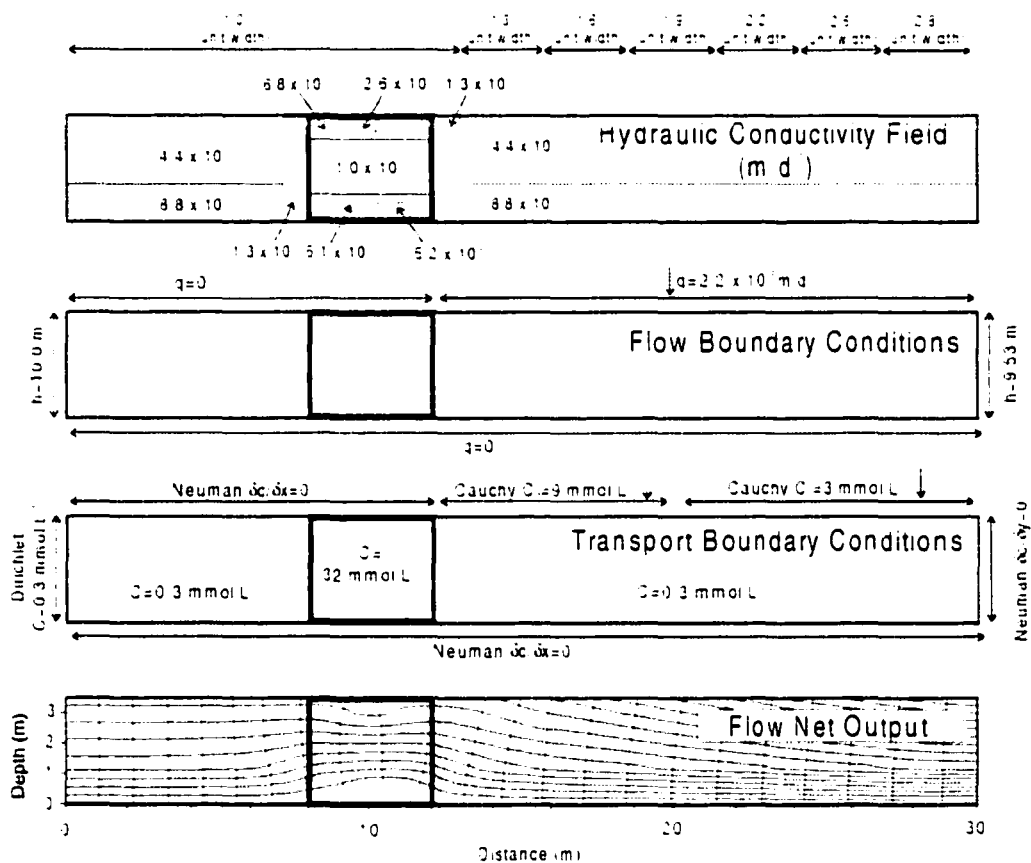


Figure 4.2. Flow and transport modeling boundary and initial conditions.

Two dimensional flow and conservative transport modeling was conducted along Transect A-A'. The flow solution was calibrated based on changes in Cl concentrations with time and constrained by field-measured hydraulic gradients and aquifer flow parameters determined by Bain et al. (1999). Model calibration was achieved by adjustment of the hydraulic conductivity field. Calibration was conducted iteratively with the determination of rates of treatment within the barrier. This process provides a

consistent model of physical flow and chemical reaction rates within the barrier but the flow solution should not be considered independent nor unique (Figure 4).

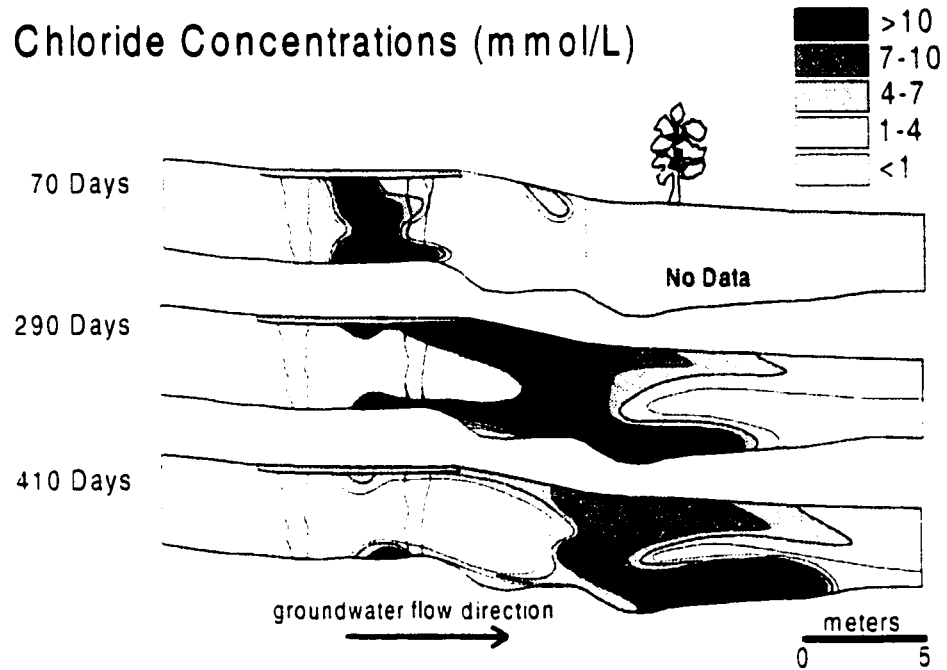


Figure 4.3 Field-measured cross-sectional profile of chloride concentrations with time

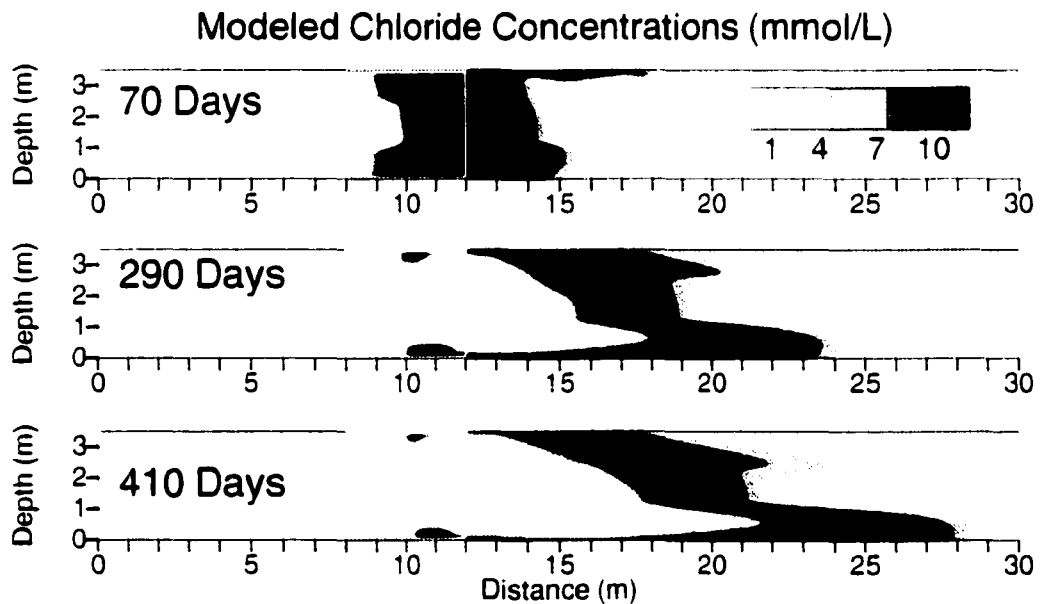


Figure 4.4 Modeled cross-sectional profiles of chloride concentrations with time

The flow modeling and field data indicate an average groundwater velocity for the aquifer of  $16 \text{ m a}^{-1}$ . With a barrier thickness of 4 m, the average residence time within the barrier is approximately 90 days. Groundwater passes through the middle of the barrier at velocities approximately three times faster (residence time = 60 days) compared to water at the top and base (residence time = 165 days).

Concentrations of Cl with time for the 12 sampling points also illustrate spatial variation in groundwater flow rates (Figure 5). After 280 days (June 96 sample date), Cl concentrations at all sampling points are less than 0.5 of the initial concentration ( $\approx 32 \text{ mmol L}^{-1}$ ). However, Cl concentrations at many points within the barrier remain elevated after the first pore volume has exited the barrier and Cl concentrations at some points remain elevated for >1000 days (10 pore volumes). This residual tailing in Cl concentrations suggests the diffusive release of Cl from aggregates of low K material (Gillham et al., 1984). The reactive mixture in the barrier is composed of a 1:1 (by volume) mixture of pea gravel and compost (Benner et al., 1997). The organic material is composed of partially degraded leafy material and wood chunks of 0.5 - 3 cm diameter. Small variations in the gravel to compost ratio can produce a large hydraulic conductivity contrast: a change of 5% in the fraction of gravel can produce an order of magnitude change in hydraulic conductivity (Benner et al., 1997).

At the scale of the observed vertical stratification in the barrier, there is a positive correlation between zones of low hydraulic conductivity (K) and lower concentrations of  $\text{SO}_4$  and Fe and higher alkalinity values. It is likely that spatial variation in water chemistry also occurs on a smaller scale within the barrier. Although the contribution of water from these small, low K zones to the flux through the barrier may be small, the contribution to the volume within the barrier may be significant. Within this conceptual model of flow through the barrier, water chemistry based on a volume-average sampling will be different from that based on a flux-averaged sample (Parker et al., 1984). A

volume-averaged sample from within the barrier will have lower concentrations of  $\text{SO}_4$  and Fe and higher alkalinity than a flux-averaged sample.

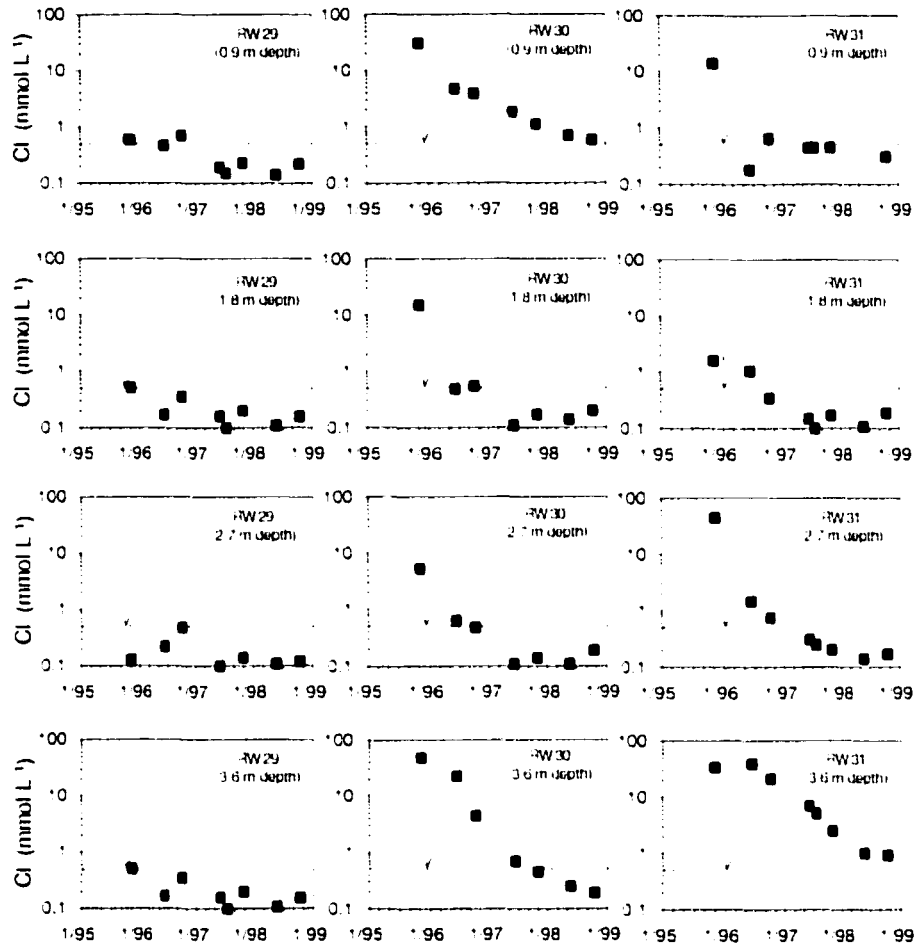


**Figure 4.5** Chloride concentrations with time for sampling points in well nests RW29, RW30 and RW31 located 0.5 m, 2 m and 3.5 m into the barrier (Figure 3). Dashed line indicates maximum observed  $\text{Cl}^-$  concentration of influent water. Arrow marks time at which background would be reached under plug flow conditions and a groundwater velocity of  $16 \text{ m a}^{-1}$ . Each plot is labeled with the approximate depth below surface.

Cross-sectional profiles of  $\text{SO}_4$ , Fe and alkalinity concentrations indicate that the difference in flow rates along Transect A-A' has a discernable impact on the degree of treatment (Figures 6, 7, and 8). Within the zone of higher flow in the central portion of the barrier, concentrations of  $\text{SO}_4$  and Fe are higher and alkalinity is lower, reflecting lower rates of removal and alkalinity generation. Less  $\text{SO}_4$  and Fe removal for a given pore volume can be attributed to shorter residence times and consequently less  $\text{SO}_4$  reduction for each pore volume passing through the central portion of the barrier.

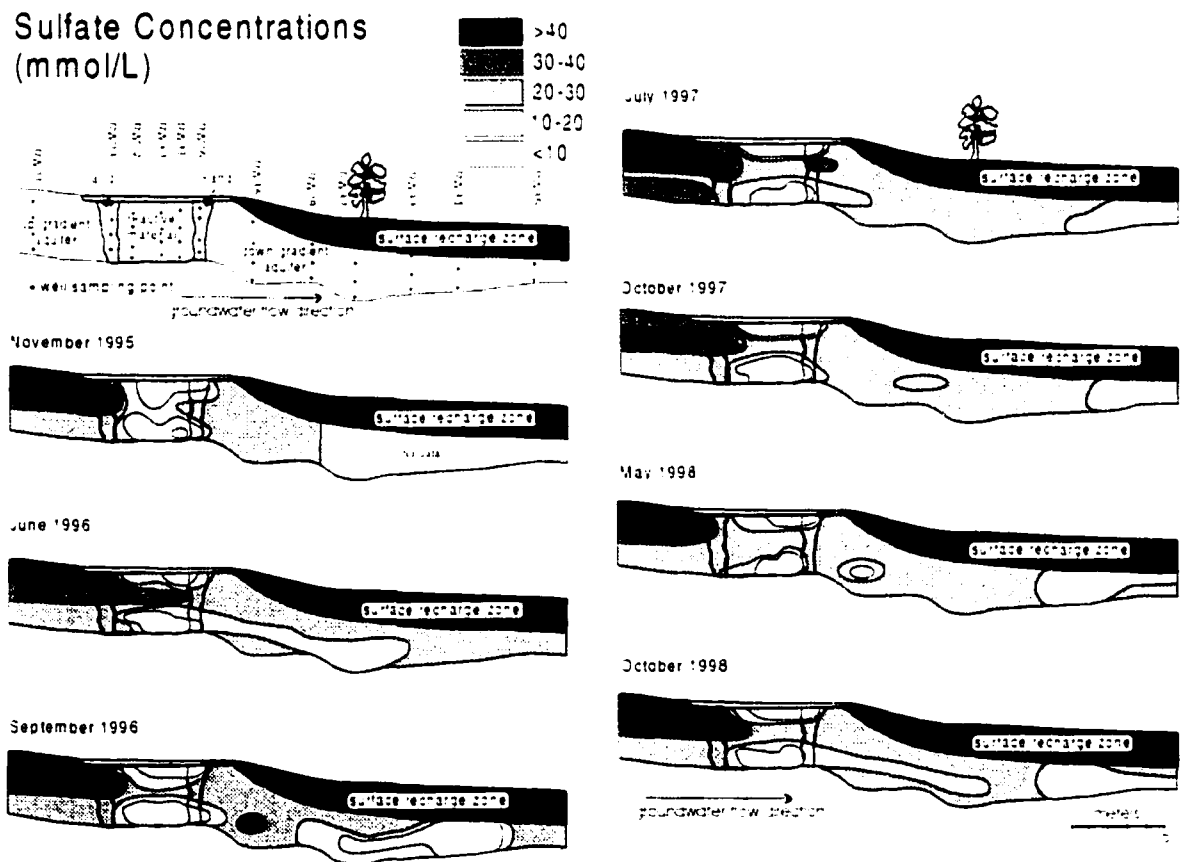


**Figure 4.6** Cross-sectional profiles along Transect A (Figure 1) of  $\text{SO}_4$  concentrations through the reactive barrier for each sampling period.

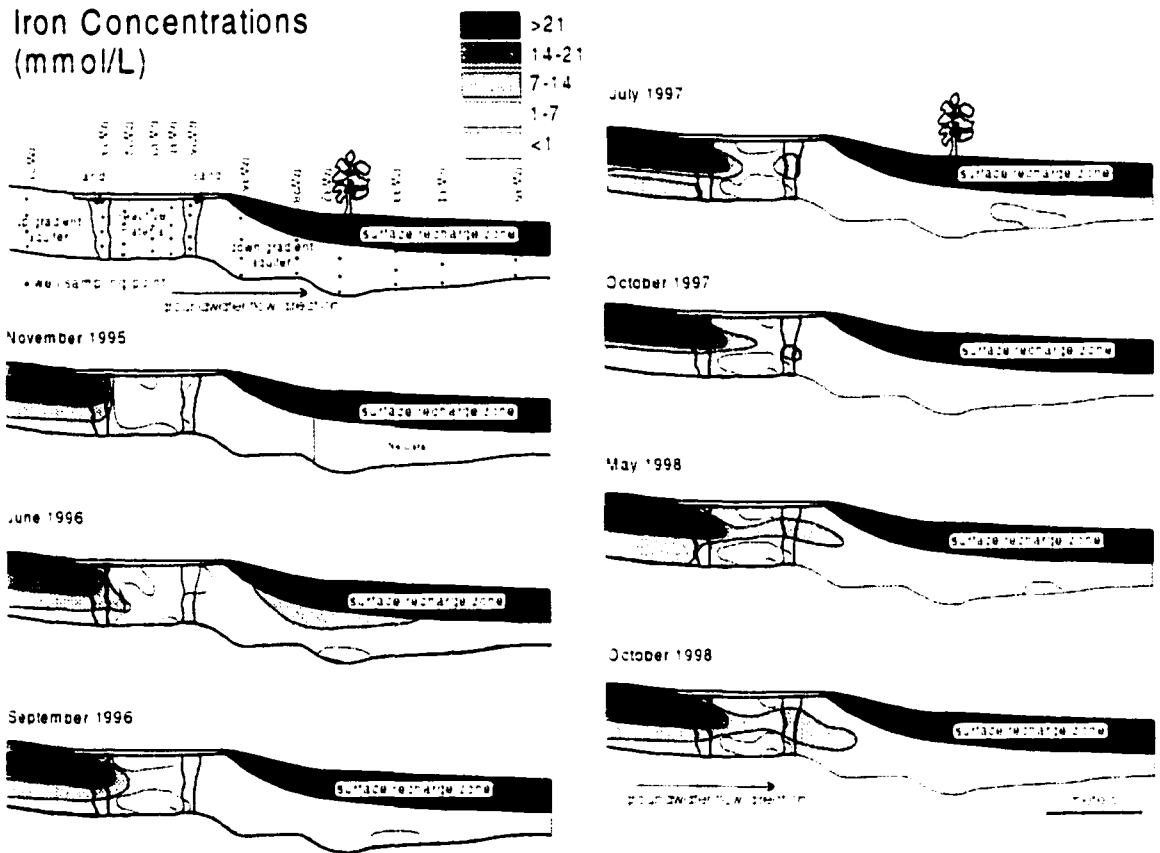


**Figure 4.7** Cross-sectional profiles along Transect A (Figure 1) of Fe concentrations through the reactive barrier for each sampling period.

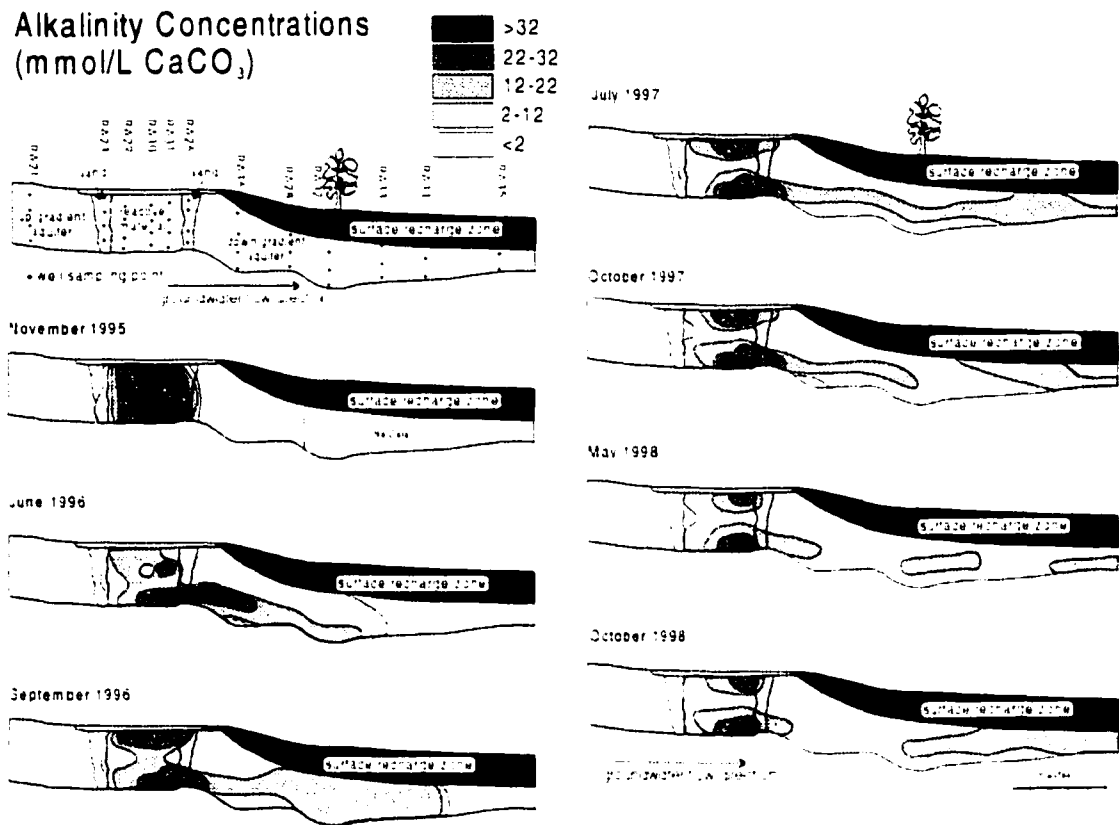


**Figure 4.8** Cross-sectional profiles along Transect A (Figure 1) of alkalinity values through the reactive barrier for each sampling period.

#### 4.4.2 Spatial Heterogeneities

Profiles along Transect A-A' show SO<sub>4</sub> concentrations decrease by 10-15 mmol L<sup>-1</sup>, Fe decrease by 5-10 mmol L<sup>-1</sup> and alkalinity (as CaCO<sub>3</sub>) increase by 5-15 mmol L<sup>-1</sup> as groundwater passes through the reactive barrier (Figures 6, 7, and 8). Sulfate concentrations up-gradient of the barrier range from >50 mmol L<sup>-1</sup> to <10 mmol L<sup>-1</sup> with the highest concentrations in the upper 2 m of the profile. Within the barrier, concentrations of SO<sub>4</sub> decline at many locations to < 10 mmol L<sup>-1</sup>. Higher values are observed in the faster flowing, central portion of the barrier. On the down gradient side, the distribution of SO<sub>4</sub> concentrations is similar to within the barrier, with the highest

values near the central part of the profile. Down gradient  $\text{SO}_4$  concentrations are lower than the up gradient values but, surprisingly, are elevated compared to those values within the barrier.

Iron concentrations are similar to those for  $\text{SO}_4$ ; concentrations decline as groundwater enters the barrier, with greater decreases in the top and bottom of the barrier where groundwater flows more slowly (Figure 7). Concentrations of Fe are also generally higher on the down-gradient side compared to within the barrier. The Fe profiles more clearly show a decline in Fe removal with time. During the first year after installation, Fe concentrations at most points within the barrier are  $< 1 \text{ mmol L}^{-1}$  but by October 1998, Fe concentrations at most points in the barrier are  $> 5 \text{ mmol L}^{-1}$ .

Alkalinity concentrations are low up gradient and increase as groundwater passes through the barrier (Figure 8). There is an inverse correlation with  $\text{SO}_4$  and Fe within the barrier: areas where flow rates are slow and concentrations of  $\text{SO}_4$  and Fe are low, alkalinity concentrations are high (20 to 45  $\text{mmol L}^{-1}$ ).

#### 4.4.3 Comparing Transects Parallel to Flow

Figures 9 and 10 compare profiles of  $\text{SO}_4$  and Fe concentrations along the 'parallel to flow' transects A, F and E for May and October 1998. Profiles along Transect F-F' show high input concentrations in the center of the aquifer and corresponding elevated concentrations through the central portion of the barrier. Transect E-E' exhibits the highest input concentrations of  $\text{SO}_4$  and Fe of the three transects. Along Transect E, the highest values within the barrier are found at the top and bottom, the inverse of Transect A. These profiles suggest that the vertical distribution of areas of high groundwater flow rates is variable.

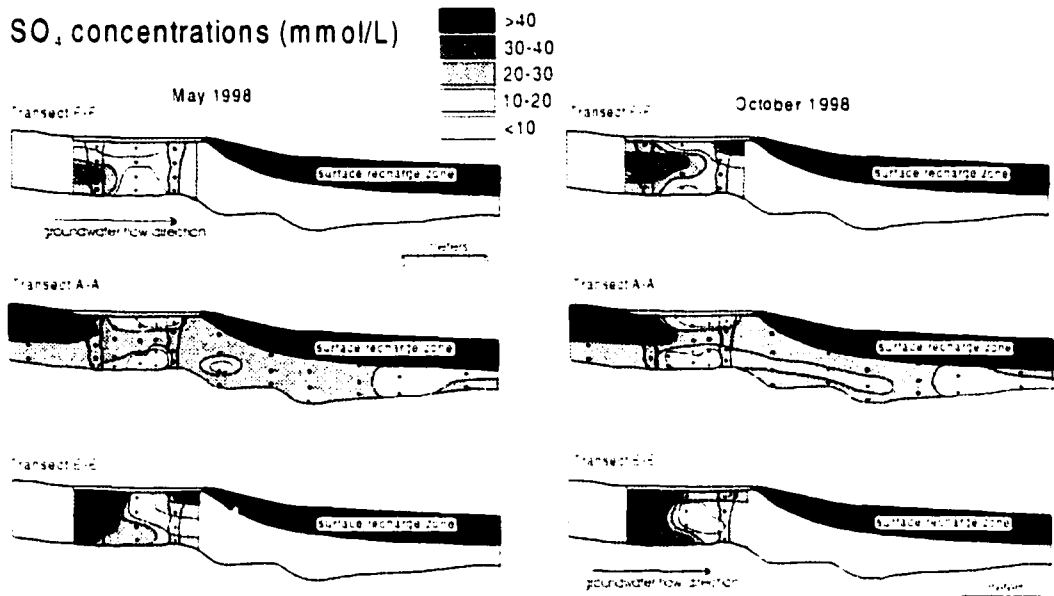


**Figure 4.9** Cross-sectional profiles along transects F, A, and E, parallel to groundwater flow, of SO<sub>4</sub> concentrations for the May and October 1998 sampling periods.

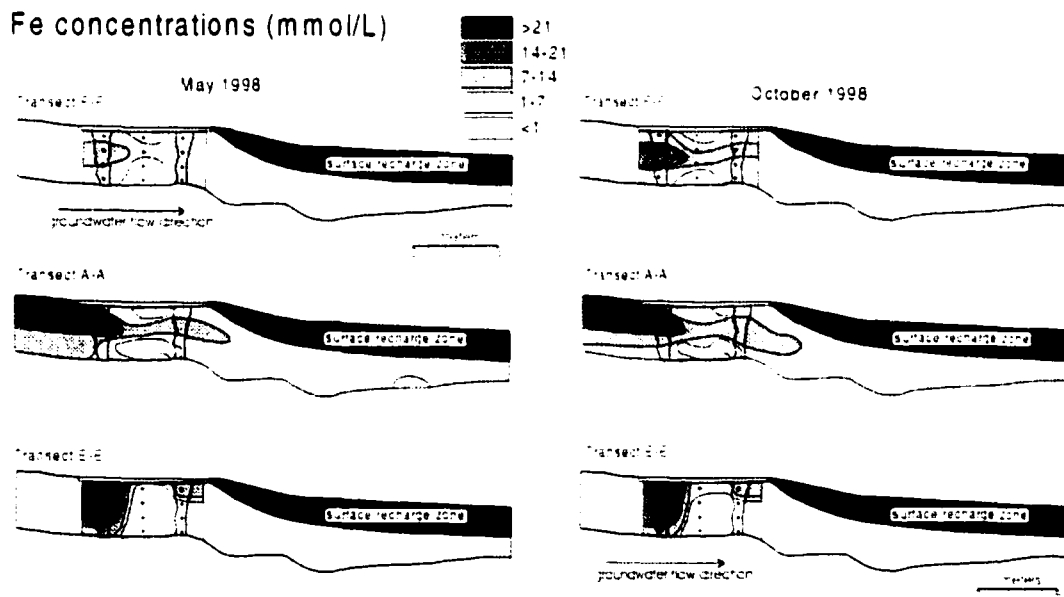


**Figure 4.10** Cross-sectional profiles along transects F, A, and E parallel to groundwater flow, of Fe concentrations for the May and October 1998 sampling periods.

In profiles A and F, flow appears to be faster through the central portion of the barrier while in Transect E, lower Fe and SO<sub>4</sub> concentrations suggest slower flow rates and longer residence times in the center of the barrier.

4.4.4 Profiles Perpendicular to Flow

Cross-sectional profiles taken perpendicular to flow (Figures 11 and 12) show SO<sub>4</sub> and Fe concentrations along transects up gradient (Transect B), within (Transect C) and down gradient (Transect D) of the barrier. These profiles exhibit the spatial trends evident in the transects parallel to the flow and also show the high degree of temporal variation for values at individual well points between sampling periods.

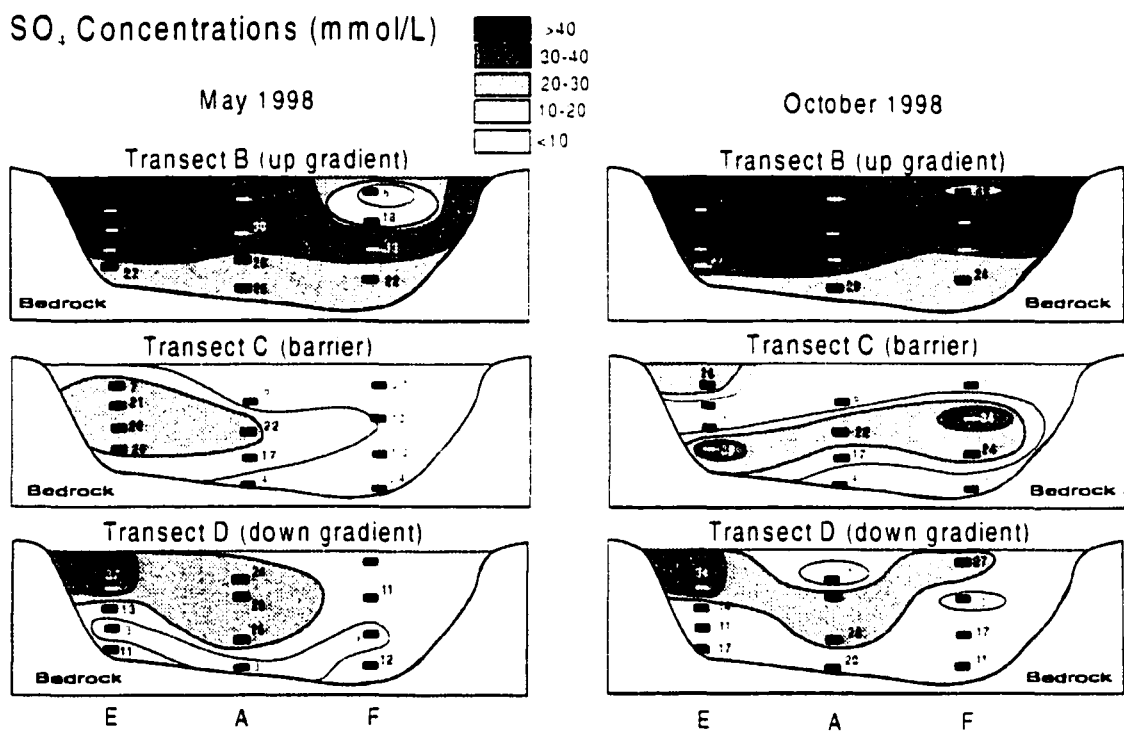
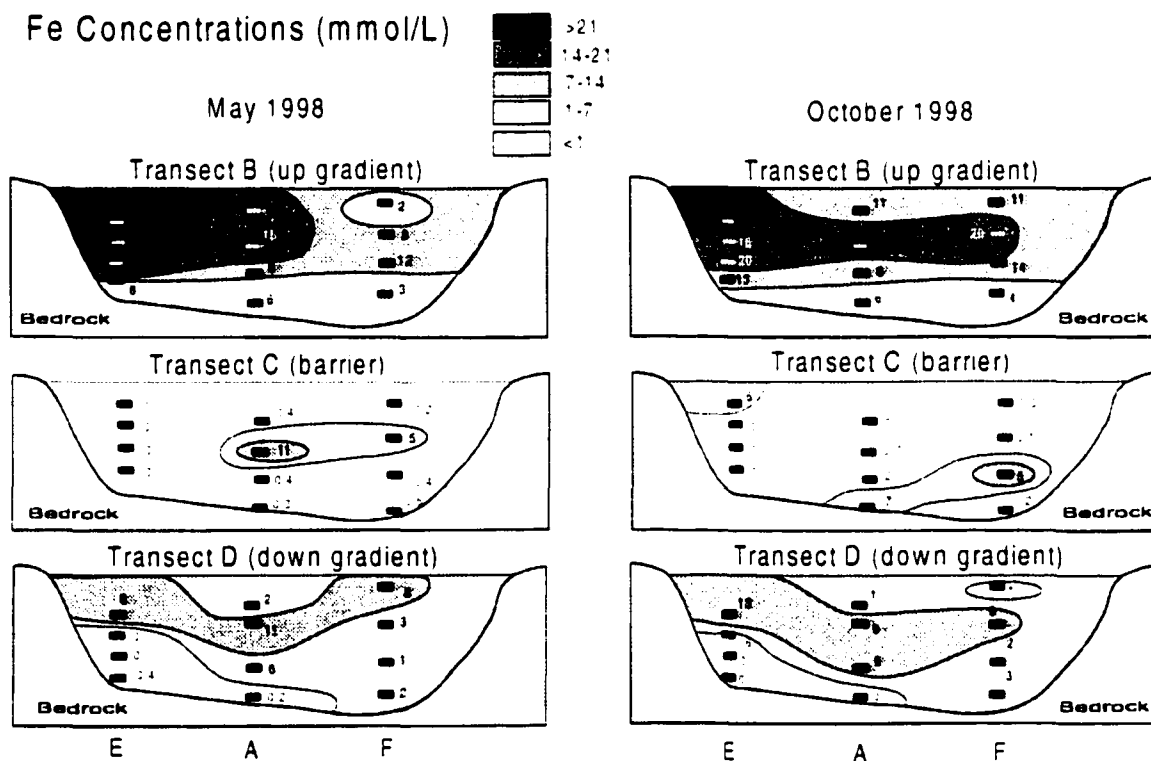


Figure 4.11 Cross-sectional profiles along transects B, C, and D, perpendicular to groundwater flow, of SO<sub>4</sub> concentrations for the May and October 1998 sampling periods. Flow direction is out of the page.

By subtracting concentrations on Transect C from values along Transect B, the amount of  $\text{SO}_4$  removed along the three transects parallel to flow (Transects A, E, and F) can be compared. The average removal for all points for the May and October data is  $17 \text{ mmol L}^{-1} \text{ SO}_4$  and  $9.1 \text{ mmol L}^{-1} \text{ Fe}$ . The vertically averaged amount removed along the centerline transect (Transect A) is  $12 \text{ mmol L}^{-1} \text{ SO}_4$ , and  $6 \text{ mmol L}^{-1} \text{ Fe}$ . This comparison indicates that, although Transect A is generally representative of changes through the barrier, this transect may underestimate, by about 1/3, the overall barrier performance. Data collection over the lifetime of the barrier was primarily along Transect A and data from this transect will be used to assess changes in the barrier with time.



**Figure 4.12** Cross-sectional profiles along transects B, C, and D perpendicular to groundwater flow, of Fe concentrations for the May and October 1998 sampling periods. Flow direction is out of the page.

#### 4.4.5 Lower Values in Barrier

Profiles perpendicular to flow within and down gradient of the barrier show that the concentrations of  $\text{SO}_4$  and Fe are often lower in sampling wells within the barrier compared to those down gradient. Groundwater bypassing treatment by flowing around the barrier could explain this trend. Flow bypassing the barrier is unlikely; the hydraulic gradient across the barrier is lower than the adjacent aquifer, indicating that there is no hydraulic force driving water around the barrier. In addition, some of the higher Fe and  $\text{SO}_4$  concentrations on the down-gradient side of the barrier are often found in sampling wells in the middle of the profile, and are not limited to the sides where bypassed water would reenter the down-gradient sand zone. Finally, concentrations of  $\text{SO}_4$ , Fe and alkalinity in down gradient well nests always reflect some degree of treatment: if a large fraction of untreated water was bypassing the barrier, some wells would likely exhibit concentrations reflective of no treatment.

An alternative explanation for higher Fe and  $\text{SO}_4$  values on the down gradient side of the barrier is heterogeneous flow. Because slower moving water in the barrier has undergone a greater degree of sulfate reduction, any bias in sampling towards a volume-average versus a flux-average will produce lower concentrations of  $\text{SO}_4$ , Fe and higher alkalinity. It is likely that water samples within the barrier reflect a volume-average bias and sampling from within the barrier underestimates the dissolved mass flux of  $\text{SO}_4$  and Fe through the barrier. In the down gradient, non-reactive zone, no correlation between hydraulic conductivity and water chemistry exists and volume biased sampling will not result in a shift in water chemistry. Therefore, the profile in the down-gradient sand zone is likely a better estimate of average mass fluxes through the barrier.

#### 4.4.6 Reactivity vs. Residence Time

Variations in the amount of  $\text{SO}_4$  and Fe removed along different flow paths through the barrier may also be caused by variations in reactivity. Because the primary

reaction, sulfate reduction, is bacterially mediated. profiles of bacterial populations and bacterial activity provide a measure of reactivity within the barrier. The dehydrogenase assay (DH) can be correlated to overall bacterial respiration, giving an indication of bacterial activity. Figure 13 shows vertical profiles of sulfate reducing bacterial populations (SRB) and dehydrogenase activity for sediment cores within the barrier taken adjacent to well nests RW29, 30 and 31.

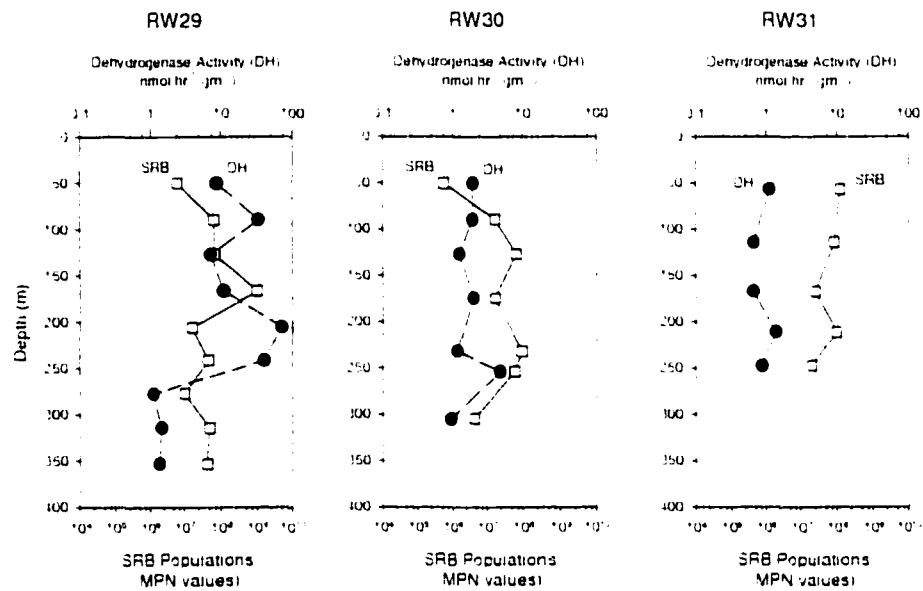


**Figure 4.13** Vertical profiles of populations of sulfate reducing bacteria (SRB) and overall bacterial activity as measured by dehydrogenase activity (DH) for cores taken adjacent to well nests RW29, RW30, and RW31.

These profiles indicate large variations in SRB populations and bacterial activity with depth in the barrier. Populations of SRB and values of DH vary by up to 2 orders of magnitude in each profile, illustrating the heterogeneous nature of bacterial population and activity within the barrier. The highest values for both SRB populations and DH are found in the central portion of the barrier where water is moving more rapidly and SO<sub>4</sub>

and Fe concentrations are highest. These limited data suggest that the bacterial populations may be responding to, and not controlling, observed vertical variations in water chemistry. Although spatial variations in reactivity cannot be discounted, the available data suggests that the observed differences in Fe and  $\text{SO}_4$  concentrations with depth in the barrier are primarily the product of variations in residence time.

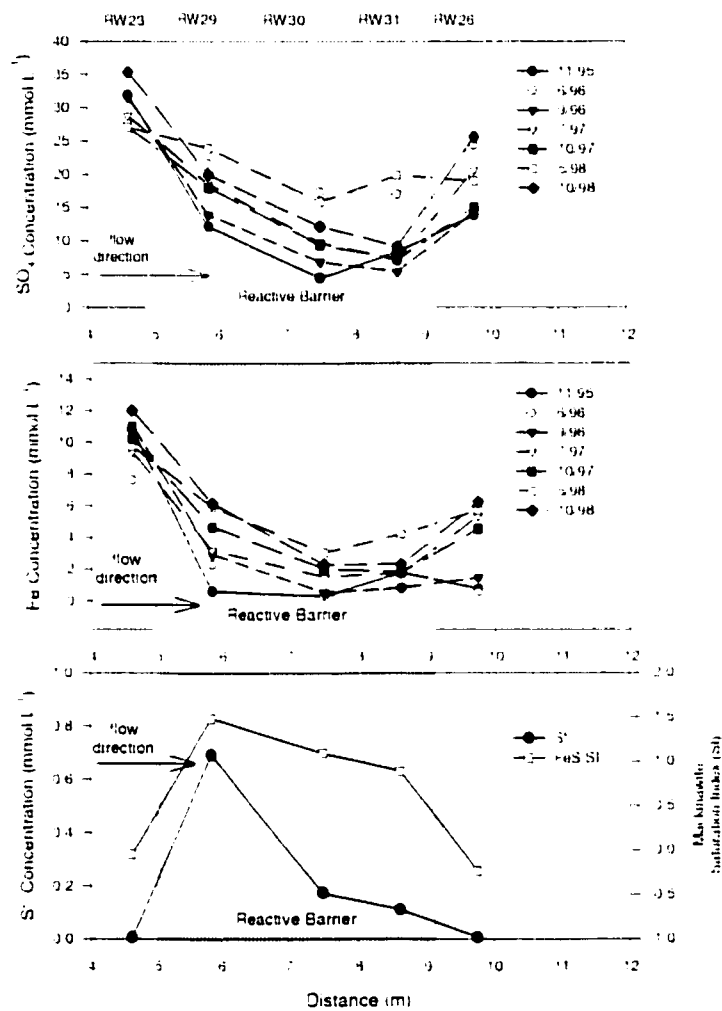


**Figure 4.14** Vertically averaged trends in concentrations of  $\text{SO}_4$ , Fe, for all sampling period, and sulfide concentrations and the saturation index for the mineral phase mackinawite for September 1996.

#### 4.4.7 Horizontal Trends

Vertically averaged concentrations along Transect A show horizontal trends in  $\text{SO}_4$  or Fe for each sampling date (Figure 14). Average input concentrations of  $\text{SO}_4$  range from 24 to 36  $\text{mmol L}^{-1}$  and average output ranges from 12 to 26  $\text{mmol L}^{-1}$ . Profiles exhibit similar trends with each sampling period. The rate of  $\text{SO}_4$  removal based on these vertically averaged values is highest at the front of the barrier. Sulfate concentrations decline by almost 20  $\text{mmol L}^{-1}$  between the input well nest (RW23) and the middle well nest (RW30), but exhibit almost no decline from the middle to the down-gradient well nest (RW31). Sulfate concentrations in the down-gradient sand zone tend to be elevated compared with those found within the barrier, likely the product of variable flow rates and subsequent volume biased sampling described previously.

The decline in the rate of sulfate removal with decreasing  $\text{SO}_4$  concentration suggests that the rate is a function of  $\text{SO}_4$  concentration. However, the rate of bacterially mediated sulfate reduction, as measured in marine sediments, is independent of sulfate concentration above about 3  $\text{mmol L}^{-1}$  (Boudreau and Westrich 1984; Roychoudhury and Van Cappellen, 1998), well below the measured concentrations within and down gradient of the reactive barrier. The heterogeneous nature of the barrier can reconcile this apparent contradiction.

Assuming that the variations in reactivity do not have a major impact on the rate of sulfate reduction, the rate, throughout the barrier, is expected to be uniform while  $\text{SO}_4$  concentrations remain above 3  $\text{mmol L}^{-1}$ . If the rate of flow were uniform through the barrier, then the profile of  $\text{SO}_4$  concentration is expected to decline linearly to 3  $\text{mmol L}^{-1}$  throughout the barrier, at which point the rate of removal would decline. However, flow rates (and residence times) vary in the barrier with flow path (Figure 15). The  $\text{SO}_4$  concentrations along the slower flow path at the base of the barrier exhibit a generally linear decline in concentration until the middle well nest where concentrations drop below the 3  $\text{mmol L}^{-1}$  level. The  $\text{SO}_4$  profile shows little decline from that point to the

down-gradient side of the barrier. Along the faster, central section of the barrier,  $\text{SO}_4$  concentrations decline less steeply and do not fall below the  $3 \text{ mmol L}^{-1}$  value. There is no obvious break in slope and concentrations of  $\text{SO}_4$  decline over the entire profile. These more discrete flow paths, produce curves that more closely follow the Boudreau and Westrich (1984) model.

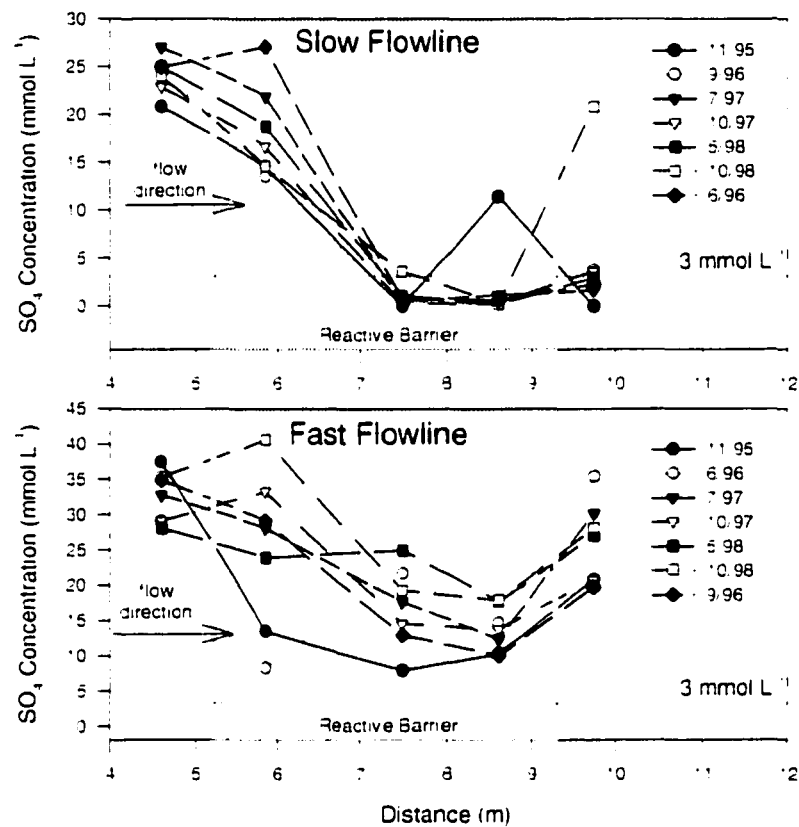


**Figure 4.15** Trends in concentrations of  $\text{SO}_4$  along slow flow path at bottom of the barrier and fast flow path in the middle of the barrier.

The distribution of flow path residence times through the barrier may be complex. However, a simplified model based on bimodal flow can explain the observed  $\text{SO}_4$  profiles within the barrier. Figure 16 shows the average field values for the slow and fast

flow paths. Predicted profiles for fast and slow flow paths are calculated using a Monod-style equation after Boudreau and Westrich (1984);

$$\text{sulfate removed} = \text{residence time} \left[ k \left( \frac{[SO_4]}{K_s + [SO_4]} \right) \right]$$

where  $SO_4$  is in  $\text{mmol L}^{-1}$   $k$  is the rate constant and the half saturation constant ( $K_s$ ) equals  $1.62 \text{ mmol L}^{-1}$  (Boudreau and Westrich, 1984). In this instance, the Monod formulation is empirically used to express the behavior of a reaction limited by availability of an electron acceptor. This equation allows the rate of sulfate reduction to remain independent of  $SO_4$  concentration above the experimentally determined half saturation constant ( $K_s$ ). As the  $SO_4$  concentration approaches this value, the rate of sulfate reduction decreases and asymptotically approaches zero as the  $SO_4$  concentration approaches zero.

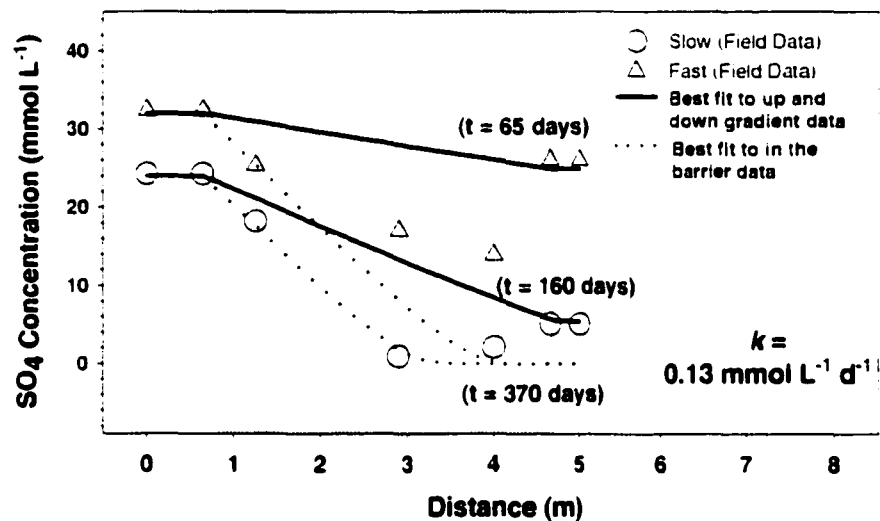


**Figure 4.16** Trends along fast and slow, and all flow paths averaged for all sampling periods and modeled rates of  $SO_4$  removal based on Monod formulation.

Along the fast flow path through the center of the barrier and slow flow path at the base of the barrier, the residence time and amount of  $\text{SO}_4$  removed is known. Therefore it is possible to solve for the rate constant ( $k$ ). Data from up and down gradient of the barrier are used to constrain curves for the fast and slow flow paths (Figure 16). The calculated rate constant ( $k$ ) equals  $0.13 \text{ mmol L}^{-1} \text{ d}^{-1}$ . This rate constant is assumed to be a function of the reactivity of the organic carbon. Using the calculated rate constant ( $k$ ), and adjusting the residence time, curves matching  $\text{SO}_4$  concentrations within the barrier can be obtained. A residence time of 370 days is consistent with these samples being biased towards a volume average. These calculated residence times also highlight the likely existence of zones of very slow moving water within the barrier.

At the front of the barrier, the  $\text{SO}_4$  concentration at all monitoring points is above  $3 \text{ mmol L}^{-1}$  (Figure 11). Along slower flow paths,  $\text{SO}_4$  concentrations drop below the  $3 \text{ mmol L}^{-1}$  level half way through the barrier. Along faster flow paths, water exits the barrier with concentrations of  $\text{SO}_4$  above  $3 \text{ mmol L}^{-1}$  (Figure 11). With greater distance through the barrier, the proportion of flow paths along which the  $\text{SO}_4$  concentration drops below the  $K_s$  value increases (Figure 11). The result of this trend is that the overall bulk rate of sulfate reduction decreases with distance into the barrier, even though the vertically averaged  $\text{SO}_4$  concentration remains above  $3 \text{ mmol L}^{-1}$  throughout (Figure 14). Limited sulfide data show elevated concentrations at the first well nest, which is consistent with the observed higher rates of sulfate reduction at the front of the barrier (Figure 14).

The rate of Fe removal is also greater at the front of the barrier (Figure 15). Concentrations of Fe decline most steeply at the front of the barrier, closely following the trend in  $\text{SO}_4$ . A previous study showing greater accumulation of acid volatile sulfides in cores taken near well RW23 compared to cores taken at RW30 and RW31 also indicates higher rates of Fe accumulations at the front of the barrier (Herbert et al., 2000). Profiles

of Fe along fast and slow flow paths exhibit similar profiles to those for  $\text{SO}_4$  (Figure 17), indicating that Fe removal is closely related to sulfate reduction.

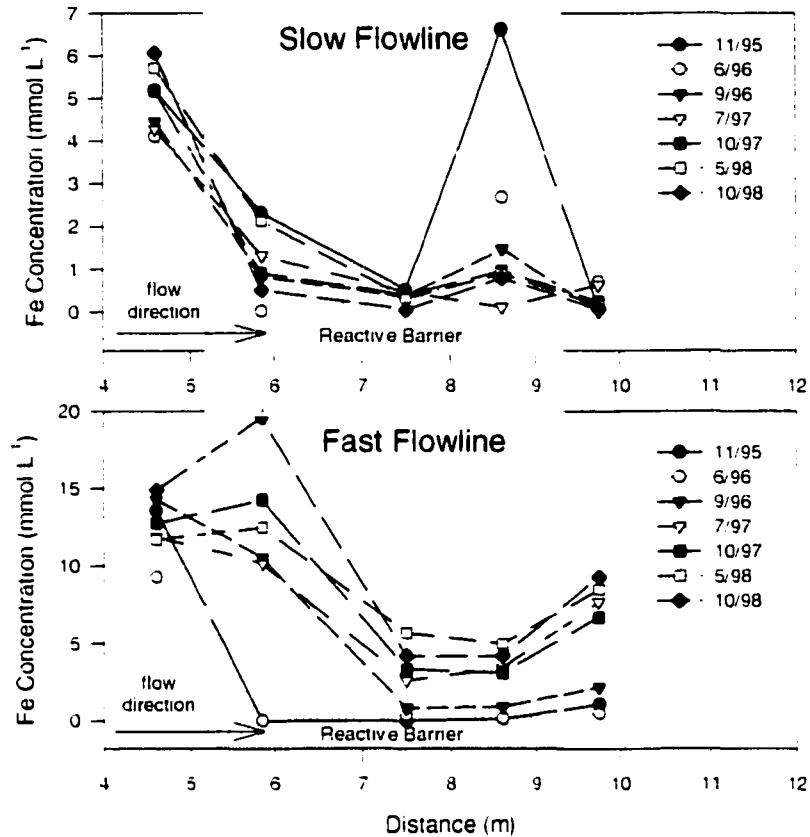


**Figure 4.17** Trends in concentrations of Fe along the slow flow path at the bottom of the barrier and the fast flow path in the middle of the barrier.

#### 4.4.8 Comparing Fe and $\text{SO}_4$ removal rates

If the rate of Fe sulfide precipitation is more rapid than sulfate reduction, then one would not expect elevated sulfide concentrations at the front of the barrier. The saturation indices for the precipitating sulfide mineral phase (mackinawite–FeS) would also be expected to remain constant across the barrier. However, elevated sulfide concentrations and higher saturation indices for mackinawite are observed at the front of the barrier, suggesting that the rate of Fe sulfide precipitation may be limiting (Figure

14). The laboratory determined rate of FeS precipitation of Rickard, 1995 is between  $10^2$  and  $10^6$  times greater than the observed rate of sulfate reduction in the barrier suggesting that FeS precipitation is transport limited.

The input ratio of  $\text{SO}_4$  to Fe is greater than the removal ratio, and there is generally excess  $\text{SO}_4$  after consumption of all of the Fe (compare Figures 11 and 12). Within zones of low flow, most of the Fe is removed and sulfide concentrations are elevated. It is likely that the effective rates of Fe removal are at least partially limited by transport of dissolved sulfide from these slow zones to adjacent zones of faster flow where Fe concentrations are higher. Dissolved sulfide concentrations (and SI values) decline by an order of magnitude by the first well nest in the down-gradient aquifer. Only limited accumulation of organic sulfides occurs in the barrier (Herbert et al., 1999), and it is likely that most of the sulfide produced is consumed by FeS precipitation. These observations suggest that, if the apparent rate of Fe sulfide precipitation is slower than that of sulfate reduction within the barrier, the difference in rates is small. Therefore, the rate of Fe removal by FeS precipitation in the barrier is primarily limited by the rate of sulfate reduction.

#### 4.4.9 Aqueous Phase Removal Rates

An overall rate of sulfate reduction and Fe sulfide precipitation for the barrier was calculated based on the change in concentrations between the vertically averaged up and down-gradient well nests along Transect A-A'. Figure 18 shows the vertically averaged molar concentrations of  $\text{SO}_4$  and Fe for well nests up (RW23) and down gradient (RW26) of the barrier with time. Although there are large variations over the three years of monitoring, profiles of water entering the barrier indicate that average  $\text{SO}_4$  concentrations are  $\approx 27 \text{ mmol L}^{-1}$  and Fe concentrations are  $\approx 10 \text{ mmol L}^{-1}$ . Profiles of down-gradient concentrations with time (RW26) show  $\text{SO}_4$  concentrations increasing from  $< 17 \text{ mmol L}^{-1}$  to  $> 23 \text{ mmol L}^{-1}$  and Fe concentrations increasing from  $< 1$  to about 6

mmol L<sup>-1</sup>. The differences between up- and down-gradient concentrations (RW23 and RW26) are plotted as regression lines in Figure 18.

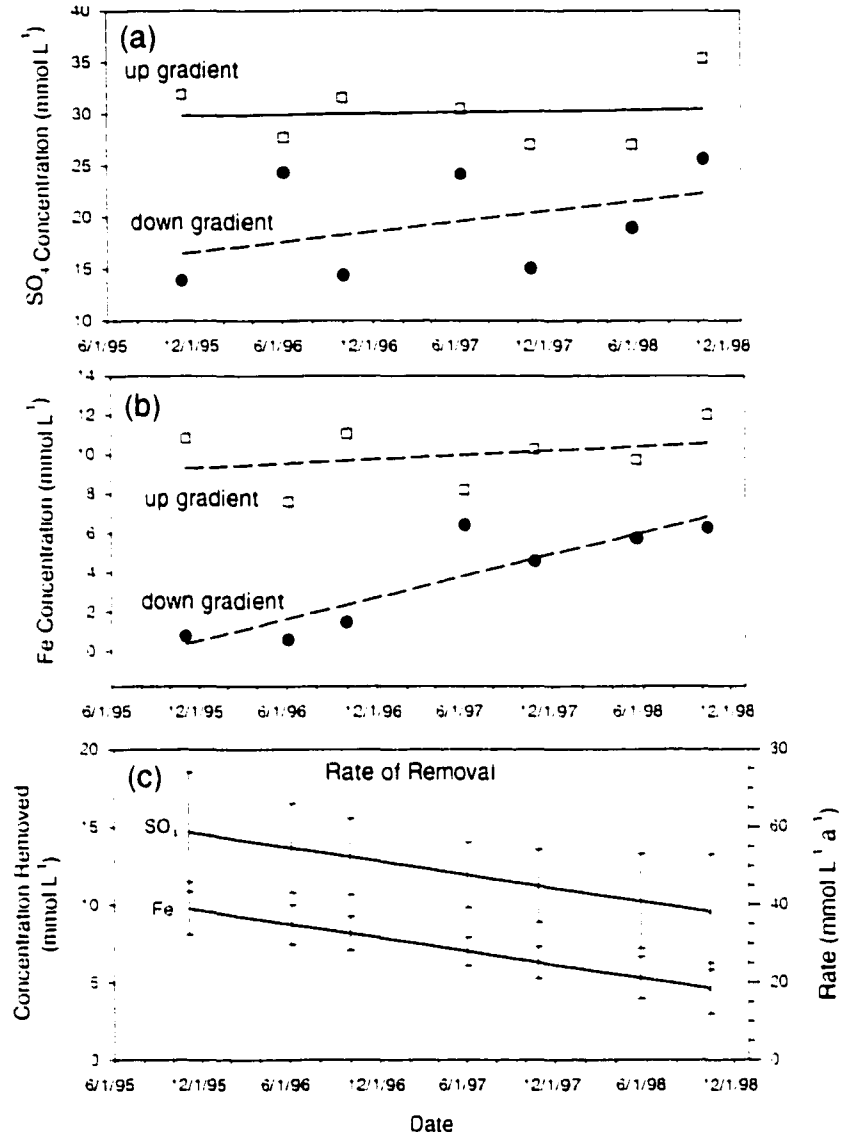


**Figure 4.18** (a) Vertically averaged concentrations of SO<sub>4</sub> in the well nests RW23 (up gradient) and RW26 (down gradient) versus time. (b) Vertically averaged concentrations of Fe in the well nests RW23 (up gradient) and RW26 (down gradient) versus time. (c) Removal of SO<sub>4</sub> and Fe based on the difference between RW23 and RW26 (up gradient - down gradient) concentrations versus time. Error bars reflect ± one standard error.

A linear fit was applied to the collected data because the limited amount of data did not suggest a more complex solution. However, the decline in rate may not be linear over the longer term. The change in constituent concentrations can be expressed as a change in concentration ( $\text{mmol L}^{-1}$ ; left-hand axis) or as a rate ( $\text{mmol L}^{-1} \text{a}^{-1}$ ; right-hand axis). Rate calculations are made using the equation:

$$\text{rate} = \frac{\Delta C}{t_R}$$

where  $\Delta C$  is the change in concentration (influent - effluent) and  $t_R$  is the residence time in days. Assuming a residence time of 90 days, the removal rate for  $\text{SO}_4$  is initially  $58 \text{ mmol L}^{-1} \text{a}^{-1}$  and declines to  $40 \text{ mmol L}^{-1} \text{a}^{-1}$  while the Fe removal rate is initially  $38 \text{ mmol L}^{-1} \text{a}^{-1}$  and declines to  $18 \text{ mmol L}^{-1} \text{a}^{-1}$ .

**Table I**

*Rates of S and Fe removal based on changes in aqueous concentrations (influent - effluent) and estimated residence times.*

Flow Path	$\text{SO}_4$ removed <sup>a</sup> (pore volume <sup>b</sup> )	Fe removed <sup>a</sup> (pore volume <sup>b</sup> )	Residence time (days)	$\text{SO}_4$ removal rate ( $\text{mmol L}^{-1} \text{a}^{-1}$ )	Fe removal rate ( $\text{mmol L}^{-1} \text{a}^{-1}$ )	S:Fe removal ratio
Ave.	13	8	90 <sup>b</sup>	53	32	1.7:1
Slow	31	12	160 <sup>c</sup>	71	27	2.6:1
Fast	5	7.7	65 <sup>c</sup>	28	43	0.65:1

a) Range in values based on (influent - effluent) sampling 3 months to 23 months after installation.  
 b) Assuming groundwater velocity of  $16 \text{ m a}^{-1}$ .  
 c) Based on groundwater velocities from flow modeling.

Table I shows the amount of  $\text{SO}_4$  and Fe removed along the fast flow path, the lower slow flow path, and the average for the A-A' Transect. As expected, the amount of  $\text{SO}_4$  and Fe removed is greater along the slow flow path. The ratio of S to Fe removal also varies: along the fast flow path the S to Fe ratio is 0.65:1, while along the slow flow path, the ratio is 2.6:1. This variation in Fe:S ratio suggests that the mechanism of

removal varies with the flow path. Along the slow flow path, most of the Fe is removed from the groundwater prior to the first well nest within the barrier (Figure 17). In contrast, approximately 60% of the  $\text{SO}_4$  removed occurs down gradient of the first well nest (Figure 15). Along the fast flow path, the rate of removal of  $\text{SO}_4$  and Fe is more uniform across the barrier. It is likely that along the slow flow path, sulfide precipitation is limited by low Fe concentrations beyond the first well nest, but the rate of sulfate reduction remains high until the middle of the barrier, resulting in greater removal of  $\text{SO}_4$  compared to Fe. Observed higher concentrations of dissolved sulfide along the slower flow path is consistent with this conclusion. However, dissolved sulfide concentrations are generally  $< 3 \text{ mmol L}^{-1}$  throughout the barrier, indicating an additional sink for reduced  $\text{SO}_4$  or dissolved sulfide exists.

#### 4.4.10 Solid Phase Accumulation Rates

Sequential extractions of sediment cores from the barrier have identified the primary solid phase sinks for S and Fe within the barrier and from this data rates of S and Fe accumulation were calculated (Herbert et al. 2000). These results indicate that the dominant sink for  $\text{SO}_4$  and Fe is solid phase mono-sulfides (Table II). However, other solid phase fractions are important. Along the slow flow path, approximately 20% of the accumulated solid phase S is as organic S while nearly all the accumulating solid phase Fe is found as sulfides. Along the fast flow path, approximately 15% of the solid phase S accumulated as sulfate and as much as 40% of the solid phase Fe accumulation is in a non-sulfide phase. Saturation indices, based on equilibrium calculations, indicate that equilibrium with respect to gypsum ( $\text{CaSO}_4 \cdot 2\text{H}_2\text{O}$ ) and siderite ( $\text{FeCO}_3$ ) is approached throughout the barrier but the groundwater is more highly saturated with respect to these minerals along the fast flow path. The precipitation of these mineral phases can account for the non-sulfide accumulation of Fe and S along the fast flow path.

**Table II**

*Rates of S and Fe removal based on solid phase digestions (from Herbert et al., 2000).*

<b>S Removal Rate (mmol L<sup>-1</sup> a<sup>-1</sup>)<sup>a</sup></b>				
Flow path	Sulfides <sup>b</sup>	Sulfate	Organic	Degassing/Other <sup>c</sup>
Slow	21	<1	4	?
Fast	30	6	<1	?
<b>Fe Removal Rate (mmol L<sup>-1</sup> a<sup>-1</sup>)<sup>a</sup></b>				
Flow path	Sulfides <sup>d</sup>	Non-sulfides <sup>e</sup>	Other <sup>c</sup>	
Slow	18	<1	?	
Fast	28	14	?	
<b>Totals (mmol L<sup>-1</sup> a<sup>-1</sup>)<sup>a</sup></b>				
Flow path	Total S	Total Fe	S:Fe ratio	
Slow	25	18	1.4:1	
Fast	36	42	0.85:1	

a) From Herbert et al. (2000), based on average accumulation from 3 months to 23 months after installation. The following ratios were used for rate conversion: barrier material composed of 40% gravel, 20% compost, and 40% water.

b) Equals acid volatile sulfur (AVS) + pyrite + elemental S.

c) Value is total inorganic sulfate - estimated pore water sulfate.

d) Sulfide Fe based on sulfide S assuming 1:1, S:Fe ratio for AVS, 2:1 for pyrite and no S as elemental S.

e) Total Fe - sulfide Fe.

#### 4.4.11 Comparing Solid and Aqueous Phase Rates

Due to a number of uncertainties, rigorous comparison of solid and aqueous phase rates is not appropriate. The solid phase data include accumulations during the first 3 months of the installation (when accumulation rates were highest) while aqueous phase sampling does not. The conversion of solid phase data to a mmol L<sup>-1</sup> a<sup>-1</sup> rate

requires an estimate of the effective porosity. The bulk porosity is around 0.4, but the nature of the organic material and the tailing observed in the chloride concentrations in the barrier (Figure 5), suggest that the effective porosity may be significantly less. Finally, the calculation of aqueous phase rates for the slow and fast flow paths is based on model-estimated residence times.

The ratios of S to Fe removal/accumulation along the different flow paths are not limited by these uncertainties. The ratios of S to Fe removal based on the solid and aqueous data are similar for the fast flow path with slightly more Fe removed relative to S. Assuming the majority of the sulfides are FeS, the excess Fe can be attributed to siderite precipitation. Along the slow flow path, the ratios of S to Fe removal for both the solid and aqueous data indicate greater removal of S relative to Fe. Assuming FeS is the primary sulfide, the difference can be partially attributed to the accumulation of organic sulfur and elevated sulfide concentrations. However, the aqueous data indicate greater than twice as much S removal compared to Fe, indicating a sink for S other than those measured by solid phase analysis.

It is possible that degassing of  $\text{H}_2\text{S}$  can account for the observed excess  $\text{SO}_4$  removed. Degassing is observed above the barrier, however this gas has not been analyzed. Potential gases that may be exsolving include  $\text{CO}_{2(g)}$ ,  $\text{CH}_{4(g)}$ , and  $\text{H}_2\text{S}_{(g)}$ . Dissolved sulfide concentrations indicate that  $\text{H}_2\text{S}_{(g)}$  is well below saturation within the reactive barrier. However,  $\text{CH}_4$  and  $\text{CO}_2$  concentrations may approach saturation and  $\text{H}_2\text{S}$  can be removed by partitioning into the  $\text{CO}_2$  or  $\text{CH}_4$  bubbles. Therefore,  $\text{H}_2\text{S}$  degassing may be primarily controlled by  $\text{CO}_2$  or  $\text{CH}_4$  bubble generation. It is unclear if this mechanism can account for a significant loss of S. Documented rates of  $\text{H}_2\text{S}$  degassing from artificial wetlands treating acid mine drainage by sulfate reduction were determined to be orders of magnitude smaller than sulfide precipitation as a sink for  $\text{SO}_4$  (Machemer et al., 1993).

Solid phase rate data (Herbert et al., 2000) suggest a rapid decline in the rate of sulfate reduction during the first 3 months and a more gradual decline from 3 to 23 months after installation. Though this trend is only based on accumulation rates over three sampling periods, it is consistent with a model of organic matter composed of fractions of varying reactivity where the most reactive material is consumed first and overall reactivity asymptotically approaches zero (Westrich and Berner, 1984; Boudreau and Rodrick, 1991). The timing of aqueous sampling sessions did not record the initial high rate and the data plotted in Figure 18, likely represent later time period of the curve where reactivity declined more gradually. Extending the trend in sulfate reduction into the future is speculative, but within the generally accepted models of organic carbon reactivity (Westrich and Berner, 1984; Boudreau and Rodrick, 1991 and references therein), the rate of sulfate reduction is predicted to decrease more gradually with time.

#### *4.4.12 Changing Groundwater Temperature*

Groundwater temperatures within the reactive barrier installation exhibit large seasonal variations (Figure 19). Ground surface temperatures range from  $>25$  °C in the summer to  $< 0$  °C in the winter and the groundwater temperature at 1 m depth varies from 2 to 19 °C. Fluctuations are dampened with depth with seasonal changes at the 3.6 meter depth of about 7 degrees. The temperature gradient inverts semi-annually with the highest temperatures at the surface during the summer and the highest temperatures at the base of the barrier during winter. These shifts in groundwater temperature are the product of two factors. First, the water table at the Nickel Rim site is at, or very near, the surface so there is no unsaturated zone to insulate the groundwater from fluctuating air temperatures. Second, surface water infiltrates the aquifer immediately up gradient of the barrier. The temperature of the surface water ranges from  $>25$  °C in the summer to 0 °C in the winter.

No measurable difference in groundwater temperature was detected spatially between the up-gradient aquifer and the groundwater within the barrier, indicating the metabolic processes within the barrier do not affect the groundwater temperature as it passes through the barrier.

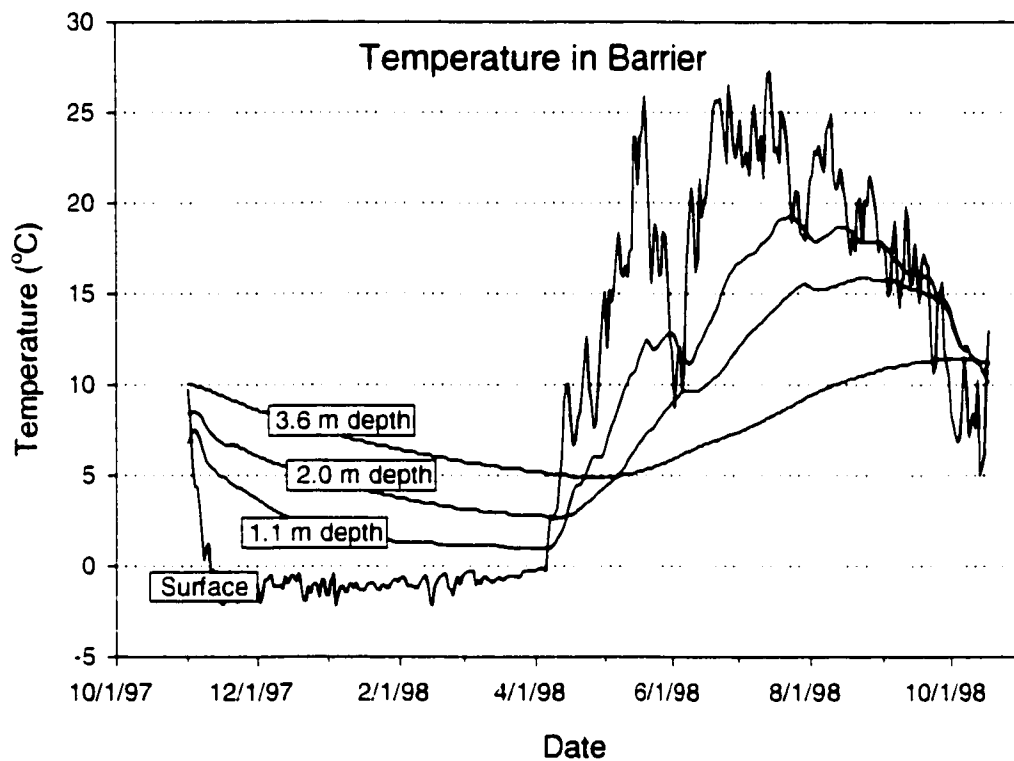


**Figure 4.19** Recorded temperature data within the barrier over a one year period. Curves are shown for ground surface temperature, 1.1 meter, 2.0 m and 3.6 m depths.

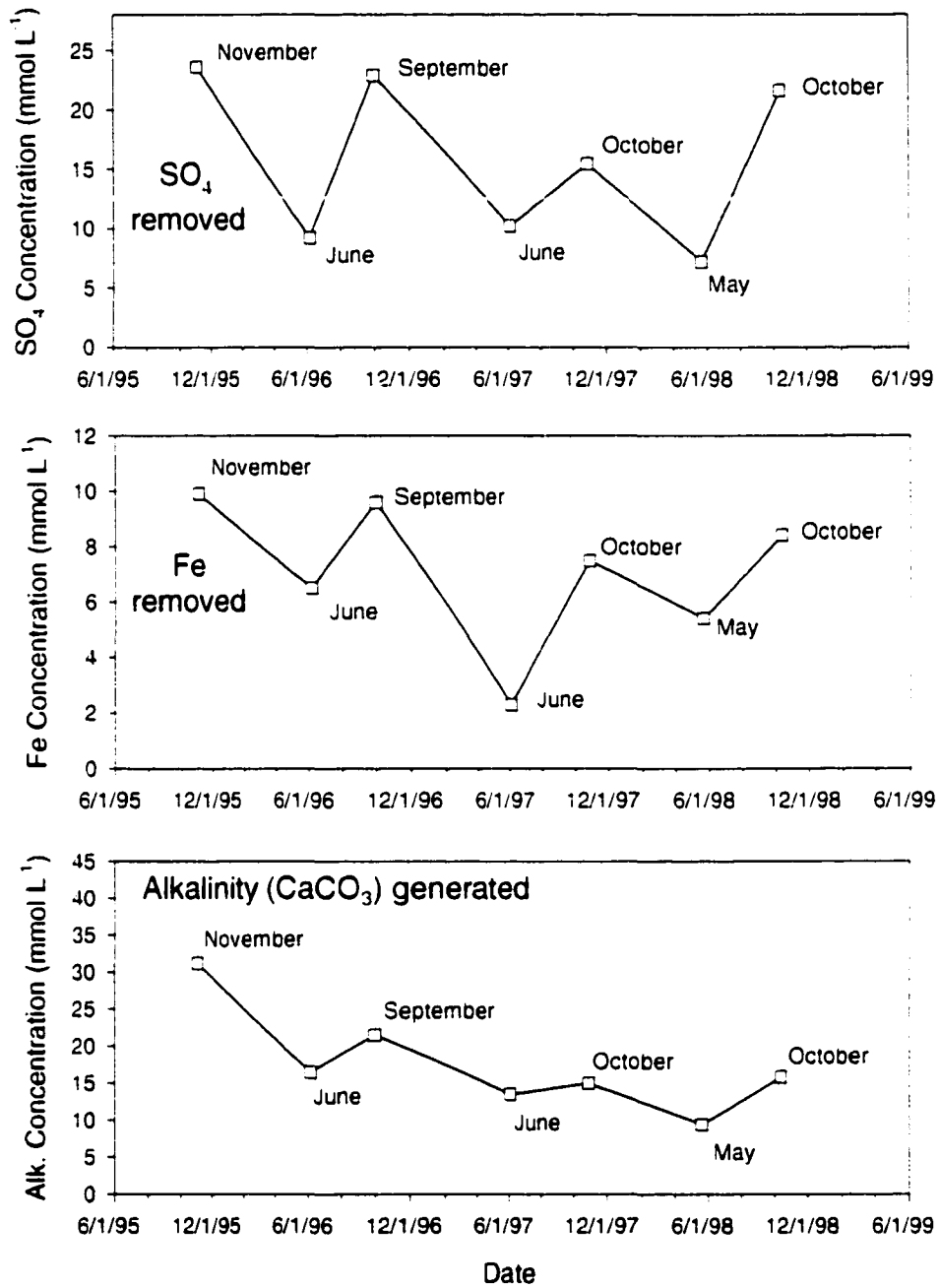


**Figure 4.20** Average concentrations of SO<sub>4</sub> and Fe removed and alkalinity added with time. Based on the RW23 concentrations - concentrations of all points (n=12) within the barrier.

#### 4.4.13 Effect of Temperature on Reactions in the Barrier

There are sufficient spatial and temporal variations in  $\text{SO}_4$  and Fe concentrations in the up gradient and down gradient waters to obscure effects of changing temperature on the rate of  $\text{SO}_4$  and Fe removal within the barrier. However, a plot of average concentration of constituents within the barrier (12 sampling points), subtracted from the average up gradient concentration does reveal seasonal cycling (Figure 20). More  $\text{SO}_4$  and Fe has been removed and more alkalinity generated in samples collected in the fall compared to spring. These seasonal fluctuations likely reflect changing rates of bacterially mediated sulfate reduction induced by higher groundwater temperatures during the summer and lower temperatures in the winter.

#### 4.4.14 Coupling Temperature to the Rate of Sulfate Reduction

The Arrhenius equation relates the effect of changing temperature on the rate of reaction. The Arrhenius equation can be expressed as:

$$\log \frac{k_1}{k_2} = \frac{E_a}{2.303R} \left[ \frac{1}{T_2} - \frac{1}{T_1} \right]$$

where  $k_1$  is the rate constant at temperature  $T_1$  (Kelvin),  $k_2$  is the rate constant at temperature  $T_2$  (Kelvin),  $R$  ( $1.987 \times 10^{-3} \text{ kcal mol}^{-1} \text{ K}^{-1}$ ) is the gas constant and  $E_a$  ( $\text{kcal mol}^{-1}$ ) is the activation energy of the reaction. Before applying this equation to the rate of sulfate reduction in the reactive barrier, the activation energy ( $E_a$ ) must be defined. The sulfate reduction reaction sequence is complex and it is likely that the rate of sulfate reduction is limited by the supply of low molecular weight compounds produced by fermentative activity (Westrich and Berner, 1984; Boudreau and Rodrick, 1991). In this application of the Arrhenius equation,  $E_a$  does not specifically refer to the activation energy of the sulfate reduction reaction but is defined as an apparent activation energy and is simply a measure of the response of the rate of sulfate reduction to a change in temperature. Previous workers have determined changes in sulfate reduction rate with

temperature and calculated a range of apparent  $E_a$  from 5 to 32 kcal mol<sup>-1</sup> (Jorgensen, 1977; Westrich and Berner, 1988; Sagemann et al., 1998; and references therein). Westrich and Berner also determined that the effective  $E_a$  increases with the age of the organic matter. These studies were conducted on sediment organic matter that is older (and probably less labile) than that used in the reactive barrier. It is likely that the  $E_a$  for sulfate reduction in the Nickel Rim reactive barrier is on the lower end of this range of  $E_a$ s.

Solving for  $k_1$  in the Arrhenius equation produces:

$$\log k_1 = \left[ \frac{E_a}{2.303R} \left( \frac{1}{T_2} - \frac{1}{T_1} \right) \right] + \log k_2$$

Letting  $k_2$  equal the effective rate constant of sulfate reduction as expressed by the zero order function from Figure 18:

$$k_2 = -0.0049(t) + 182.72$$

where  $t$  is the date in number of days,  $T_2$  equals the average annual temperature at 2 m depth (9 °C), while  $T_1$  is equal to the temperature function expressing the 2 m depth field-measured temperature data (Figure 21):

$$T_1 = 8.9843 - 5.8 \left[ \sin(2(\pi)(t)/365 - 150.55) \right]$$

where  $t$  is the date expressed as number of days.

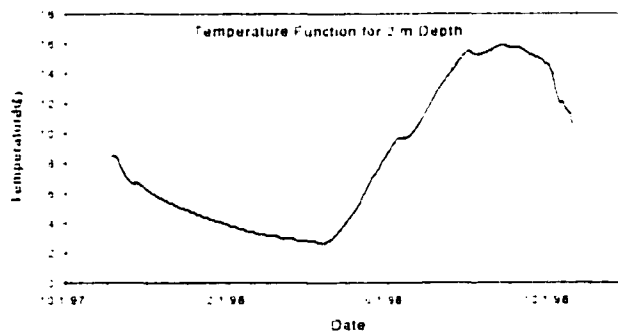


**Figure 4.21** Temperature at 2 m depth (solid line) and plot of four parameter sine function (dotted line) for those data.

The only unknown variable is the activation energy ( $E_a$ ) term. If an effective  $E_a = 25$  kcal mol<sup>-1</sup> is arbitrarily assumed, the value of  $k_1$  can be calculated with time. The temperature adjusted rate ( $k_1$ ) is plotted with time in Figure 22, showing that the rate of sulfate removal is predicted to decline sinusoidally with time.

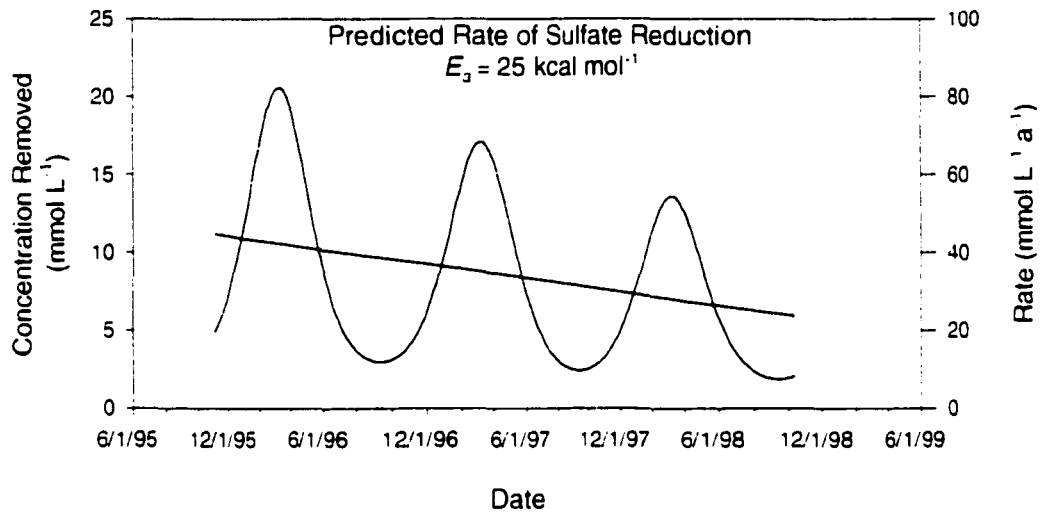


**Figure 4.22** Predicted rate of sulfate removal versus time based on average removal rate (Figure 18), the Arrhenius equation and an apparent activation energy of  $E_a = 25$  kcal mol<sup>-1</sup>.

#### 4.4.15 Calculating an effective $E_a$

If the rates are known at different temperatures, the Arrhenius equation can be used to solve for the apparent activation energy ( $E_a$ ). The slope of the average rate of SO<sub>4</sub> removal from Figure 18 is specified as  $k_2$ . Since the primary interest is the change in rate, it is not necessary to specify the y intercept. The average temperature for the 2 m depth (9 °C) is specified as  $T_2$  and the sinusoidal temperature function for the 2 m depth is input for  $T_1$ . The  $k_1$  variable is the field-collected SO<sub>4</sub> values in Figure 20.

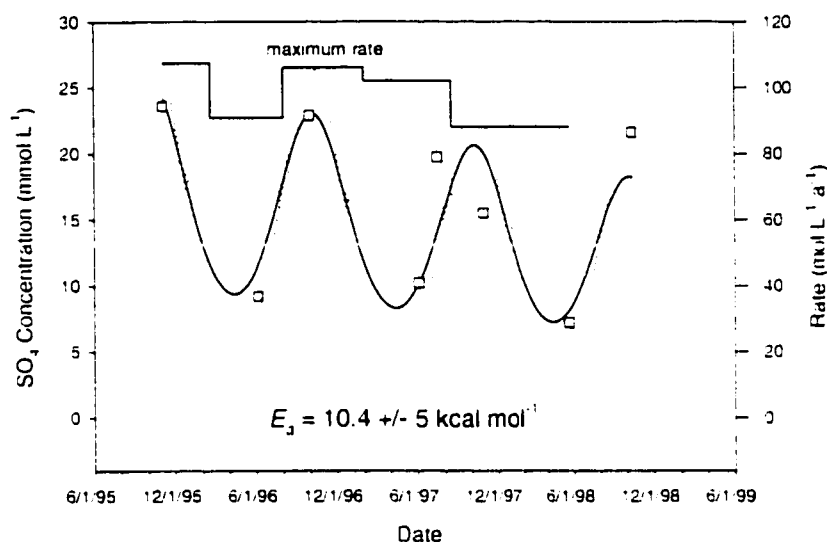


**Figure 4.23** The curve based on Arrhenius equation (solid line) for observed temperature induced fluctuations in  $\text{SO}_4$  removal (square boxes) yielding an apparent activation energy  $E_a = 10 \text{ kcal mol}^{-1}$ . Dashed curve shows sensitivity of fit to changing  $E_a$  by  $\pm 5 \text{ kcal mol}^{-1}$ . Stepped solid line indicates maximum rate based on observed removal in well nest RW23 (down gradient).

Therefore the unknowns are the y-intercept and the apparent activation energy  $E_a$ . A solution is obtained by simultaneously solving for the y-intercept and  $E_a$  to achieve a best fit to the field-collected  $\text{SO}_4$  concentration data ( $k_1$ ) (Figure 23). The predicted effective  $E_a$  is  $10 \text{ kcal mol}^{-1}$ , which is at the lower end of the range of values determined in previous studies. This low value confirms that the organic material used in the barrier is labile and reactive.

Specifying a range of  $E_a$  values and solving for the best fit to the field data suggests the range of effective  $E_a$  that provide a reasonable fit (values shown as dashed lines in Figure 23). These plots indicate that the field data constrain the minimum  $E_a$  value, but do not constrain the maximum  $E_a$  value. However, the lowest measured  $\text{SO}_4$  concentration (maximum removal value) provides an upper limit on the  $E_a$ . Concentrations in well nest RW31 during the fall sampling event reflect water that

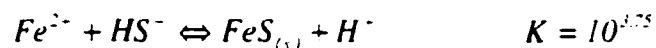
passed through the barrier during the period of highest sulfate reduction rates (the month of August). The lowest vertically averaged concentration measured for  $\text{SO}_4$  for RW31 is  $5 \text{ mmol L}^{-1}$ . This value, subtracted from the input concentration, can be used to constrain the maximum sulfate reduction rate in the barrier (stepped horizontal line, Figure 23). With this constraint on the highest rate of  $\text{SO}_4$  reduction, the range of potential  $E_a$  is limited to a value very close to the best fit  $10 \text{ kcal mol}^{-1}$  value. The modeled curve fits the observed field data quite well indicating that the observed seasonal variations in sulfate removal can be attributed to the effect of changing temperature on the rate of sulfate reduction.

#### 4.4.16 Effect of Temperature on Sulfide Solubility

Because  $\text{SO}_4$  reduction is the rate-limiting step in Fe removal, the rate of sulfide precipitation may approach thermodynamic equilibrium. To estimate the potential effect that the changing temperature has on the removal of Fe from the barrier, the effect of changing temperature on the solubility product of the precipitating mineral phase mackinawite can be calculated. The van't Hoff equation can be used to calculate the effect of changing temperature on the equilibrium constant:

$$\log K_2 = \log K_1 + \frac{\Delta H_R}{2.303R} \left[ \frac{1}{T_1} - \frac{1}{T_2} \right]$$

where  $K_1$  is the equilibrium constant at temperature  $T_1$ ,  $K_2$  is the equilibrium constant at  $T_2$  and  $\Delta H_R$  is the enthalpy of reaction and is assumed to be constant with changing temperature. A similar approach to calculating the affect of temperature on reaction rate can be taken. If the precipitation reaction is written as:



$K_1$  equals  $K_{\text{mackinawite}}$  (Benning et al., 1999) at  $T_1 = 25 \text{ }^\circ\text{C}$ .  $T_2$  is defined by the 2 m depth temperature function and the enthalpy ( $\Delta H_r$ ) for mackinawite is specified as  $-12.46 \text{ kcal mol}^{-1}$  (Benning et al., 1999). The equation can be solved for the remaining unknown,  $K_2$ .

Assuming equilibrium conditions and that Fe and  $\text{HS}^-$  vary equally, the theoretical change in Fe concentration can be calculated (Figure 24). This sinusoidal plot is inverse to the observed changes in Fe and  $\text{SO}_4$ , suggesting that the changes in Fe concentration can not be attributed to the fluctuating solubility of mackinawite.

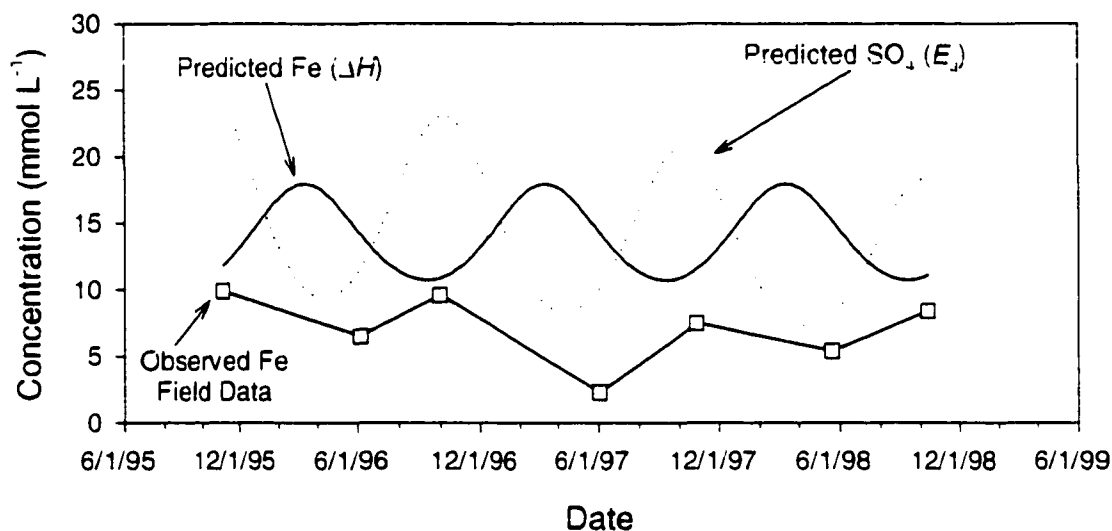


**Figure 4.24** Observed (square boxes) and predicted Fe concentrations with time based on: 1) changing solubility of mackinawite (based on van't Hoff equation,  $\Delta H$ ) and 2) changing rates of  $\text{H}_2\text{S}$  generation expressed as  $\text{SO}_4$  removal (based on Arrhenius equation,  $E_a$ ).

The changing solubility of the potentially important secondary precipitating phases siderite ( $\text{FeCO}_3$ ) and gypsum ( $\text{CaSO}_4 \cdot 2\text{H}_2\text{O}$ ) may also contribute to the observed seasonal changes in dissolved  $\text{SO}_4$  and Fe. The enthalpy of reaction ( $\Delta H_R$ ) for siderite precipitation is  $5.3 \text{ kcal mol}^{-1}$  (Allison et al., 1990) indicating that siderite is less soluble at higher temperatures. Therefore, the seasonal variation in Fe concentrations may also be attributable to the changing solubility of siderite. The enthalpy of reaction ( $\Delta H_R$ ) for gypsum is near zero ( $0.109 \text{ kcal mol}^{-1}$ ) and the annual  $17^\circ\text{C}$  change within the barrier will have little effect on gypsum solubility or  $\text{SO}_4$  concentrations. It should be noted that siderite and gypsum solubilities are also directly dependent on  $\text{CO}_3^{2-}$  and  $\text{Ca}^{2+}$  activities.

respectively, and the seasonal changes in the solubilities of both of these minerals are difficult to predict with simple calculations.

#### 4.4.17 Implications for Barrier Performance and Design

The calculated bulk rates for  $\text{SO}_4$  and Fe removal for the barrier represent an average of the rates along different flow paths, are a function of barrier thickness and cannot be used to retrieve globally applicable rate constants. This is best illustrated by noting that rates based on flow through the first half of the barrier (or the same barrier, half as thick) would be much greater (Figure 14). The rate constant based on slow and fast flow paths more closely approximates a global rate constant. Despite the noted limitations in this rate constant, it can be used to estimate required residence times for the treatment of water containing a known  $\text{SO}_4$  and Fe concentration. Assuming the average input concentrations of  $\text{SO}_4$  ( $30 \text{ mmol L}^{-1}$ ) and Fe ( $10 \text{ mmol L}^{-1}$ ) and a 1:1 removal ratio, the minimum residence time for removal of >95% of the Fe in the Nickel Rim barrier is approximately 90 days. Despite an average residence time approximately equal to the minimum required residence time of 90 days, complete removal of Fe is not achieved. Less Fe is removed than predicted because the low flow zones are underutilized: along these slower flow lines all Fe is removed and excess sulfide is not utilized for mackinawite precipitation. In addition, when the  $\text{SO}_4$  concentration drops near the half saturation constant ( $K_s$ ), the rate of  $\text{SO}_4$  reduction will decline.

Specific enhancements to the reactive mixture composition to improve homogeneity and barrier performance may include increasing the gravel fraction or selecting a different particle size distribution for the organic mixture. Ultimately, however, barriers must be designed to account for preferential flow, and a thickness must be selected to ensure that the residence time of all flow paths is sufficient to provide acceptable removal rates.

Changing groundwater temperature has a large impact on barrier performance. Using the apparent activation energy value of  $10 \text{ kcal mol}^{-1}$ , a decrease in groundwater temperature of  $10 \text{ }^\circ\text{C}$ , will decrease the rate by nearly half. At the Nickel Rim site, the average air temperature is only a few degrees lower than at the bottom of the aquifer. Therefore, application of an insulating layer above the aquifer will produce a more uniform sulfate reduction rate but will result in only a small increase in the annually averaged rate. At sites where the average groundwater temperature is significantly greater than the average air temperature, insulating the aquifer may boost barrier performance. Conversely, when the average air temperature is greater than the average groundwater temperature, insulating the aquifer may decrease performance.

The rate of sulfate reduction controls the treatment capacity of the Nickel Rim barrier. A higher rate may be achieved by selection of a material that can be more rapidly metabolized by sulfate reducing bacteria. An organic carbon source containing a higher fraction of labile short chain organic compounds will be more reactive yielding higher performance for a given barrier thickness. Sulfate reducing bacteria can also utilize  $\text{H}_2$  as an electron donor, and a substrate that provides  $\text{H}_2$  may also produce higher rates of treatment. A reactive barrier in Elizabeth City, North Carolina, composed of zero valent iron, generates large amounts of  $\text{H}_2$ . The rate of sulfate reduction in this barrier is higher than the rates calculated for the Nickel Rim barrier (Mayer, 1999). Therefore, the addition of zero valent iron to an organic carbon barrier may result in increased rates of sulfate reduction and improved reactive barrier performance. The additional costs of any changes in reactive material must be weighed against simply increasing the barrier thickness using inexpensive compost materials.

The calculated  $E_a$  allows comparison to previous laboratory column studies (Waybrant, 1995). In this laboratory study, flow-through columns containing organic carbon were used to simulate a reactive barrier for sulfate reduction and metal sulfide precipitation. The input water for the laboratory column was chosen to match the

groundwater in the Nickel Rim aquifer and the organic mixture used in the barrier was based on the mixtures used in the column studies. In this laboratory study, conducted over a two year period at 25 °C, the SO<sub>4</sub> reduction rate was 280 mmol L<sup>-1</sup> a<sup>-1</sup>. Normalizing this rate to the average temperature in the Nickel Rim aquifer (9 °C) results in a rate of 103 mmol L<sup>-1</sup> a<sup>-1</sup>, approximately 2 times the rate observed in the aqueous phase field data. The similarity between these two values is good considering the uncertainty associated with the residence time for the Nickel Rim barrier. That the rates are similar indicates that, within a factor of 2, the laboratory values correctly predicted the treatment capacity of the field installation.

#### 4.5 REFERENCES

- Allison, J.D., Brown, D.S., and Nova-Gradac, K.J. 1990. *MINTEQA2/PRODEFA2, A geochemical assessment model for environmental systems: Version 3.0 user's manual*. Athens, GA, U.S. E.P.A.
- Bain, J.G.; Blowes, D.W.; and Robertson, W.D. 1999. Hydrogeochemistry of a sand aquifer affected by drainage from the Nickel Rim tailings. *J. Contam. Hydrol.* In Press
- Ball, J.W.; Nordstrom, D.K. 1991. *User's manual for WATEQ4F, with revised thermodynamic data base*. U.S.G.S., O.F.R. 91-183.
- Benner, S.G.; Blowes, D.W.; Gould, W.D.; Herbert Jr., R.B.; Ptacek, C.J. 1999. Geochemistry of a permeable reactive barrier for metals and acid mine drainage. *Environ. Sci. Tech.*, 33, 2793-2799.
- Benner, S.G.; Blowes, D.W.; Ptacek, C.J. 1997. Full-scale porous reactive wall for the prevention of acid mine drainage. *Ground Water Monit. Remed.*, 17, 99-107.
- Benner, S.G.; Gould, W.D.; Blowes, D.W. 2000. Microbial populations associated with the generation and treatment of acid mine drainage. *Chem. Geol.* In Press
- Benning, L.G., Wilkin, R.T., and Barnes, H.L. 1999. Reaction pathways on the Fe-S system below 100 degrees C. In Press *Chem. Geol.*
- Boudreau, B.P.; Ruddick B.R. 1991. On a continuum representation of organic matter diagenesis. *Amer. J. Sci.*, 291, 507-538.
- Boudreau, B.P.; Westrich, J.T. 1984. The dependence of bacterial sulfate reduction on sulfate concentration in marine sediments. *Geochim. Cosmochim. Acta*, 48, 2502-2516.

- Gillham, R.W.; Sudicky, E.A.; Cherry, J.A.; Frind, E.O. 1984. An advection-diffusion concept for solute transport in heterogeneous unconsolidated geologic deposits. *Water Resour. Res.*, 20 (3), 369-378.
- Guiguer, N., Molson, J., Franz, T., and Frind, E. 1994. FLOTRANS User Guide Ver. 3.0: Two-Dimensional Steady-State Flownet and Advective-Dispersive Contaminant Transport Model. Waterloo Hydrogeologic Inc. Waterloo, Ontario, Canada.
- Herbert Jr., R.B.; Benner, S.G.; Blowes, D.W. 2000. Solid phase iron - sulfur geochemistry of a reactive barrier for treatment of mine drainage. *Appl. Geochem.* In Press
- Jorgensen, B.B. 1977. The sulfur cycle of a coastal sediment (Limfjorden, Denmark). *Limnol. Oceanogr.*, 22 (5), 814-832.
- Ladd, J.N. 1978. Origin and range of enzymes in soil. *Soil Enzymes*. Burns, R.G., Eds. Academic Press, p. 51-96.
- Machemer, S.D.; Reynolds, J.S.; Laudon, L.S.; Wildeman, T.R. 1993. Balance of S in a constructed wetland built to treat acid mine drainage. Idaho Springs, Colorado, USA. *Appl. Geochem.*, 8 587-603.
- Mayer, K.U. 1999. A Numerical Model for Multicomponent Reactive Transport in Variably Saturated Porous Media. Ph.D. Thesis, University of Waterloo, Waterloo Ontario.
- Parker, J.C.; van Genuchten, M.T. 1984. Flux-averaged and volume-averaged concentrations in continuum approaches to solute transport. *Water Resources Research*. 20 (7), 866-872.
- Rickard, D. 1995. Kinetics of FeS precipitation: Part I. Competing reaction mechanisms. *Geochim. Cosmochim. Acta*, 59 (21), 4367-4379.
- Roychoudhury, A.N.; Viollier, E.; Van Cappellen, P. 1998. A plug flow-through reactor for studying biogeochemical reactions in undisturbed aquatic sediments. *Appl. Geochem.*, 13, 269-280.

- Sagemann, J.; Jorgensen, B.B.; Greeff, O. 1998. Temperature dependence and rates of sulfate reduction in cold sediments of Svalbard, Arctic Ocean. *Geomicrobiol. J.*, 15, 85-100.
- Waybrant, K.R. 1995. *The Prevention of Acid Mine Drainage Using In Situ Porous Reactive Walls: A Laboratory Study*. M. Sc.Thesis. University of Waterloo, Waterloo, Ontario, Canada.
- Westrich, J.T.; Berner, R.A. 1988. The effect of temperature on rates of sulfate reduction in marine sediments. *Geomicrobiol. J.*, 6, 99-117.
- Westrich, J.T.; Berner, R.A. 1984. The role of sedimentary organic matter in bacterial sulfate reduction: the *G* model tested. *Limnol. Oceanogr.*, 29, 236-249.

## Chapter 5

### *Microbial Populations Associated with the Generation and Treatment of Acid Mine Drainage*

#### 5.1 CHAPTER SUMMARY

Bacterial populations and water chemistry were profiled throughout the groundwater flow system associated with the Nickel Rim mine tailings impoundment Ontario, Canada. Groundwater containing high concentrations of sulfate (2000-12000 mg/L) and iron (500-4000 mg/L) flows from the tailings into an adjacent aquifer. A portion of the plume then discharges to the surface where ferrous iron is oxidized creating low pH (pH<3) conditions. The remaining groundwater passes through a permeable reactive barrier which induces sulfate reduction and metal sulfide precipitation. Elevated populations of iron (IOB) and sulfur (SOB) oxidizing bacteria are restricted to hydrologically defined zones of recharge and discharge. Sulfur oxidizers are highest in the tailings ( $1.27 \times 10^3$  MPN/g) where sulfide minerals are exposed to oxygen and oxygen-rich recharge water. Iron oxidizing bacteria were highest ( $9.56 \times 10^5$  MPN/g) where tailings-derived effluent, rich in Fe(II), discharges to the aerobic surface water environment. Populations of both iron and sulfur oxidizing bacteria in the zone of active oxidation are low compared to those found at other, less mature, tailings sites. Active oxidation in the Nickel Rim tailings is occurring immediately above the water table where the water content is high. The high water content limits oxygen ingress and sulfide oxidation, and the associated populations of oxidizing bacteria are low. Populations of sulfate reducing bacteria (SRB) are elevated in the tailings and in portions of the down-gradient aquifer where organic carbon concentrations are high. The highest population ( $3.73 \times 10^7$  MPN/g) of SRB were found where sulfate-bearing water migrates through the organic carbon-rich permeable reactive barrier. At locations with high populations of SRB, elevated populations of SOB were also found, suggesting SOB in these zones are metabolizing the reduced sulfur species produced by the SRB in adjacent, but disparate, redox microenvironments.

## 5.2 INTRODUCTION

The oxidation of sulfide minerals in mine waste material can produce high concentrations of dissolved sulfate and iron and generate acidic conditions that enhance mobility of dissolved metals in the pore water. A hydrogeological flow system often develops within waste rock pile or tailings impoundments that transports this sulfate and iron-rich, acidic water downwards into underlying or adjacent aquifers and the effluent eventually discharges to nearby surface water bodies (Dubrovsky et al., 1985). Dissolution of mineral phases along the flow path within the aquifer buffers the pH of the acidic effluent to near neutral (Morin et al., 1988). Upon discharge, dissolved ferrous iron oxidizes and precipitates as ferric oxyhydroxide minerals, principally ferrihydrite and goethite, producing further acidity.

Oxygen is the ultimate oxidant of sulfide minerals in natural surface systems and is the direct oxidant at pH >4 (Nordstrom and Alpers, 1999). Where the pH is below 4, sulfides are oxidized by ferric iron. In most mine wastes however, oxygen is the primary oxidizing agent of ferrous iron to ferric. Because of this limitation, sulfide oxidation generally occurs only in areas where dissolved or gaseous oxygen is present.

The primary mechanism of bacterial catalysis of sulfide oxidation is indirect, through the oxidation of ferrous to ferric iron. A variety of bacteria, including *Thiobacillus ferrooxidans*, mediate the oxidation of sulfides and ferrous iron. The rate limiting step in sulfide oxidation is often the oxidation of ferrous to ferric iron and the bacterial rate of iron oxidation is estimated to be up to  $10^5$  greater than rates under abiotic conditions (Singer and Stumm, 1970, Nordstrom and Southam, 1997). Enumerations of sulfur and iron oxidizing bacteria in tailings show high populations of these bacteria within the zone of active oxidation. Acidophilic iron oxidizers (*i.e.* *Thiobacillus ferrooxidans*, *Leptosprillum ferrooxidans*) have been found in tailings at populations of up to  $10^8$  MPN/g (Southam and Beveridge, 1992, Blowes et al., 1995, Blowes et al., 1998). Populations of acidophilic, sulfur oxidizing bacteria (*i.e.*

*Thiobacillus thiooxidans*) are elevated in tailings and may also play an important role in sulfide oxidation. *Thiobacillus ferrooxidans* have been shown to oxidize reduced sulfur compounds but *Thiobacillus thiooxidans* are unable to oxidize iron (Nordstrom and Southam, 1997). Where effluent containing high concentrations of ferrous iron discharges to the surface as seeps or flows from mine workings, populations of acidophilic iron oxidizing bacteria are also high (up to  $10^9$  cells/mL) (Schrenk et al., 1998).

Promotion of sulfate reduction and metal sulfide precipitation using organic carbon may provide an effective remediation mechanism for acid mine drainage. Reduction of sulfate to sulfide and the subsequent precipitation of Fe and other metal sulfide phases can greatly decrease the potential acidity and trace metal content of the water. At surface temperatures and pressures, sulfate reduction is bacterially mediated, and abiotic rates are negligible. Sulfate reduction is mediated by the phylogenically diverse anaerobes, Sulfate Reducing Bacteria (SRB).

### 5.2.1 The Nickel Rim Research Site

The Nickel Rim tailings were deposited between 1953 and 1958. The deposited tailings contain approximately 5 wt.% sulfide sulfur of which 98% is pyrrhotite ( $\text{Fe}_{1-x}\text{S}$ ) with minor amounts of chalcopyrite ( $\text{Cu}_2\text{S}$ ), pentlandite ( $(\text{Fe,Ni})_9\text{S}_8$ ), pyrite ( $\text{FeS}_2$ ) and marcasite ( $\text{FeS}_2$ ) (Jambor and Owens, 1993, Johnson et al., 1999). The water table in the tailings is at a depth of 1-2 meters. A groundwater plume, containing high concentrations of ferrous Fe and  $\text{SO}_4$  emanates from the tailings. Approximately 50% of this plume water discharges to the surface at the foot of the tailings dam. The remaining 50% of the plume discharges to Moose Lake about 160 m down-gradient (Figure 1) (Bain 1996, Johnson et al., 1999, Bain et al., 1999). An in situ, permeable reactive barrier was installed into the path of this plume approximately 110 m down gradient of the tailings impoundment (Benner et al., 1997). The reactive barrier, composed of organic compost

material, promotes sulfate reduction and metal sulfide precipitation, improving groundwater quality by removing metals and generating alkalinity (Benner et al., 1999).

We have examined the distribution of sulfur and iron oxidizing and sulfate reducing bacteria along groundwater flow paths from the zone of active sulfide oxidation in the mine tailings impoundment to discharge at the surface.

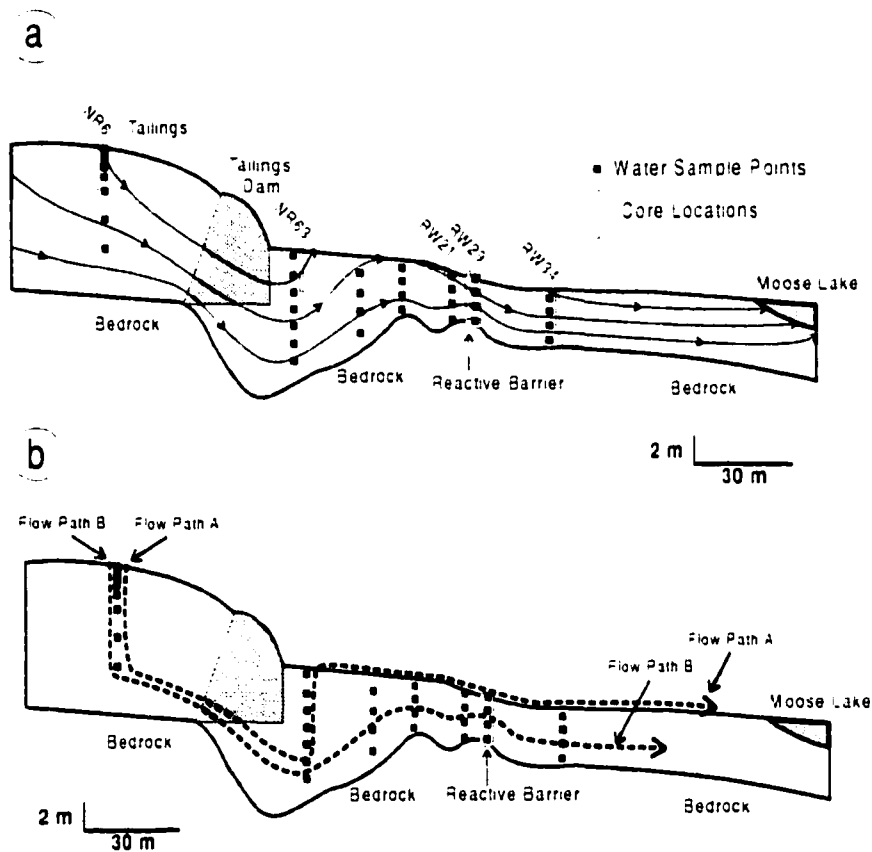


**Figure 5.1** a) Shows the flow system for the Nickel Rim Aquifer based on hydrologic flow modeling of Bain et al. (1999). Diagram also shows water sampling points and sediment core locations. (b) Shows idealized flow paths: Both flow paths originate in the tailings, but Flow Path A discharges to the surface at the base of the tailings dam, while Flow Path B remains in the aquifer and passes through the reactive barrier.

### 5.3 METHODS

Monitoring wells were installed in nests along a transect roughly parallel to groundwater flow. A detailed description of well installation, water sampling and field and laboratory analysis can be found in Benner et al. (1997). Aqueous samples were obtained from the unsaturated zone by immiscible displacement of pore water from 30 cm sections of sediment cores (Patterson et al., 1978) and from the saturated zone by peristaltic pump. Sediment samples for bacterial analysis were collected using a 5 cm diameter driven coring device. Cores, collected in aluminum tubing, were cut into 25 cm sections, capped, sealed and immediately stored in ice packed coolers. Field sampling was conducted in July 1997. The samples were delivered to the Mineral Sciences Laboratory at CANMET within 24 h of collection where they were stored under refrigeration (4°C) until analysis. Samples were analyzed within 14 days of sample collection. In the laboratory, the cores were placed in an anaerobic chamber, the aluminum casing was cut perpendicular to its long axis, and the sediment was removed to an autoclaved storage bottle. The material was homogenized by stirring and five 1 g replicate samples were taken from the bulk sample material for each most probable number (MPN) determination.

The sulfate reducing bacteria were grown in a modified Postgate medium C in 20 mL serum bottles (Postgate, 1984). The medium had the following composition in g/L:  $\text{KH}_2\text{PO}_4$ , 0.5;  $\text{NH}_4\text{Cl}$ , 1.0;  $\text{Na}_2\text{SO}_4$ , 4.5;  $\text{CaCl}_2 \cdot 2\text{H}_2\text{O}$ , 0.04;  $\text{MgSO}_4 \cdot 7\text{H}_2\text{O}$ , 0.06; Na lactate (60%), 2.92; Na acetate, 1.28; yeast extract, 1.0;  $\text{FeSO}_4 \cdot 7\text{H}_2\text{O}$ , 0.004; Na citrate  $\cdot 2\text{H}_2\text{O}$ , 0.3; resazurin, 0.005 (pH adjusted to 7.5 using NaOH). The medium was boiled under nitrogen until it became clear. The medium was allowed to cool and transferred to an anaerobic chamber where it was dispensed (9.0 mL per bottle) into 20 mL serum bottles containing a small iron nail. The serum bottles were sealed with a septum and an aluminum crimp top. The bottles were autoclaved, allowed to cool and then placed in the anaerobic chamber.

In the anaerobic chamber, 1 g sediment was added to each of five serum bottles. Inoculated samples were sequentially diluted and incubated in an anaerobic glove box for 30 days. Positive growth of SRB was indicated by precipitation of Fe-sulfides. Values are reported as Most Probable Number (MPN) determinations (Alexander, 1965).

Acidophilic iron oxidizers were grown in a medium consisting of 0.5 g/L of  $K_2HPO_4$ , 0.5 g/L of  $(NH_4)_2SO_4$ , 0.5 g/L of  $MgSO_4 \cdot H_2O$ , which was autoclaved and 33.4 g/L of  $FeSO_4 \cdot 7H_2O$ . (Tuovinen and Kelly, 1973). The ferrous sulfate solution with a pH of 3.0 was prepared, filter sterilized, and then the two solutions were combined and pH adjusted to 2.2. A 9 mL volume was dispensed into sterile test tubes, and 1 g of sample was added to each of 5 tubes. The samples were serially diluted in a series of tubes up to ten dilutions. During each dilution the samples were vortexed vigorously for 10 s. Controls were not inoculated. The samples were incubated for 4 weeks. A positive result was indicated by a presence of oxidized iron in the tube and the populations were calculated from MPN tables (Alexander, 1965).

Acidophilic sulfur oxidizers were grown in Medium B (ATCC medium 23) (Ghera et al., 1989) containing 0.1 g  $NH_4Cl$ , 3.0 g  $KH_2PO_4$ , 0.2 g  $MgCl_2 \cdot 6H_2O$ , 5 g  $Na_2S_2O_3 \cdot 5H_2O$ , and 0.1 g  $CaCl_2$ . The pH was adjusted to 4.2, a five-tube MPN/g method was used, and the tubes were incubated for 4 weeks. A positive result was indicated by the presence of a sulfur deposit and a pH < 4.

The 95% confidence interval for the MPN values is calculated as described in Alexander, 1965. The upper confidence level for the 95% level is obtained by multiplying the value by a 3.3 and the lower confidence level is obtained by dividing by 3.3. A useful 'rule of thumb' for interpreting these MPN values is that changes of an order of magnitude are significant.

The enumeration of microbial populations performed here reflects the presence of these functionally defined bacterial groups. It does not indicate activity and therefore interpretation of these results is presented in the context of the observed changes in water

chemistry which provide some connection to activity. Because growth and reproduction require metabolic activity, elevated bacterial populations reflect elevated activity either presently or at some time in the past. Within this groundwater system, physiochemical changes occur on a time scale of years. Therefore, changing environmental conditions within the aquifer that could result in high populations of bacteria in a setting where they are not active is less likely than in more rapidly changing environments.

## **5.4 RESULTS AND DISCUSSION**

Vertically collected cores and profiles of water chemistry within the tailings and adjacent aquifer provide a unique view of the distribution of microbial populations throughout the system. A profile through the recharge zone of the tailings will be examined first, then we will present profiles along idealized flow paths from recharge to discharge. Finally, trends in vertical profiles throughout the aquifer will be examined.

### *5.4.1 Recharge Zone (Tailings)*

The Nickel Rim tailings mineralogy are described in detail in Johnson et al., 1999 and Jambor and Owens, 1993. The tailings have undergone oxidation for approximately 40 years and the oxidation front has migrated downwards to a depth of approximately 1 m. The contact between the oxidized tailings and the underlying unoxidized tailings is very distinct, with the oxidized tailings orange and the tailings below colored gray to black. Figure 2 shows the location of the mineralogically defined zone of active oxidation at the contact between the oxidized (orange) and unoxidized (gray) tailings. In this narrow (2-5 cm) zone, the primary sulfides are oxidizing and sulfide minerals present are partially altered and typically exhibit alteration rims of goethite ( $\alpha\text{FeOOH}$ ) and native sulfur ( $\text{S}^0$ ). In this zone, and in the 10 cm directly above (the transition zone), the secondary mineral phases goethite, jarosite ( $\text{KFe}_3(\text{SO}_4)_2(\text{OH})_6$ ) and covellite ( $\text{CuS}$ ) are precipitating and are present at the highest concentrations in the profile. Above the

transition zone, the precipitated jarosite is unstable and is dissolving releasing  $\text{SO}_4$ , Fe and acidity to the pore water. Within this oxidized zone, Fe is reprecipitating as goethite. At the top 10 cm of the profile, there is a zone where all the jarosite has dissolved and the only remaining secondary mineral phase is goethite. In the unoxidized zone, below the zone of active oxidation, sulfide mineral phases show little evidence of alteration (Jambor and Owens, 1993, Johnson et al., 1999).

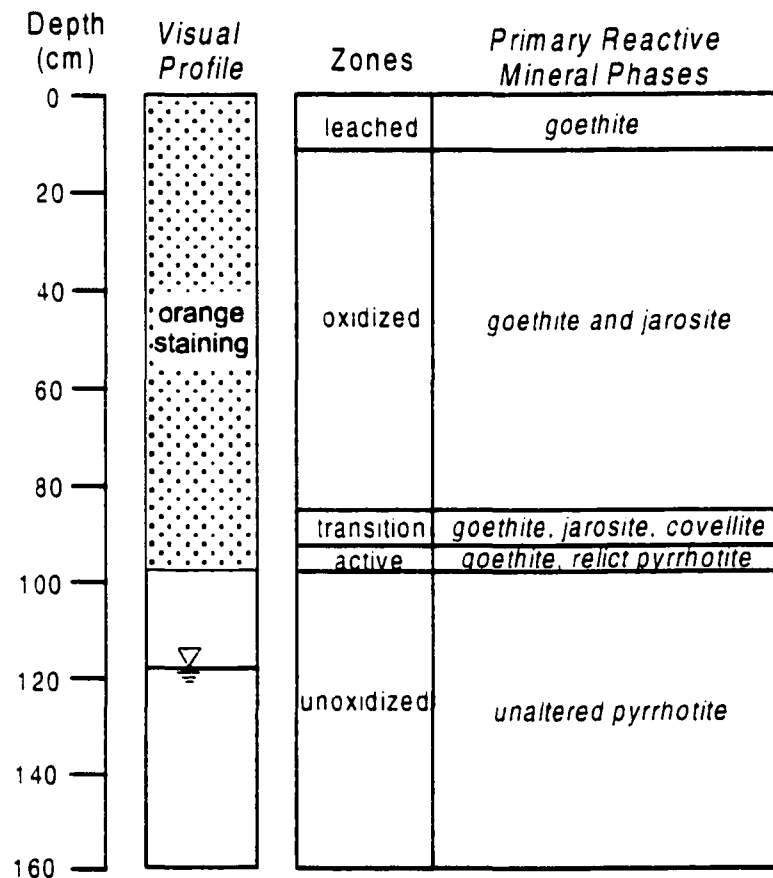


**Figure 5.2** The mineralogy of the tailings from the surface to the 1.6 m depth (Adapted from Jambor and Owens (1993)). The narrow (2-5 cm) zone of active sulfide oxidation is located at bottom of the previously oxidized, orange-stained, tailings.

Groundwater flow is downward at NR6 (Figure 1a, Figure 3) and, at the time of sampling, the water table was located 1.2 meters below ground surface. The water table

fluctuates between a depth of approximately 0.9 and 2.0 m below ground surface. The capillary fringe extends about 0.2 - 0.4 m above the water table and water saturations as high as 70% extend up to a 80 cm above the water table (Johnson, 1993). Therefore, the zone of active oxidation is often located at or near the water table and, under high water levels, is located within the capillary fringe.

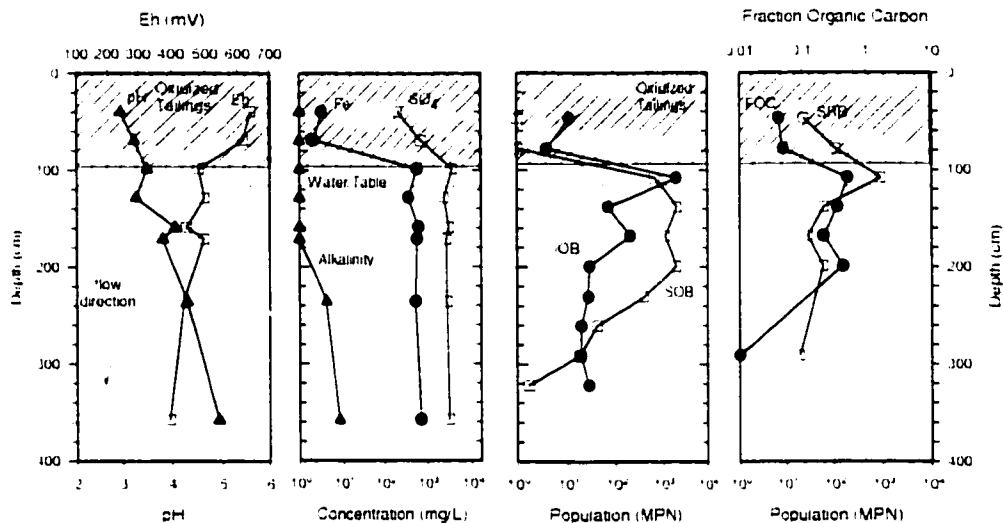


**Figure 5.3** Vertical profiles for location NR6 in the tailings impoundment of pH, Eh, Alkalinity, Fe, SO<sub>4</sub>, IOB (iron oxidizing bacteria), SOB (sulfur oxidizing bacteria), SRB (sulfate reducing bacteria) and FOC (solid phase fraction organic carbon). Hashed marks denotes oxidized tailings, horizontal dotted line indicates the location of the water table. See Figure 1 for location of profile.

Figure 3 shows water chemistry and bacterial populations from the surface of the tailings to a depth of approximately 3.5 m. The profile of water chemistry at this location is very similar to profiles of Johnson et al. (1999) and Bain et al. (1996), indicating little measurable change over the intervening 5 years. At the first sampling point at 0.4 m depth, concentrations of total dissolved Fe are 3 mg/L, SO<sub>4</sub> is 220 mg/L, pH is 3.0, and alkalinity is <1 mg/L (as CaCO<sub>3</sub>) (Figure 3). Both Fe and SO<sub>4</sub> increase rapidly (to 600 and 3700 mg/L, respectively) at 1.0 m and remain at similarly high levels for the

remainder of the profile to a depth of 3.5 m. The pH increases to 4.9 at the bottom of the profile. Alkalinity values remain low (<10 mg/L) but increase slightly with depth.

The population of iron oxidizing bacteria (IOB) is between  $10^0$  and  $10^1$  MPN/g above 1.0 m depth. There is a single isolated maximum value of  $2 \times 10^3$  MPN/g at 1.0 m depth and the population then declines to  $2 \times 10^1$  MPN/g at the bottom of the profile. The population of sulfur oxidizing bacteria (SOB) is  $<10^0$  MPN/g above 1 m depth, between  $4 \times 10^2$  MPN/g and  $2 \times 10^3$  MPN/g from 1.0 m to 2.0 m and then declines to  $<10^1$  MPN/g at 3.2 m depth.

Comparing the profiles of bacterial populations with profiles of Fe and  $\text{SO}_4$  concentrations, there is a correlation between the rapid increase in Fe and  $\text{SO}_4$  and the maximum in IOB, SOB MPN/g values. This population maximum also correlates to the change from altered to unaltered sulfide minerals in the tailings sediment. Iron and sulfur oxidizing bacteria are high at this location because this is where active sulfur and iron oxidation is occurring.

Populations of SOB and IOB within the zone of active sulfide oxidation in the Nickel rim tailings are 3-5 orders of magnitude lower than previous studies of similar tailings environments (Southam and Beveridge, 1992, Blowes et al., 1995, Blowes et al., 1998). We believe these low populations reflect lower rates of sulfide oxidation in the Nickel Rim tailings. Sulfide oxidation in the Nickel Rim tailings has been ongoing for 40 years. The oxidation front has nearly reached the water table and the zone of active oxidation is often occurring within a zone of high water saturation. The high water content decreases the rate of oxygen diffusion, greatly reducing the rate of sulfide oxidation. The low pH and relatively high concentrations of Fe and  $\text{SO}_4$ , despite the apparently slow rates of oxidation, may be the product of dissolution of the secondary mineral phase jarosite (Johnson et al., 1999).

Populations of SRB also exhibit a spike at 1 m to  $9 \times 10^2$  MPN/g and are generally  $< 1 \times 10^2$  MPN/g over the rest of the profile. Elevated populations of SRB have

been previously observed in tailings (Fortin et al., 1996, Fortin and Beveridge, 1997). Fortin and coworkers suggested that the SRB survive in more alkaline and reducing microenvironments utilizing organic carbon generated by oxidizing bacteria to reduce sulfate. The profile of solid phase organic carbon (FOC), which mirrors populations of SRB, is consistent with the conclusion of Fortin and Beveridge, (1997). The increase in SRB populations does not correspond to a decrease in sulfate concentrations, indicating that the presence of these bacteria does not affect the bulk aqueous chemistry of the tailings.

The profile of the SOB population exhibits a broad zone of elevated values across a 1 m distance from 1.0 to 2.0 m depth. This distribution is not consistent with the results of the mineralogical study, which indicates a distinct and narrow zone of active sulfide oxidation. However, the MPN/g values for SOB across this elevated zone are low and likely reflect relatively low rates of sulfide oxidation. The electron acceptor these microorganisms are utilizing is unclear. Transport of oxygen or ferric iron from the unsaturated zone downwards through one meter of unaltered sulfides requires a travel time of approximately 2 years (Bain et al., 1999).

#### *5.4.2 Profiles along Flow Lines*

The dissolved products of sulfide oxidation derived from above the water table in the tailings, are transported downward and into the adjacent aquifer. Figure 1b shows two idealized flow paths for water recharging the tailings. These flow paths do not precisely match actual flow lines, but they do follow the general direction of groundwater flow as indicated by groundwater flow and transport modeling conducted by Bain et al. (1999). These flow paths are used to illustrate microbial and chemical changes as water passes through the aquifer.

Flow Path A passes downward through the tailings and into the underlying and adjacent aquifer before discharging to the surface-water flow system at the base of the tailings dam. This surface water then flows to nearby Moose Lake. Flow Path B also originates in the tailings but discharges to the deeper portion of the aquifer, and passes through the reactive barrier before eventually discharging to Moose Lake. In Figures 4 (Flow Path A) and 5 (Flow Path B) water chemistry and bacterial populations are plotted along these two flow paths. When the flow path passes perpendicular through a vertical profile (NR 63, RW21, RW29, and RW34) an average value has been calculated.

#### 5.4.2.1 Flow Line A

The Flowline A profile (Figure 4) is presented as three sections (tailings, aquifer, and surface) each plot with a different horizontal scale. Along the profile, concentrations of Fe and  $\text{SO}_4$  remain high from the recharge zone to discharge to the surface, exhibiting a gradual increase and then decrease over that distance. Both pH and alkalinity also increase along the flow path through the tailings and aquifer. These changes in water chemistry can be attributed to historical variations in the rate of sulfide oxidation and to the precipitation and dissolution of the pH buffering mineral siderite (Bain et al., 1999).

Upon discharge to the surface, the water chemistry changes dramatically. The pH decreases from 6.1 to 4.2, Eh increases from 200 to 440, alkalinity declines from 90 to <1 mg/L (as  $\text{CaCO}_3$ ), Fe concentrations decline from 1300 to 790 mg/L and  $\text{SO}_4$  concentrations decline from 4200 to 3200 mg/L. Sediment at the surface is covered by 2 to 5 cm of water. In the surface water, Fe concentrations decline from 800 mg/L at discharge to 420 mg/L at the final sampling point approximately 100 m downstream. There is a corresponding decrease in pH from discharge (pH=4) to 100 m downstream (pH=2.5). The decrease in Fe,  $\text{SO}_4$ , and pH upon discharge are the result of oxidation of  $\text{Fe}^{2+}$  and subsequent precipitation of ferric oxyhydroxide and hydroxysulfate mineral phases. The presence of red-orange and yellow precipitates at the surface is consistent

with this conclusion. These changes in water chemistry and accompanying precipitating secondary mineral phases are typical for discharging groundwater containing high ferrous iron concentrations.

Populations of IOB are generally low ( $<7 \times 10^1$ ) along the flow path from the zone of active oxidation in the tailings to discharge to the surface. Within 0.1 m of the surface, however, the population of IOB increases to  $5.2 \times 10^2$  MPN/g in the surface sediment. The population of IOB continue to increase downstream to a high of  $>10^6$  MPN/g.

Populations of SRB correlate well to solid phase organic carbon concentrations along this flow path with the highest values ( $5 \times 10^5$  MPN/g) found in the sediment immediately below the ground surface. This observation suggests that SRB are using this solid-phase organic carbon to reduce sulfate. Unfortunately, the peak in SRB population occurs immediately below the surface and it is not possible to determine the impact that this sulfate reduction has on the bulk water chemistry.

The population of SOB are generally low throughout the aquifer and surface water sections along this flow path but are highest just prior to discharge to the surface and exhibit a positive correlation with solid phase organic carbon concentrations and SRB populations.

With the exception of areas of high organic carbon, populations of the measured bacterial populations are low throughout the aquifer. The lack of large bacterial populations is indicative of the lack of electron acceptors (oxygen) for IOB and SOB and the lack of electron donors (organic carbon) for SRB. The groundwater pH along most of the aquifer profile is about 6, beyond the optimal range for acidophilic IOB and SOB. However, at other tailings sites where bulk pore water pH is near neutral and sulfides and oxygen is present, populations of IOB and SOB populations are elevated (Southam and Beveridge, 1992, Blowes et al., 1995, Blowes et al., 1998). From a geochemical perspective the creation of acidic micro-niches in the nickel rim aquifer would be

relatively easy given the low aqueous alkalinity and the absence of the Ca and Mg carbonate buffering mineral phases. It is unlikely that pore water pH is a primary limiting factor to the presence of IOB and SOB in this aquifer.

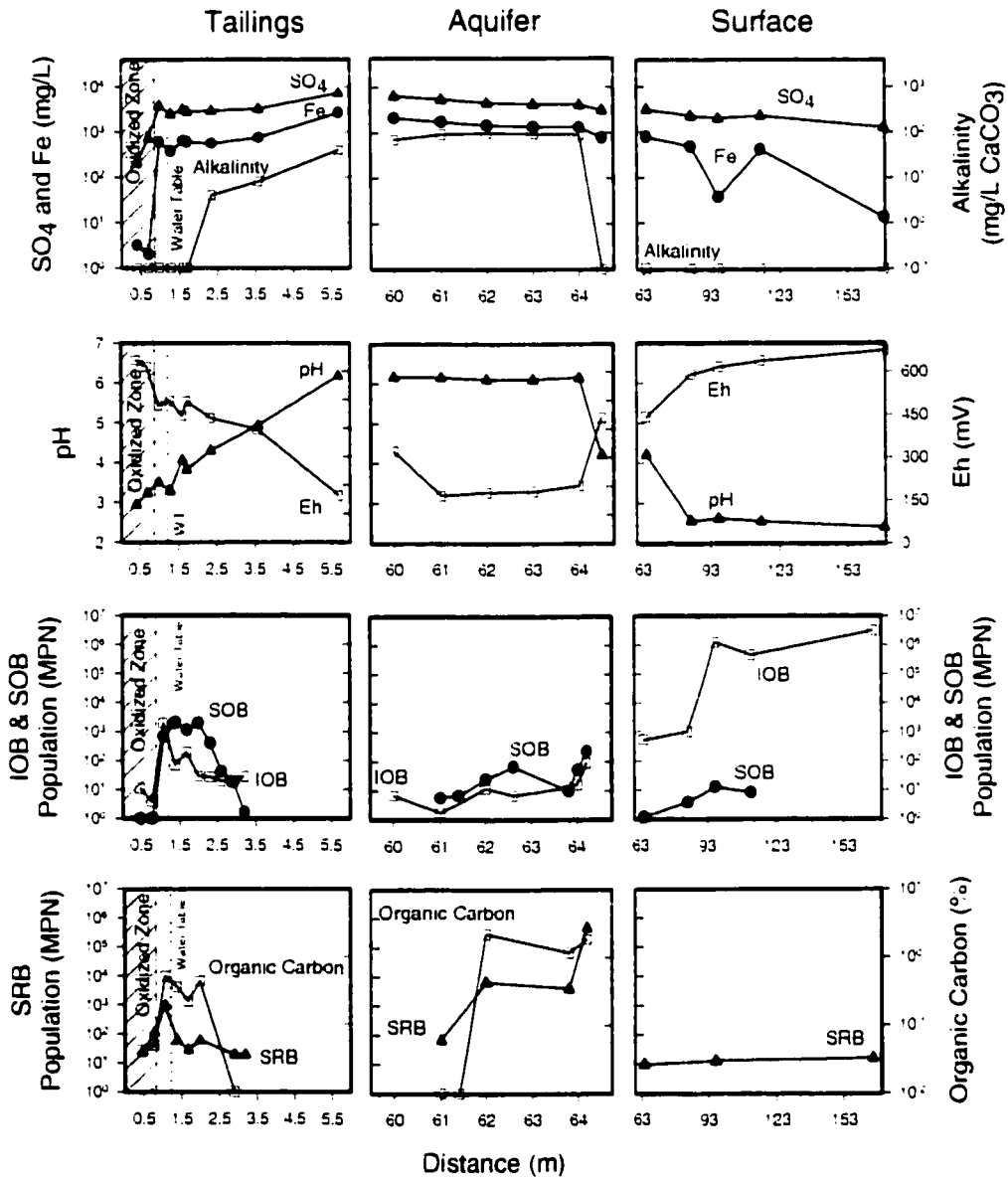


Figure 5.4 Flow Path A profiles of pH, Eh, Alkalinity, Fe, SO<sub>4</sub>, IOB (iron oxidizing bacteria), SOB (sulfur oxidizing bacteria), SRB (sulfate reducing bacteria and

*DOC (dissolved phase organic carbon). See Figure 1 for location of Flow Path A.*

At the point of discharge, reduced groundwater containing high ferrous iron concentrations enters the aerobic, oxygen-rich, surface water system. Populations of IOB are elevated because of the high concentrations of electron donors (oxygen) and acceptors (ferrous iron) necessary for IOB metabolism. The absence of metabolizable electron acceptors (reduced sulfur species) limits the populations of SOB to very low levels. Although SRB populations may be limited by low organic carbon concentrations (unfortunately, no DOC or FOC data is available for the surface sediment), it is more likely that the aerobic conditions inhibit SRB growth. Given the existence of high SRB populations in the acidic tailings environment, SRB are probably not limited by low pH conditions in the surface water.

#### 5.4.2.2 Flow Line B

Flow Line B (Figure 5) begins with the same tailings profile as Flow Line A, but does not discharge to the surface at the base of the dam. This flow path remains within the aquifer and passes through the reactive barrier before eventually discharging to Moose Lake. Over the 100 m travel distance prior to passage through the reactive barrier, the aquifer water chemistry is very similar to Flow Path A, with only small, gradual changes in plotted constituents.

Flow Path B includes samples from the aquifer over a much greater distance than Flow Path A, and therefore provides a more comprehensive profile of bacterial distribution in the aquifer. Populations of IOB and SOB remain low throughout this flow path with all values  $< 5 \times 10^1$  MPN/g after the 2.5 m depth in the tailings. These low values indicate little bacterially mediated S or Fe oxidation in the aquifer. The population of SRB is elevated at points in the aquifer where organic carbon concentrations are high. The population of SRB increases to  $3 \times 10^8$  MPN/g within the reactive barrier, 4 orders of magnitude higher than at any other point along the entire flow path. This high

population reflects the presence of high concentrations of electron donors and electron acceptors under optimal pH conditions. Somewhat surprisingly, average populations of SOB are also slightly elevated in the barrier compared to the adjacent aquifer.

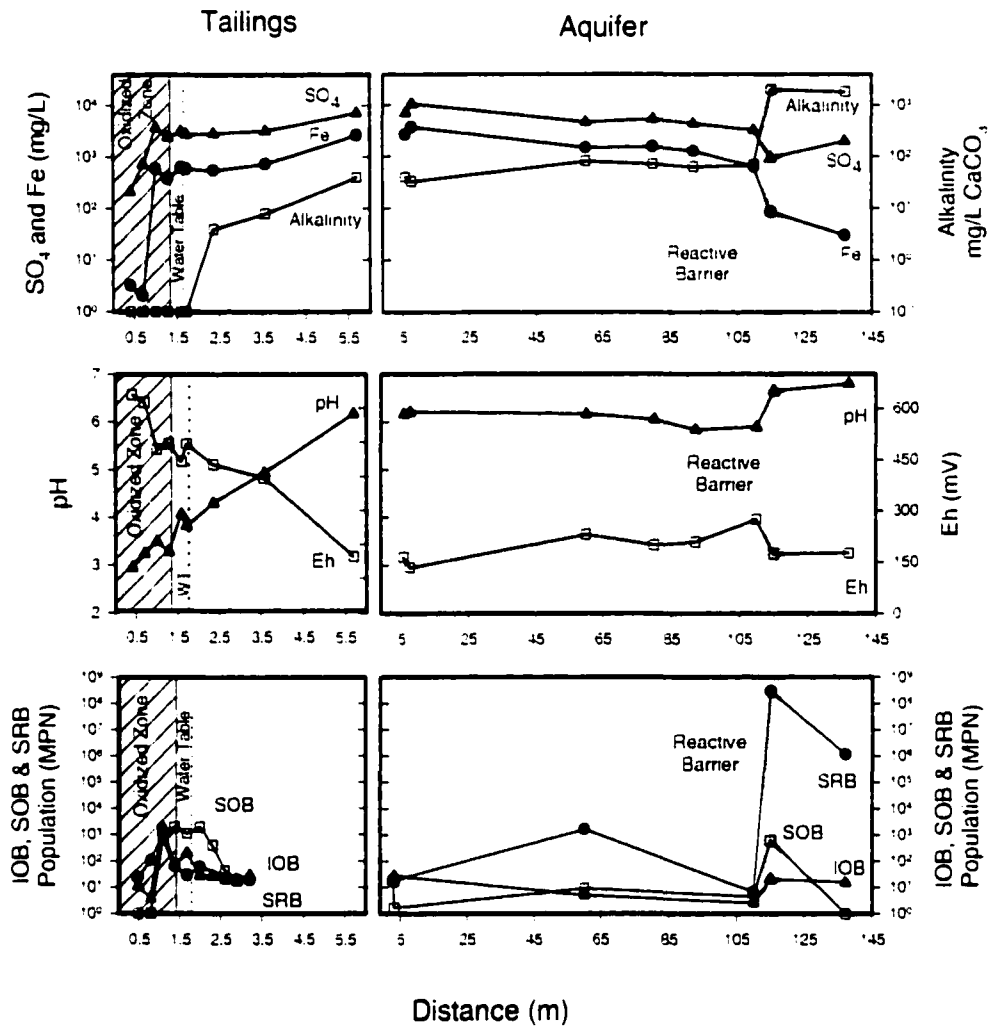


**Figure 5.5** Flow Path B profiles of pH, Eh, Alkalinity, Fe, SO<sub>4</sub>, IOB (iron oxidizing bacteria), SOB (sulfur oxidizing bacteria), SRB (sulfate reducing bacteria. See Figure 1 for location of Flow Path B.

Sulfate reducing bacteria are also abundant in the aquifer down-gradient of the barrier ( $>10^6$  MPN). Dissolved organic carbon concentrations increase from  $<10$  mg/L in the up-gradient aquifer to  $>100$  mg/L down-gradient of the barrier (Benner et al., 1999). The high population of SRB is likely metabolizing elevated concentrations of dissolved organic carbon emanating from the reactive barrier.

#### *5.4.3 Vertical Profiles within the Aquifer*

Examination of vertical profiles within the aquifer further illustrates the control that the hydraulic regime and organic carbon concentration have on bacterial distribution. Profile NR63 (Figure 6 and Figure 1) is located in the discharge zone at the foot of the tailings dam and groundwater flow is upward and to the right. There is a thick peat layer (20-40 cm) in the upper meter of the profile. Populations of SOB, IOB and SRB are all high at the top of the profile due to the abundance of organic carbon and high disequilibrium concentrations of dissolved  $\text{SO}_4$  and Fe created by the discharge of reduced groundwater to the surface. At Profile RW21 (Figure 7), the aquifer sediment is similar to that at NR63, however only a minor ( $<10$  cm thick) organic-rich layer is found near the top of the profile. Groundwater flow is predominantly horizontal from left to right but the upper third of the aquifer receives recharging acidic water from the surface (Figure 1). This profile also exhibits elevated populations of IOB, SOB and SRB near the surface where oxic, acidic surface water recharges the aquifer and organic material is present. The flow regime for Profile RW29 (Figure 8) within the permeable reactive barrier is unique because a protective clay cap prevents recharge of surface water. Within the barrier, groundwater flow is entirely from the left to the right. The distribution of organic material is uniform across the profile (Benner et al., 1997). There are variations in bacterial populations within the barrier. However, there are not elevated populations of bacteria near the surface as is observed in the other aquifer profiles. The absence of these higher populations can be explained by the presence of the protective clay layer, which

prevents surface water recharge or discharge, and by the uniform organic material distribution. Profile RW34 (Figure 9) is located in the aquifer approximately 15 m down-gradient from the reactive barrier. The aquifer at this location is stratigraphically similar to RW21 but does not contain a peat layer in the upper portion of the aquifer. As at Profile RW21, there is surface water recharging the aquifer (Figure 1). The highest populations of IOB and SOB are found in the upper portion of the aquifer where surface water is recharging the aquifer. The absence of a layer of organic material results in low populations of SRB at the top half of the profile. High populations of SRB are found at the bottom of the profile where groundwater, containing elevated concentrations of dissolved organic carbon, is released from the reactive barrier. In most cases, areas that contain elevated populations of SRB, also contain elevated populations of SOB (i.e. NR6, NR63, RW21, RW29).

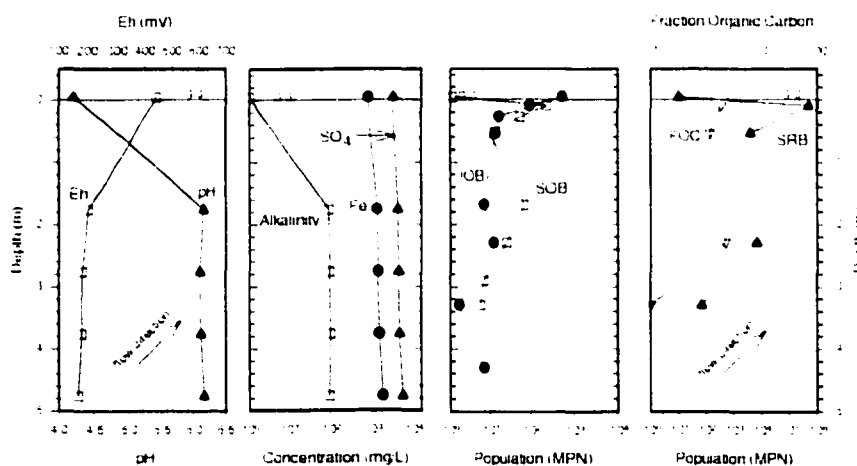


**Figure 5.6** Vertical profiles for location NR63 at the base of the tailings dam of pH, Eh, Alkalinity, Fe,  $SO_4$ , IOB (iron oxidizing bacteria), SOB (sulfur oxidizing bacteria), SRB (sulfate reducing bacteria) and FOC (solid phase fraction organic carbon). Horizontal line indicates the ground surface (G.S.). See Figure 1 for location of profile.

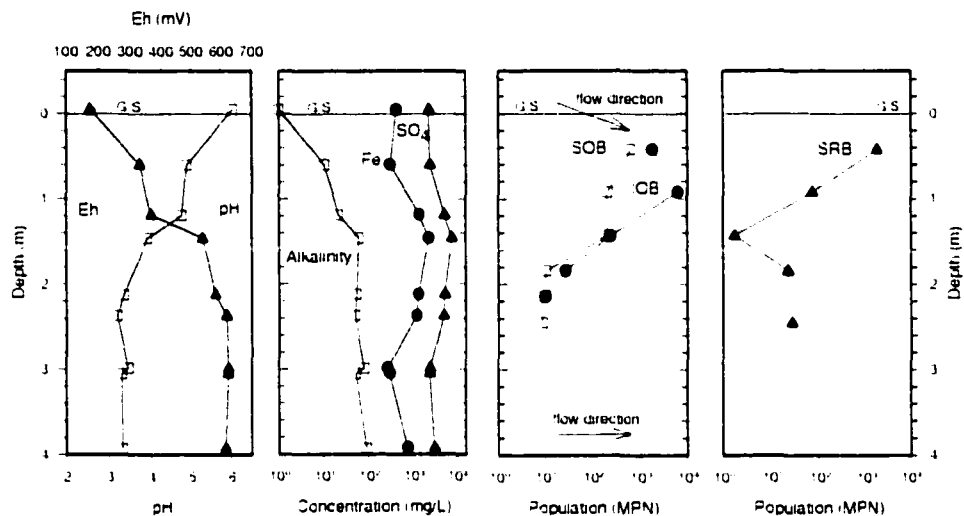


**Figure 5.7** Vertical profiles for location RW21 up-gradient of the reactive barrier of pH, Eh, Alkalinity, Fe, SO<sub>4</sub>, IOB (iron oxidizing bacteria), SOB (sulfur oxidizing bacteria), SRB (sulfate reducing bacteria). Horizontal line indicates the ground surface (G.S.). See Figure 1 for location of profile.

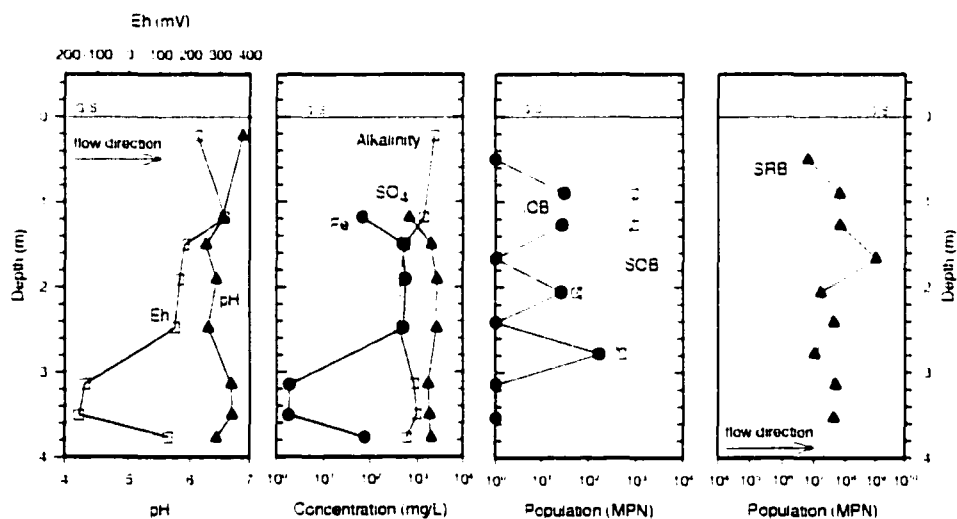


**Figure 5.8** Vertical profiles for location RW29 within the reactive barrier of pH, Eh, Alkalinity, Fe, SO<sub>4</sub>, IOB (iron oxidizing bacteria), SOB (sulfur oxidizing bacteria), SRB (sulfate reducing bacteria). Horizontal line indicates the ground surface (G.S.). See Figure 1 for location of profile.

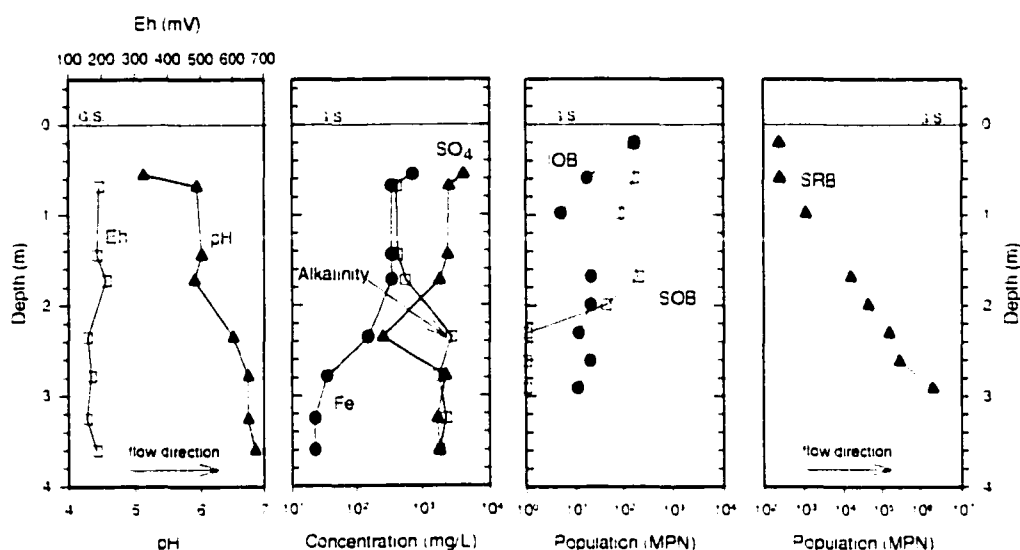


**Figure 5.9** Vertical profiles for location RW24 down-gradient of the reactive barrier of pH, Eh, Alkalinity, Fe, SO<sub>4</sub>, IOB (iron oxidizing bacteria), SOB (sulfur oxidizing bacteria), SRB (sulfate reducing bacteria). Horizontal line indicates the ground surface (G.S.). See Figure 1 for location of profile.

## 5.5 CONCLUSIONS

The Nickel Rim tailings impoundment is relatively mature with respect to sulfide oxidation. The narrow zone of active oxidation in the tailings has nearly reached the water table and is often located in a zone of high water content. Low gas porosity limits O<sub>2</sub>-gas diffusion to the depth where sulfide minerals are present, and consequently limits the rate of sulfide oxidation. A consequence of lower rates of sulfide oxidation is lower populations of sulfur and iron oxidizing bacteria within the zone of active oxidation. The presence of high concentrations of dissolved Fe and SO<sub>4</sub>, despite apparently low rates of sulfide oxidation, can be attributed to the dissolution of secondary minerals.

Examination of the water chemistry and bacterial populations throughout the flow system illustrates the control that the hydrogeologic regime has on the distribution of the sulfur and iron oxidizing bacterial populations. Elevated populations of these

bacteria are largely limited to zones of recharge where gaseous oxygen and oxygen-rich water enters the tailings and zones of discharge where reduced water comes in contact with the atmosphere. Bacterial populations are generally low in the rest of the aquifer. These profiles also show the difference in bacterial distribution between the recharge and discharge zone: in the recharge zone both sulfur and iron oxidizing bacteria are present, while at discharge, only populations of iron oxidizing bacteria are high. Solid phase and dissolved organic carbon also creates zones of disequilibrium within the aquifer. Within these zones, high populations of sulfate reducing bacteria are found. Outside these zones of disequilibrium, where electrochemically active dissolved species approach equilibrium, measured bacterial populations are low.

In many locations along the flow path, there is an apparent coexistence of elevated populations of SRB and SOB. This can be explained by the presence of solid phase-controlled, disparate redox microenvironments that are linked by advective or diffusive transport of electroactive species. These elevated SOB populations are likely metabolizing the reduced sulfur species produced by the SRB and the SOB may be dependent on the SRB populations to provide these electron donors. Conversely, SRB may benefit from the presence of SOB which consume oxygen that would inhibit sulfate reduction.

**5.6 REFERENCES**

- Alexander, M. 1965. Most-probable-number method for microbial populations. Black, C.A., (Ed.) *Agronomy, Vol. 9. Methods of Soil Analysis Part 2: Chemical and Microbiological Properties*. pp. 1467-1471.
- Bain, J.G. 1996. *The Physical and Chemical Hydrogeology of a Sand Aquifer Affected by Drainage from the Nickel Rim Tailings Impoundment*. M.Sc. Thesis, University of Waterloo, Waterloo, Ontario.
- Bain, J.G., Blowes, D.W., and Robertson, W.D., 1999. Hydrogeochemistry of a sand aquifer affected by drainage from the Nickel Rim tailings. *J. Contam. Hydro.* In Press.
- Benner, S.G., Blowes, D.W., Gould, W.D., Ptacek, C.J., and Herbert Jr., R.B., 1999. Geochemistry of a permeable reactive barrier for metals and acid mine drainage. *Environ. Sci. Tech.*, 33, 2793-2799.
- Benner, S.G., Blowes, D.W., Ptacek, C.J., 1997. Full-scale porous reactive wall for the prevention of acid mine drainage. *Ground Water Monit. Remed.*, 17 (4), 99-107.
- Blowes, D.W., Jambor, J.L., Hanton-Fong, C.J., Lortie, L., Gould, W.D., 1998. Geochemical, mineralogical and microbiological characterization of sulphide-bearing carbonate-rich gold-mine tailings impoundment, Joutel, Quebec. *Appl. Geochem.*, 13 (6), 687-705.
- Blowes, D.W., Al, T.A., Lortie, L., Gould, W.D., Jambor, J.L., 1995. Microbiological, chemical, and mineralogical characterization of the Kidd Creek Mine Tailings Impoundment, Timmins Area, Ontario. *Geomicrobiol. J.*, 13, 13-31.

- Dubrovsky, N.M., Cherry, J.A., Reardon, E.J., Vivyurka, A.J., 1985. Geochemical evolution of inactive pyritic tailings in Elliot Lake uranium district. *Can. Geotech. J.*, 22, 110-128.
- Fortin, D. and Beveridge, T.J., 1997. Microbial sulfate reduction within sulfidic mine tailings: formation of diagenetic Fe sulfides. *Geomicrobiol. J.*, 14, 1-21.
- Fortin, D., Davis, B., Beveridge, T.J., 1996. The role of *Thiobacillus* and sulfate-reducing bacteria in iron biocycling in oxic and acidic mine tailings. *FEMS Microbiol. Ecol.*, 21 (1), 11-24.
- Gherna, R., Pienta, P. and Cote, R. eds. 1989. *American Type Culture Collection, Catalog of Bacteria and Phages*, 17th ed. Rockville, MD: American Type Culture Collection.
- Jambor, J.L. and Owens, D.R., 1993. Mineralogy of the tailings impoundment at the former Cu-Ni deposit of Nickel Rim Mines Ltd., Eastern edge of the Sudbury Structure, Ontario. Report # MSL 93-4 (CF), Canada Centre for Mineral and Energy Technology, Energy, Mines and Resources, Ottawa, Canada.
- Johnson, R.H., 1993. The Physical and Chemical Hydrogeology of the Nickel Rim Mine Tailings Sudbury, Ontario. M.Sc. Thesis, University of Waterloo, Waterloo Ontario, Canada.
- Johnson, R.H., Blowes, D.W., Robertson, W.D., and Jambor, J.L., 1999. The hydrogeochemistry of the Nickel Rim mine tailings impoundment, Sudbury, Ontario. *J. Contam. Hydro.*, In Press.

- Morin, K. Cherry, J.A., Dave, N.K., Lim, T.P., Vivyurka, A.J., 1988. Migration of acidic groundwater seepage from uranium-tailings impoundments. 1. Field study and conceptual hydrogeochemical model. *J. Contam. Hydro.*, 2, 271-303.
- Nordstrom, D.K. and Alpers, C.N. 1999. Geochemistry of Acid Mine Waters. In: Plumlee, G.S., Logsdon, M.J. (Eds.), *The Environmental Geochemistry of Mineral Deposits. Part A. Processes, Methods, and Health Issues*. Society of Economic Geologists, Littleton, CO. Society of Economic Geologists, *Reviews in Economic Geology*, v. 6A, chapter 6, 28 p.
- Nordstrom, D.K. and Southam, G. 1997. Geomicrobiology of sulfide mineral oxidation. In: *Geomicrobiology: Interactions Between Microbes and Minerals*. Banfield, J.F., Nealson, K.N., Eds. Mineralogical Society of America, Washington, D.C. pp. 361-390.
- Patterson, R.J., Frappe, S.K., Dykes, L.S., McLeod, R. 1978. A coring and squeezing technique for the detailed study of subsurface water chemistry. *Can. J. Earth Sci.* 15, pp. 162-169.
- Postgate, J.R. 1984. *The Sulphate-Reducing Bacteria*. Cambridge University Press, Cambridge, England.
- Schrenk, M.O., Edwards, K.J., Goodman, R.M., Hamers, R.J., Banfield, J.K. 1998. Distribution of *Thiobacillus ferrooxidans* and *Leptospirillum ferrooxidans*: Implications for generation of acid mine drainage. *Sci.*, 279, 1519-1522.
- Singer, P.C. and Stumm, W. 1970. Acid mine drainage: the rate determining step. *Sci.*, 167, 1121-1123.

- Southam, G., and Beveridge, T.J., 1992. Enumeration of thiobacillus within pH-neutral and acidic mine tailings and their role in the development of secondary mineral soil. *Appl. Environ. Microbiol.*, 58 (6), 1904-1912.
- Tuovinen, O.H. and Kelly, D.P. 1973. Studies on the growth of *Thiobacillus ferrooxidans*. I. Use of membrane filters and ferrous iron agar to determine viable numbers and comparison with  $^{14}\text{CO}_2$ -fixation and iron oxidation as measures of growth. *Arch. Mikrobiol.*, 88, 285-298.

## Chapter 6

### *Modeling Flow in Reactive Barriers: Implications for Performance and Design*

#### **6.1 CHAPTER SUMMARY**

Reactive barriers are passive and in situ groundwater treatment systems. The hydraulic conditions and contaminant levels within the aquifer dictate barrier design. Heterogeneities in hydraulic conductivity ( $K$ ) within the aquifer or the reactive barrier may result in reduced residence times or higher flux rates through portions of the barrier. These spatial variations in flux have the potential to compromise the treatment capacity of the barrier. Numerical flow modeling shows that heterogeneities in  $K$  can result in spatial variations in flux within the barrier. However, the impact of these high  $K$  layers will be a function of their location and distribution: the more localized the high  $K$  zone, the greater the preferential flow. The geometry of the reactive barrier will also strongly influence flow distribution. Aquifer heterogeneities can produce greater preferential flow in thinner barriers compared to thicker barriers. The  $K$  of the barrier will affect the flow distribution: decreasing the  $K$  of the barrier will result in more even distribution of flow. If the reactive material within the barrier is heterogeneous, the thicker the barrier, the greater the preferential flow. This modeling indicates more uniform flow can be attained utilizing thicker homogeneous barriers.

## 6.2 INTRODUCTION

Permeable reactive barriers can provide effective treatment for a variety of groundwater contaminants including halogenated organic compounds (*Gillham and O'Hannesin, 1994*), nitrate (*Robertson and Cherry, 1995*), phosphate (*Ptacek et al., 1994, Baker, 1996*), chromate (*Blowes and Ptacek, 1992*), arsenic and selenium (*McRae, 1999*) other trace metals (*McGregor et al., 1999*) and water contaminated by mine wastes (*Blowes and Ptacek, 1994; Benner et al., 1997*). Reactive barriers are installed by placing an appropriate reactive mixture into the aquifer so that the contaminated groundwater is treated during passage through the material under natural gradient conditions.

Installations are "keyed" into an underlying layer of low permeability or may be "hanging" with no boundary to flow at the base. Because aquifers tend to be laterally continuous, the sides of a barrier are often not keyed to an impermeable boundary and are designed to extend beyond the lateral extent of the contaminant plume. Reactive barriers can also be installed in a Funnel and Gate configuration where impermeable boundaries (e.g. sheet piling) are installed into the aquifer extending at some angle laterally from the reactive mixture (*Starr and Cherry, 1995*). These walls then funnel the groundwater through the reactive zone.

The hydraulic conductivity ( $K$ ) of the reactive material will greatly influence the manner in which water passes through the barrier. If the  $K$  is lower than that of the aquifer, water will diverge around the barrier, if the  $K$  is greater than the aquifer, flow will converge into the barrier. Converging flow indicates a capture zone that is wider than the barrier, while diverging flow indicates a capture zone that is smaller than the width of the barrier. To ensure that the contaminated water passes through and not around the barrier, installations are often designed with a  $K$  that is greater than the

surrounding aquifer. Any variation in  $K$  within the barrier will result in different residence times and may compromise performance (*Devlin and Barker, 1999*).

Reactive barriers have a finite treatment capacity. Treatment capacity can be expressed as reactivity where the treatable flux through the barrier is limited by the reaction rate and the thickness of the barrier. Treatment capacity can also be expressed as longevity where the treatment capacity is consumed over time by the flux of contaminants passing through the barrier. Reactive barrier thickness is dictated by the required barrier reactivity and the desired longevity of the specific site conditions. In some installations, the reaction rate will be sufficiently rapid that complete treatment occurs in the front portion of the barrier (*Bennett, 1997*). For this class of installation, the reactivity does not limit the barrier treatment capacity but barrier thickness will dictate barrier longevity. For other installations, the reactive mechanism may be sufficiently slow that the full thickness of the barrier is required to achieve treatment (*Benner et al., 1999*). The thickness of reactive barriers can vary from centimeters to meters (*U.S. Environmental Protection Agency (EPA), 1999*).

All reactive barriers will have some finite longevity and reactivity, however the particular reaction mechanism and barrier design will dictate which factor is of greater concern. In either case, changes in the flux rate through the barrier will affect reactive barrier performance (*Tratnyek et al., 1997*). Higher flux rates, which result in shorter residence times, limit the exposure of the contaminant to the treatment material. This limitation may lead to incomplete contaminant removal. In addition, higher contaminant flux through portions of the barrier may more rapidly consume treatment material along those flow paths.

The porosity and hydraulic conductivity of the barrier can change with time (*Mackenzie et al., 1997*). Secondary mineral precipitation within the barrier can decrease flow, while dissolution of barrier material can increase flow. In a barrier with a heterogeneous flow field, these effects may be preferential: greater dissolution or

precipitation will occur in those areas receiving a higher flux. The loss or accumulation of material has the potential to increase or decrease the pre-existing preferential flow paths.

Reactive barrier design and assessment involves prediction and calculation of flux rates through the reactive barrier. Computer flow modeling is often performed to compare conceptual models of how the groundwater passes through the barrier. Modeling has been performed on the configuration of funnel and gates associated with reactive barriers (*Starr and Cherry, 1994; Bennett, 1997, Teutsch et al., 1997*), and varying barrier width (*Tramcyek et al., 1997*) to optimize performance with respect to treatment capacity and contaminant capture.

Four variables control contaminant mass flux rates through a reactive barrier: concentration of the contaminant, hydraulic gradient, porosity and hydraulic conductivity. Spatial and/or temporal variations in these parameters will result in different mass flux rates, potentially affecting reactive barrier performance by exceeding the reactivity or longevity of the reactive material. This paper assesses the impact of spatial variations in hydraulic conductivity on flow through reactive barriers. Two-dimensional flow modeling illustrates the importance of reactive barrier thickness on barrier performance and provides assistance for reactive barrier design and assessment.

### **6.3 METHODS**

The two-dimensional finite element model FLOTRANS (*Guiguer et al., 1994*) was used to conduct the simulations. A uniform grid of 100 by 100 nodes was used to represent a 10 by 10 m domain. The left and right boundaries were assigned specified head so that a gradient of 0.001 was established with flow from left to right. A specified flux of zero was assigned to the top and bottom boundaries of the domain. The stream function output of each simulation was used to contour flow lines and to calculate horizontal flux along a centerline.

Modeling simulations have been performed for two barrier boundaries. In the first, the barrier is keyed to a low permeable boundary. In the second, the barrier is hanging with nothing preventing flow around the barrier. The primary difference between these two simulations is that in the first, flow can diverge away from or converge into the reactive barrier while in the second, little divergent flow occurs. These simulations produce results that can represent cross sections taken vertically or horizontally through a barrier, depending on the specific configuration of the installation (Figure 1). For clarity, the simulations will be discussed as vertical cross-sections, the water flowing from the left to the right with the top of the diagram toward ground surface. Most reactive barriers are installed from the water table downward, but for these simulations water flows over the top of the barrier. This approach was taken eliminate the potential artificial influence of the top boundary condition. The flow fields that develop in reactive barriers with Funnel and Gate systems can be quite complex and this work does not attempt to address these complexities, however many of the conclusions can be applied to Funnel and Gate installations. These simulations are not meant to match specific field conditions, but are idealized and designed to illustrate broadly applicable concepts of flow through reactive barriers.

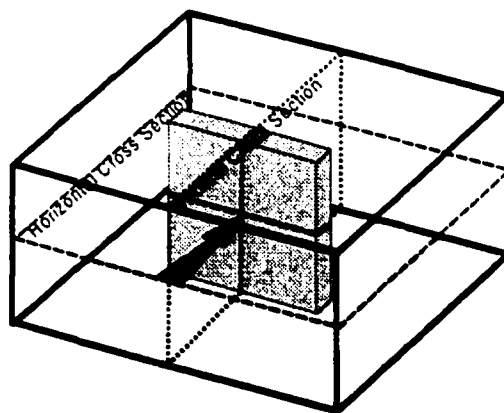


**Figure 6.1** Shows a three dimensional view of idealized reactive barrier. Simulations can represent horizontal or vertical cross sectional views of flow through the barrier.

For the base case series of simulations (Scenario I) an isotropic and homogeneous hydraulic conductivity ( $K$ ) of 4 m/day was assigned to the aquifer and an isotropic, homogeneous  $K$  of 40 m/day was assigned to the barrier. For all subsequent simulations, isotropic conditions were maintained. The specific distribution of  $K$  within the aquifer and the barrier is shown on the contoured plot of flow lines.

## **6.4 RESULTS AND DISCUSSION**

### **6.4.1 Homogeneous Conditions**

In Scenario I (Figure 2), the results of flow modeling for an aquifer and reactive barrier of homogeneous hydraulic conductivity is simulated. Output for each simulation consists of a x-sectional diagram showing flow lines and a plot of horizontal flux distribution along the centerline of the domain. The centerline flux distribution provides a close approximation of the barrier residence time; higher velocities indicate shorter residence time.

The height of the reactive barrier is 5 meters perpendicular to flow. Three barrier widths (300 cm, 100 cm, and 20 cm) are modeled. The simulation for the narrow (20 cm) barrier represents an installation with anticipated rapid reaction rates and/or low contaminant flux. The thick (300 cm) barrier is more typical of an installation utilizing a slower reaction mechanism and/or high contaminant flux. In simulations (a), (b), and (c) the barrier is unbounded at the top and bottom, while in simulation (d) the barrier is keyed into low  $K$  material (0.04 m/day).

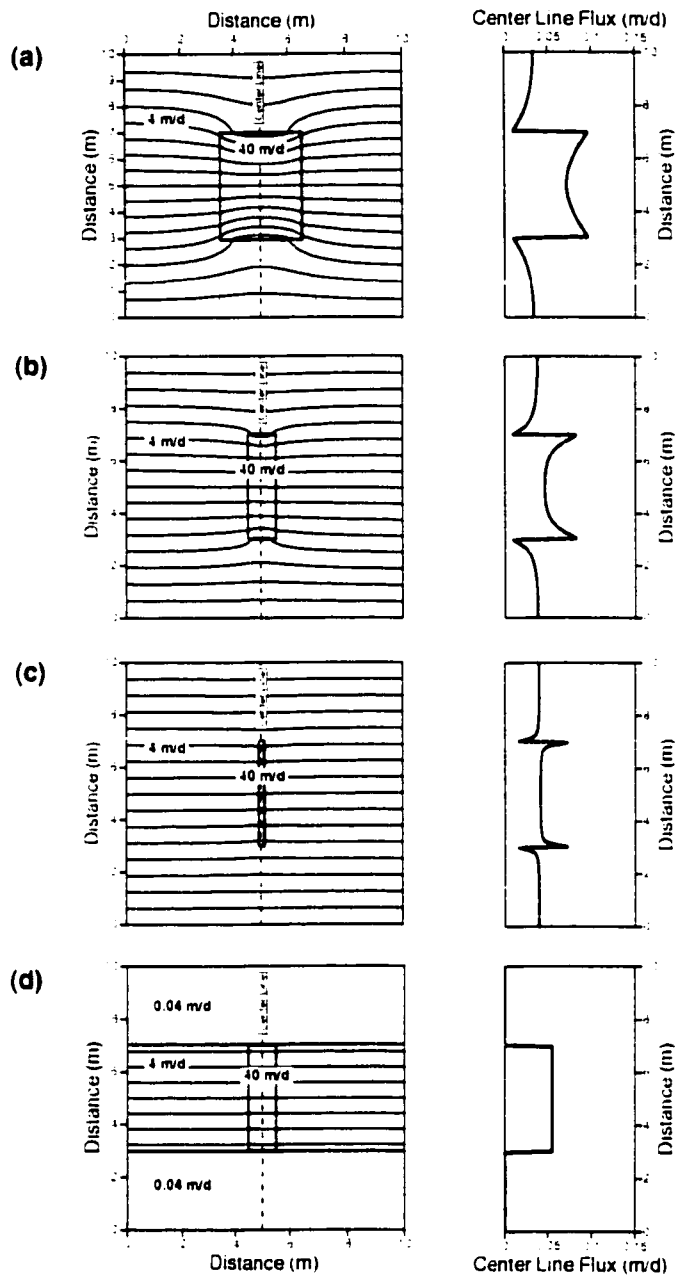


**Figure 6.2** Scenario I shows flow with a homogenous  $K$  distribution in the aquifer and barrier. The barrier  $K$  is ten times greater than the aquifer. a) 3.0 m thick barrier. b) 1.0 m thick barrier. c) 0.2 m thick barrier. d) same as (b), but with low  $K$  material bounding top and bottom of domain.

The hydraulic conductivity ( $K$ ) of the barrier is greater than the surrounding aquifer. When the barrier is unbounded, (simulations a, b and c) flow converges into the barrier on the up gradient side and diverges from the barrier on the down gradient side. This results in higher velocities through the barrier compared to the adjacent aquifer (see Centerline flux profiles simulations a, b, and c). The 300 cm thick barrier induces greater convergence of flow and exhibits a greater difference in flux rates compared to the aquifer. The distribution of flux within the barrier is not intuitive. As the flux profiles indicate, there are higher velocities through the edges in contact with the adjacent aquifer compared to the center of the barrier. There is a corresponding decrease in flux in the aquifer immediately adjacent to the barrier. This is caused by the continuity in potential across the boundary between the two different  $K$  fields: the gradient in the barrier and aquifer at the boundary must be equal. Because there is an order of magnitude difference in  $K$ , the flux immediately within the barrier is 10 times greater than the flux immediately outside the barrier. The flux is lower in the central portion of the barrier compared with the sides because converging flow must travel a greater distance, with a corresponding greater drop in hydraulic head, to reach the central portion of the barrier. These simulations illustrate that, even under homogeneous conditions, flux through reactive barriers will vary spatially. The edges of the barrier will receive greater flux and, all else being equal will achieve a lower level of treatment and/or achieve treatment for a shorter period of time compared to the central portion of the barrier. In simulation d, which has the same barrier configuration as (b) but with low  $K$  boundaries at the top and bottom, there is no convergent flow, this edge effect is not observed and flux distribution is uniform across the barrier.

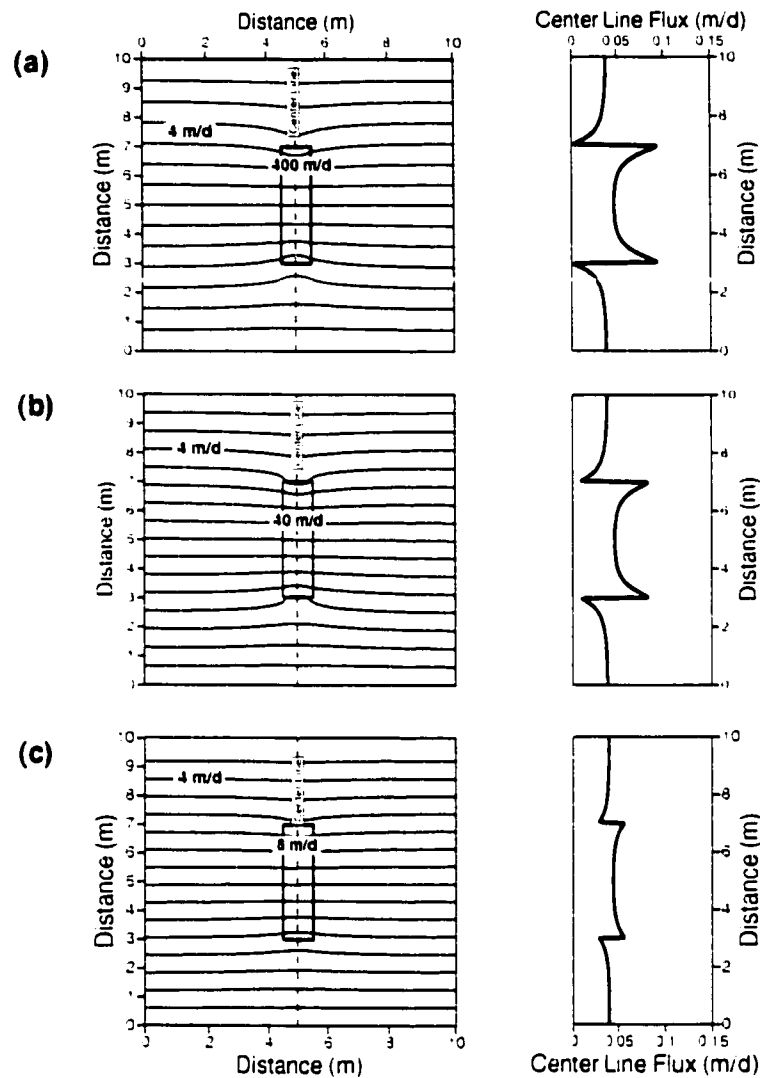


**Figure 6.3** Scenario II shows the affect of varying the barrier  $K$  on the "edge effect". Homogenous  $K$  distribution in the aquifer and barrier. All simulations the same as Scenario I (b), but the barrier  $K$  is varied. Barrier is a) 100 times greater than the aquifer, b) 10 times greater than the aquifer, c) 2 times greater than the aquifer.

6.4.1.1 Varying  $K$  of the Barrier

In Scenario II (Figure 3) the impact of varying the  $K$  of the barrier on this edge effect is illustrated. The  $K$  of the barrier is 100 times that of the aquifer in simulation (a).

10 times greater in (b) and 2 times greater in simulation (c). When the K of the barrier is increased by an order of magnitude (compare simulations (a) and (b)), there is more convergent flow into the barrier and the overall flux increases. The relative difference in flux from edge to the center of the barrier, however, remains essentially unchanged. When the K of the barrier is decreased to twice the K of the aquifer (Compare (b) to (c)), the amount of convergent flow decreases and the edge effect largely disappears. From these simulations, it is apparent that the edge effect results from convergent flow; as the difference in K between the barrier and the aquifer decreases, the edge effect declines.

#### 6.4.2 Heterogeneous Aquifer

At most field sites, the K of the aquifer is heterogeneous and the flux entering an installed barrier will vary spatially. Scenario III (Figure 4) demonstrates the impact of aquifer heterogeneities on flux distribution through the barrier. Each simulation is identical to Scenario I (Figure 2), but a one meter thick layer of high K (40 m/day) has been inserted into the aquifer, extending from the left to the right boundary of the domain. For all simulations, the presence of the high K layer increases the total flux through the barrier. However, flux profiles for the three barrier thicknesses (20, 100 and 300 cm) indicate that the impact of the high K layer on flux distribution within the barrier is variable. For the 300 cm thick barrier, flux remains relatively well distributed (a). The 20 cm barrier, however, exhibits large variations in flux along the center line as a result of the high K layer in the adjacent aquifer. The flux through the central portion of the 20 cm barrier is 8 times greater than along the outer two thirds, nearly maintaining the 10:1 flux ratio present in the aquifer. The 20 cm barrier is not thick enough to allow water from the high K layer to diverge, and the heterogeneous flux profile of the aquifer is transferred to the barrier. The thicker, 300 cm, barrier permits greater divergence of flow

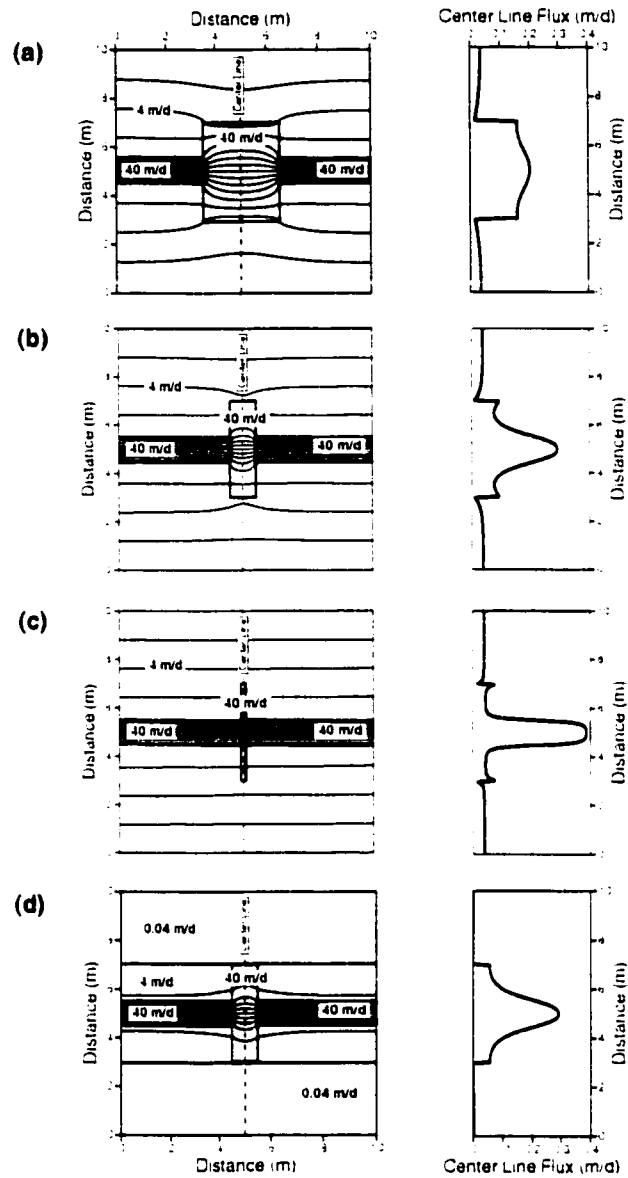


**Figure 6.4** Scenario III shows the affect of an aquifer with heterogeneous *K* distribution. Same as Scenario I, but a 1.0 m thick high *K* layer (10 times rest of aquifer) has been placed up and down gradient of the barrier.

from the high *K* layer in the aquifer and, consequently, flux is more evenly distributed across the reactive zone. Existence of low *K* confining units at the top and bottom of the barrier has little influence on flux distribution for this scenario (simulation d). These

simulations illustrate that the thinner the barrier the more closely the flux distribution will resemble that of the aquifer. Thicker barriers will tend to dampen flux heterogeneities from the aquifer, producing more evenly distributed flow.

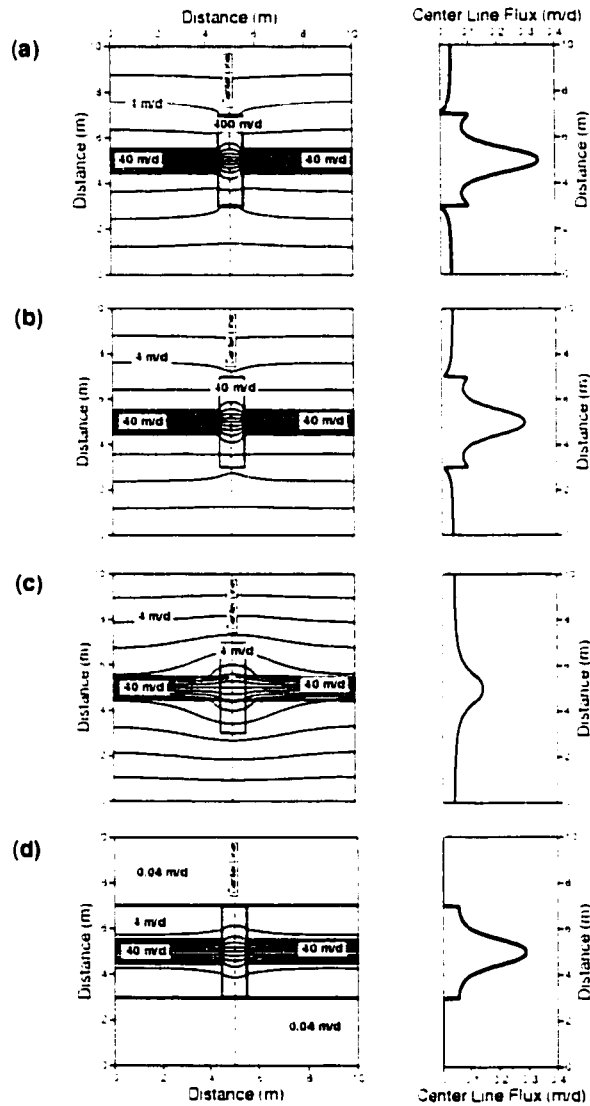


**Figure 6.5** Scenario IV shows the affect of varying barrier  $K$  on flow in heterogeneous aquifer. The barrier  $K$  is varied. Barrier  $K$  is a) 100 times greater, b) 10 greater, c) equal to, the  $K$  of the aquifer, d) same as (b), but with low  $K$  material bounding top and bottom of domain.

#### 6.4.2.1 Varying K of the Barrier

The previous simulations showed that adjusting the barrier thickness can result in a more even flow distribution. Here we investigate how the hydraulic conductivity of the barrier affects the distribution of flow in a homogeneous aquifer. In Scenario IV (Figure 5), the barrier geometry is unchanged and only the K of the barrier is varied. In simulation (a) the K of the barrier is decreased an order of magnitude (to 4 m/day) and in (c) the K is increased an order of magnitude (to 400 m/day). When the K of the barrier is increased, the total flux increases and greater preferential flow through the central portion of the barrier is observed. As the barrier K is decreased, flow convergence and overall flux through the barrier declines, but a more even flux distribution is achieved. Designing a barrier with a K that is lower than the aquifer may be problematic because of the negative impact on capture zone size. However, for barriers in heterogeneous aquifers it may be a disadvantage for the K of the barrier to be orders of magnitude greater than the K of the aquifer.

#### 6.4.2.2 Impact of K Distribution in Aquifer

The nature of K heterogeneities in aquifers varies: the distribution and magnitude of high K layers will vary from aquifer to aquifer. In Scenario V (Figure 6), the effect of different K distributions in the aquifer on flux through the barrier is explored. In each of these simulations the K and geometry of the barrier and the average horizontal K for the aquifer is the same. Total flux across the domain is also constant, but the distribution of high K layers in the aquifer is varied. In simulation (a), the high K layer in the aquifer is half as wide and the K is twice as high (80 m/day) as in simulation (b). This distribution increases the preferential flow, with flux through the central portion 5 times greater than through the rest of the barrier.

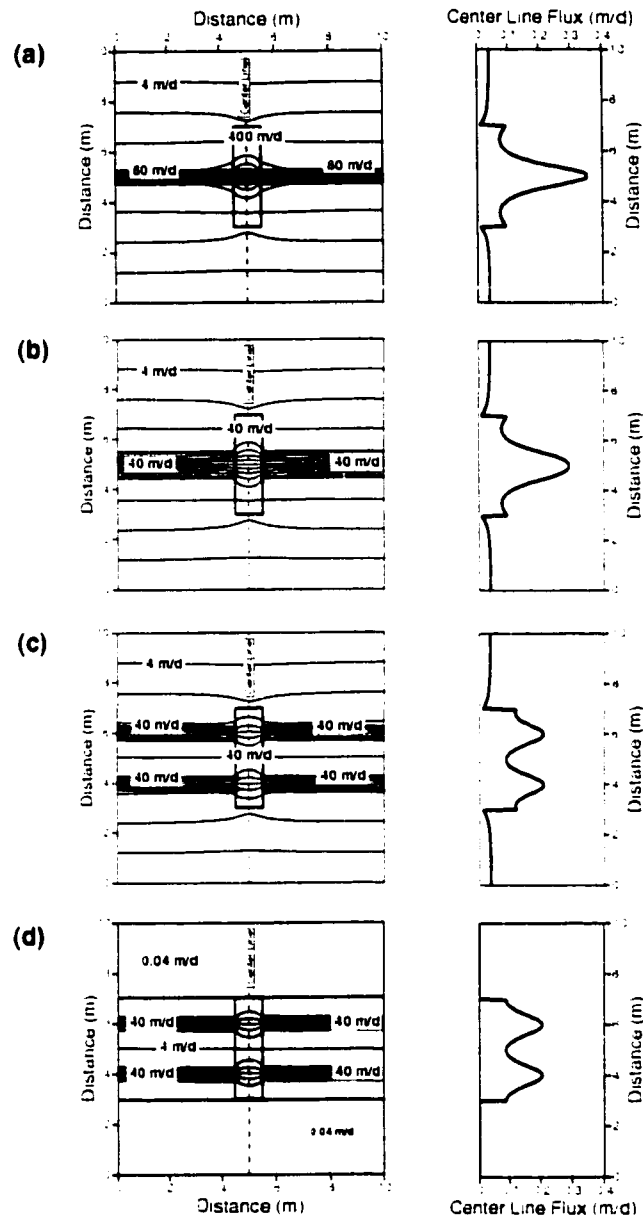


**Figure 6.6** Scenario V shows the affect of varying the  $K$  distribution in aquifer. The total flux across the domain remains constant, but the distribution of high  $K$  layers is varied. a) The high  $K$  layer in the aquifer is 0.5 m wide with a  $K$  20 times that of the rest of the aquifer. b) The high  $K$  layer is 1.0 m wide with a  $K$  10 times that of the rest of the aquifer. c) The high  $K$  layer is split into 2 layers each 0.5 m wide with a  $K$  10 times that of the rest of the aquifer. d) same as (c), but with low  $K$  material bounding top and bottom of domain.

In simulation (c) the high K layer has the same conductivity value as in simulation (b) (40 m/day) but has been split into two layers each half as wide. Splitting the high K layer results in a more even flow distribution with the difference in flux between the high and low zones declining from 3 to 2 times. These simulations indicate that the more localized and greater the magnitude of the high K zones, the greater the preferential flow through the barrier. Therefore, barriers installed into heterogeneous aquifers containing many, well distributed, high K layers will have a more even flow distribution than in aquifers containing fewer, more localized, high K layers. Existence of aquitards at the top and bottom of the barrier has little influence on flux distribution for this series of simulations (d).

#### 6.4.2.3 Adding Mixing Zones

The previous simulations indicated that thicker barriers result in a more even distribution of flux. At some field installations, it may be appropriate to install homogeneous zones adjacent to an existing barrier, or concurrently during a new installation, to produce more evenly distributed flow. Scenario VI (Figure 7) illustrates how homogeneous zones up and down-gradient of the reactive barrier affect flow distribution in the barrier. Simulation (a) is identical to the 20 cm barrier simulation in Scenario III, while simulations (b), (c), and (d) have additions of a homogeneous zone. In (b), a 200 cm homogeneous zone is placed up gradient of the barrier. In (c), 100 cm zones are placed both up and down gradient so that the thickness of the high K zone is identical to (b) but the location of the reactive zone varies. Simulation (d) is identical to (c) but the 100 cm zones are separated from the barrier by 50 cm meters of the heterogeneous aquifer. There is significant flow divergence within the barrier in simulation (a), with the flux distribution largely reflecting the distribution in the heterogeneous aquifer. The presence of the homogeneous zone upstream of the barrier in simulation (b) does not significantly

improve flow distribution through the reactive barrier. When flow enters the reactive zone in this simulation, significant convergence to re-enter the high K zone of the aquifer has already occurred and the homogeneous zone has little effect on the flux profile.

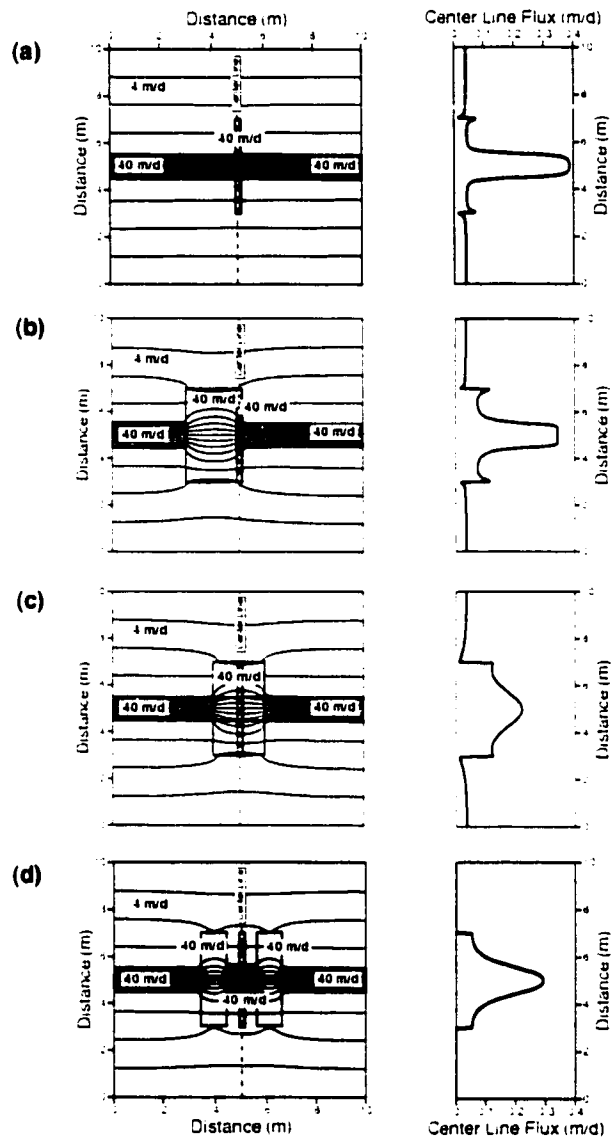


**Figure 6.7** Scenario VI shows the affect of adding homogeneous mixing zones. Mixing zones are added up and down gradient of the barrier. a) Same as Scenario III (c). b) High K, 2 m thick block added up gradient of the barrier. c) High K, 1 m blocks added up and down gradient of the barrier. d) Same as (c) but high K blocks are separated from the barrier by 0.5 m of aquifer.

However, when the homogeneous zone is placed on either side of the barrier, nearly all preferential flow is eliminated (simulation c). Homogeneous zones placed up and down gradient but separated by a portion of aquifer (simulation d), are ineffective at redistributing flux and flux profiles continue to reflect heterogeneities of the adjacent aquifer. From these simulations, it is apparent that the placement of homogeneous zones relative to the reactive mixture is very important. Geometries that place the reactive zone in the middle of immediately adjacent homogeneous zones will achieve the most uniform flow distribution.

#### 6.4.3 Heterogeneous Barrier

All previous scenarios have assumed that the barrier hydraulic conductivity is homogeneous. However, variations in the reactive mixture composition or installation process may result in a heterogeneous K distribution within the barrier. In addition, *in-situ* reactions resulting in the preferential precipitation or dissolution of solid phases within the barrier may result in an initially homogeneous barrier becoming heterogeneous with time. In Scenario VII (Figure 8), the aquifer is homogeneous but a high K zone ( $K = 400$  m/day) 100 cm wide has been inserted into the central portion of each barrier. In the thin barrier simulation, the zone of high K has little impact on the flow field or the flux rates with only a slight increase in flux of approximately 10% observed. However, in the 300 cm barrier simulation, there are significant changes in the flow field and flux distribution through the barrier as a result of the high K layer. Flux rates through the middle third portion of the thick barrier are on the order of 3 times greater than the outer two thirds. The thicker barrier permits greater convergence of flow into the high K layer while in the thin barrier little convergence is observed. Aquitards at the top and bottom of the barrier eliminate convergent flow and decrease the total flux through the barrier but has little influence on flux distribution (simulation d). These simulations indicate

that variation in hydraulic conductivity within the barrier will have a greater impact on flux distribution in thicker barriers.

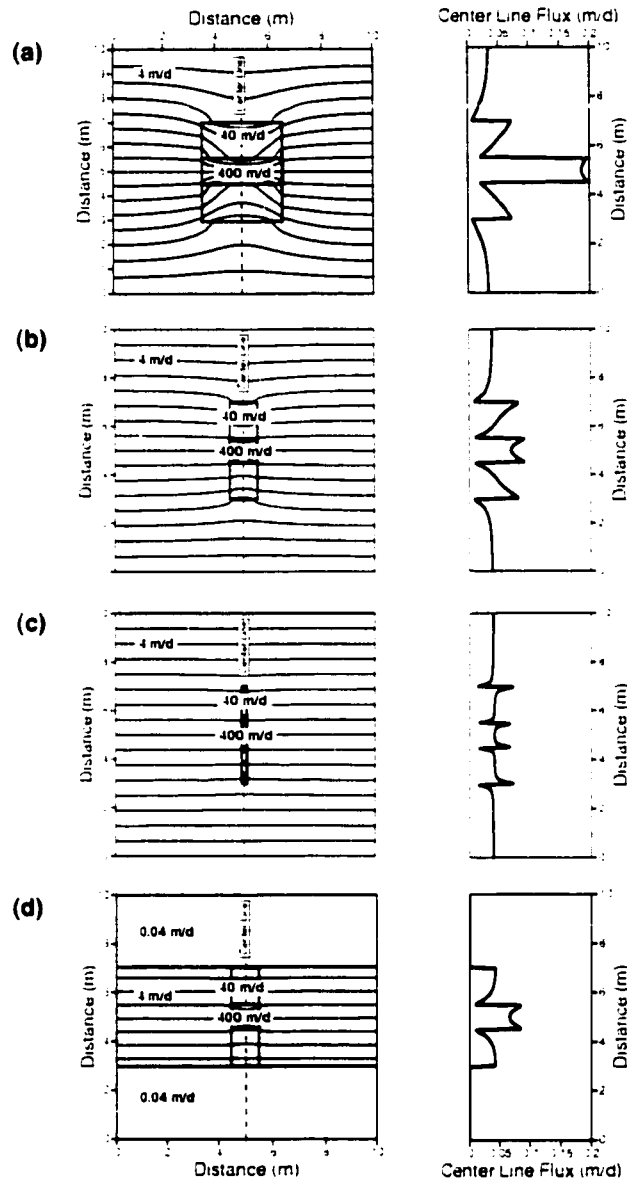


**Figure 6.8** Scenario VII shows the affect of heterogeneous  $K$  in the barrier. Same as Scenario I but 1.0 m wide high  $K$  layer added to barrier. a) 3.0 m thick barrier. b) 1.0 m thick barrier. c) 0.2 m thick barrier. d) same as (b), but with low  $K$  material bounding top and bottom of the domain.

## **6.5 CONCLUSIONS**

These simulations illustrate the importance of hydraulic conductivity variations on potential reactive barrier performance. Spatial variations in  $K$  of the aquifer, as well as in the barrier, will result in uneven flux distribution. These differences in flux will translate into decreased treatment capacity of the reactive barrier. The distribution and magnitude of the variations in  $K$  within the aquifer and barrier will effect the flux distribution. The geometry of the reactive barrier can attenuate or exaggerate these flux variations.

The thinner the barrier, the more sensitive the flux distribution to variations in the  $K$  of the aquifer. Minimum residence times and barrier lifetime in thin barriers will be potentially controlled by small layers of high  $K$  material in the aquifer. Therefore in-depth characterization of spatial distribution of  $K$  are necessary to design and assess performance of these barriers. In contrast, thicker barriers will more evenly distribute high flux inputs from a heterogeneous aquifer, and more uniform treatment over a longer period of time will be achieved. Thicker barriers are more sensitive to  $K$  variation within the barrier and therefore great care must be taken in the design, mixing and installation of these barriers to achieve and maintain a homogeneous  $K$  distribution.

The more convergent and divergent flow, the greater the impact of hydraulic conductivity variations on flux distribution. This trend suggests that flow in hanging barriers will tend to have more uniform compared with flow in Funnel and Gate systems.

Nearly all aquifers contain variations in  $K$  and the precise characterization of the  $K$  distribution is difficult. In these aquifers, thicker barriers will result in more even flux distribution and will optimize reactive barrier performance and increase the potential of correctly predicting barrier lifetime. However, reactive materials can be costly and barriers are often designed to minimize the volume of reactive material. In these cases, it may be advantageous to mix the reactive mixture with inert, less expensive material to

maximize the reactive barrier thickness without increasing the volume of reactive material required. For thinner barrier installations, placement of inert homogeneous zones up and down gradient may increase the performance of the barrier. However, significant redistribution of flow will be achieved only by installing the high K material immediately adjacent to reactive barrier on both the up and down gradient sides. Adjusting the K of the barrier will also affect flow distribution. Increasing the K of the barrier in a heterogeneous aquifer will result in increased preferential flow. Minimizing the K of the barrier, without compromising the required capture zone, will most effectively redistribute flux from high K layers within the aquifer.

The conclusions of this work are not applicable to heterogeneities in contaminant concentration. Changing the K or the geometry of the barrier will be ineffective at redistributing heterogeneous contaminant mass and even thick barriers should be designed to treat the highest concentrations found in the aquifer.

## 6.6 REFERENCES

- Benner, S.G., Blowes, D.W., Gould, W.D., Ptacek, C.J., and Herbert Jr., R.B. 1999. Geochemistry of a permeable reactive barrier for metals and acid mine drainage. *Environ. Sci. Tech.* In Press.
- Benner, Blowes, and Ptacek 1997. Full-scale porous reactive wall for the prevention of acid mine drainage. *Ground Water Monit. Remed.* 17, (4) p. 99-107.
- Bennett, T.A. 1997. An In Situ Reactive Barrier for the Treatment of Hexavalent Chromium and Trichlorethylene in Groundwater. M.Sc. Thesis. University of Waterloo, Waterloo, Ontario, Canada.
- Blowes, D.W. and Ptacek, C.J. 1992. Geochemical remediation of groundwater by permeable reactive walls. Removal of chromate by reduction with iron bearing solids. In Proceedings of the Subsurface Restoration Conference, Third International Conference on Groundwater Quality Research, Dallas, Texas, June 21-24, p. 214-216.
- Blowes, D.W. and Ptacek, C.J. 1994. System for Treating Contaminated Groundwater. U.S. Patent # 5514279.
- Devlin, J.F., Barker, J.F. 1999 Field demonstration of permeable reactive wall flushing for biostimulation of a shallow sandy aquifer. *Ground Water Monit. Remed.* 19 (1) p. 75-83.
- Gillham and O'Hannesin 1994. Enhanced degradation of halogenated aliphatics by zero-valent iron. *Ground Water*, 32 (6) p. 958-967.
- Guiguer, N., Molson, J., Franz, T., and Frind, E. 1994. FLOTRANS User Guide Ver. 3.0: Two-Dimensional Steady-State Flownet and Advective-Dispersive Contaminant Transport Model. Waterloo Hydrogeologic Inc. Waterloo, Ontario, Canada.

- Mackenzie, P.D., Sivavec, T.M., Horney, D.P. 1997. Mineral precipitation and porosity losses in iron treatment zones. American Chemical Society, National Meeting San Francisco, California, April 13-17.
- McGregor, R., Blowes, D.W., Ludwig, R., Pringle, E., and Pomeroy, M. 1999. Remediation of heavy metal plume using a reactive wall. In Proceedings In Situ and On-Site Bioremediation: The Fifth International Symposium, April 19-22, 1999. Battelle, Columbus Ohio. In Press.
- McRae, C.W.T. 1999. Evaluation of Reactive Materials for In Situ Treatment of Arsenic(III), Arsenic(V) and Selenium(VI) Using Permeable Reactive Barriers: Laboratory Study. M.Sc. Thesis. University of Waterloo, Waterloo, Ontario, Canada.
- Ptacek, C.J., Blowes, D.W., Robertson, W.D., and Baker, M.J. 1994. Adsorption and mineralization of phosphate from septic system effluent on aquifer materials. In Proceedings of the Waterloo Centre for Groundwater Research Annual Septic System Conference, Waterloo, Ontario, June 6, 26-44. Waterloo Centre for Groundwater Research Waterloo, Ontario.
- Robertson, W.D. and Cherry, J.A. 1995. In situ denitrification of septic system nitrate using reactive porous media barriers: Field trials. *Groundwater* 33(1) p. 99-111.
- Smyth, D.J.A., Shikaze, S.G., Cherry, J.A. 1997 Hydraulic performance of permeable barriers for in-situ treatment of contaminated groundwater. 1997 International Containment Technology Conference and Exhibition, St. Petersburg, Florida, February 9-12. In Press.
- Starr, R. Cherry, J.A. 1994. In situ remediation of contaminated groundwater: The funnel-and-gate system. *Ground Water*, 97 (2) p. 465-476.
- Teutsch, G., Tolksdorff, J., Schad, H., 1997 The design of in situ reactive wall systems – A combined hydraulic-geochemical-economical simulation study. *Land Contamination & Reclamation* 5 (2) p. 125-130.

Tratnyek, P.G., Johnson, T.L., Scherer, M.M., Eykholt, G.R. 1997 Remediating ground water with zero-valent metals: chemical considerations in barrier design. *Ground Water Monit. Remed.* 17 (4) p. 108-114.

U.S.Environmental Protection Agency (EPA) 1999. Permeable Reactive Barrier Installation Profiles. <http://www.rtdf.org/public/permbarr/barrdocs>.

## Chapter 7

### *Conclusions*

This thesis has demonstrated that a full-scale reactive barrier can be installed into an aquifer contaminated with high sulfate and dissolved metals. Using standard excavation methods and utilizing readily available and inexpensive municipal waste products this reactive barrier was installed in less than 4 days at a cost of approximately \$30,000.00 (U.S.).

The installation has resulted in a dramatic improvement in groundwater quality over the three years of monitoring. The dominant process leading to improved groundwater quality within the barrier is sulfate reduction. Sulfate reduction promotes the removal of acid generating Fe (II) by metal sulfide precipitation. Trace metals are also removed by sulfide precipitation. In addition to metal removal, sulfate reduction also generates significant alkalinity which greatly enhances the buffering capacity of the groundwater. Secondary processes that may contribute to improved groundwater quality include siderite precipitation and calcite dissolution.

Bacterially mediated sulfate reduction is the rate-limiting step in the removal of iron and the generation of alkalinity. The Monod formulation can predict the rate of treatment within the barrier:

$$\text{sulfate reduction rate} = k \frac{[SO_4]}{K_s + [SO_4]}$$

where  $K_s$  equals  $1.6 \text{ mmol L}^{-1}$  and  $k$  equals  $0.13 \text{ mmol L}^{-1} \text{ a}^{-1}$  (at  $9^\circ\text{C}$ ). The product of this rate and the residence time within the barrier indicates the amount of  $SO_4$  removed. In

the Nickel Rim barrier, preferential flow results in a range of residence times from approximately 65 to 370 days. The reactivity, as expressed by the rate constant ( $k$ ), is a function of groundwater temperature. The effect of temperature on the rate can be predicted using the Arrhenius Equation and an apparent activation energy  $E_a = 10 \text{ kcal mmol}^{-1}$ .

More homogeneous flow and improved barrier performance may be achieved by changes in the reactive barrier mix composition. Numerical flow modeling also indicates that barrier geometry will impact flow distribution. In general, if greater homogeneity in hydraulic conductivity can be achieved within the barrier than within the adjacent aquifer, a thicker (longer flow path) barrier will produce more uniform flow distribution.

Populations of sulfur and iron oxidizing bacteria within the Nickel Rim aquifer are limited to hydrologically defined zones of recharge and discharge. Populations of these bacteria in the tailings are relatively low compared to other tailings sites reflecting the presently low rates of sulfide oxidation at the Nickel Rim tailings. The zone of active oxidation has nearly reached the water table and high water saturation is now limiting oxidation rates. This suggests that the Nickel Rim tailings are nearing the end of their oxidation life cycle and remediation should focus on treating the oxidation products already produced.

Future work on reactive barriers of this type should focus on two topics: reactivity and physical flow. The Nickel Rim barrier performance is ultimately limited by the rate of sulfate reduction. It is likely that this is a function of the organic carbon reactivity. It is postulated that a change in organic carbon lability produces the decline in organic carbon reactivity. Establishing the relationship between organic carbon reactivity and barrier performance is necessary so that other possible factors such as trace nutrients or other unidentified phyiochemical factors can be discounted. Additional work should also be performed on increasing the reactivity of the reactive mixture.

The nature of flow through the barrier also impacts barrier performance. In the Nickel Rim barrier preferential flow through the central portion of the barrier resulted in decreased overall barrier performance. Understanding the scale and cause of the preferential flow is essential to eliminating this problem in the future. In addition, the relationship between faster flow paths and higher concentrations within the barrier to sampling bias within the barrier. Understanding the nature and cause of this sampling bias would assist in developing effective sampling protocols for assessing barrier performance.